GA–A26933

RESEARCH AND DEVELOPMENT AND FABRICATION OF INERTIAL CONFINEMENT FUSION TARGETS, COMPONENTS, AND COMPONENT TECHNOLOGY

ANNUAL REPORT TO THE U.S. DEPARTMENT OF ENERGY FOR THE PERIOD OCTOBER 1, 2009 THROUGH SEPTEMBER 30, 2010

by
PROJECT STAFF

DATE PUBLISHED: MARCH 2010

GENERAL ATOMICS

DISCLAIMER

GENERAL ATOMICS

GA–A26933

RESEARCH AND DEVELOPMENT AND FABRICATION OF INERTIAL CONFINEMENT FUSION TARGETS, COMPONENTS, AND COMPONENT TECHNOLOGY

ANNUAL REPORT TO THE U.S. DEPARTMENT OF ENERGY FOR THE PERIOD OCTOBER 1, 2009 THROUGH SEPTEMBER 30, 2010

by
PROJECT STAFF

Prepared under
Contract No. DE-AC52-06NA27279
for the U.S. Department of Energy

GENERAL ATOMICS PROJECT 30272
DATE PUBLISHED: MARCH 2010

GENERAL ATOMICS

LIST OF ACRONYMS

AES	Auger electron spectroscopy
AFM	atomic force microscope
ALD	atomic layer deposition
AuB	gold boron
BSE	Back Scattered Electron
CCD	charge coupled device
CD	carbon deuterium
CFTA	capsule fill tube assembly
CH	carbon hydrogen
CompRad	Compton Radiography
CPM	Center for Precision Manufacturing
CR	contact radiography
CryoTARPOS	cryogenic target positioner
CTS	cryogenic target system
D_2	deuterium
DEP	dielectrophoresis
DG	droplet generator
DImE	Defect Implosion Experiment
DOE	Department of Energy
DT	deuterium-tritium
DU	depleted uranium
E&EMS	Energy and electromagnetics systems
EDM	Electrical discharge machining
EDS	energy dispersive spectroscopy
EDX	energy dispersive x-ray
EDXS	energy dispersive x-ray spectroscopy
EOS	Equation of state
EP	Extended performance
EW	Electrowetting
FWHM	full width half maximum
GA	General Atomics
GDP	glow discharge polymer
GXD	Gated X-ray Detector
HAPL	high average power laser
HED	high energy density

HEDP	high energy density plasma
hGXI	hardened Gated X-ray Imager
ICF	Inertial Confinement Fusion
IDC	Indirect Drive Capsule Center
IFT	Inertial Fusion Technology – or – Inter Facial Tension
I-TIC	ignition target inserter cryostat
LANL	Los Alamos National Laboratory
LBS	Laboratory basic science
LEH	Laser Entrance Hole
LLE	Laboratory for Laser Energetics
LLNL	Lawrence Livermore National Laboratory
LMM	Laser Micromachining Center
MIFEDS	magneto inertial fusion electrical discharge system
NC	non-concentricity
NIC	National Ignition Campaign
NIF	National Ignition Facility
NLUF	National Laser Users Facility
NNSA	National Nuclear Security Administration
PAMS	poly-α-methyl styrene
PR	Precision Radiography
PSDI	phase-shifting diffraction interferometer
PVA	polyvinyl alcohol
PVD	Physical vapor deposition
R/F	resorcinol formaldehyde
SBS	styrene-butadiene-styrene
SEM	scanning electron microscopy
Si-GDP	silicon-doped glow discharge polymer
SNL	Sandia National Laboratory
SNRT	Supernova Rayleigh-Taylor
SSP	Stockpile Stewardship Program
T_2B	trans-2-butene
TARPOS	Target Positioner
TEM	Transmission electron microscopy
Ti-GDP	titanium-doped glow discharge polymer
TMP	thermo mechanical package
TMS	tetramethyl silane
UR/LLE	University of Rochester Laboratory for Laser Energetics
USAXS	ultra small angle x-ray scattering

XRF	x-ray fluorescence

TABLE OF CONTENTS

1 INTRODUCTION

This report documents General Atomics' (GA) fiscal year 2010 (FY10) activities for Inertial Confinement Fusion (ICF), a research and development program of the U.S. Department of Energy (DOE) National Nuclear Security Administration (NNSA). The program goals are controlled nuclear fusion at laboratory scales using large laser and pulsed power facilities in the U.S., and conducting experiments relevant to high energy density physics (HEDP) using those same facilities. The ICF Campaign, which includes the National Ignition Campaign (NIC) and HEDP experiments, is presently executed at the following facilities: Los Alamos National Laboratory (LANL), Lawrence Livermore National Laboratory (LLNL), Sandia National Laboratories (SNL), the University of Rochester Laboratory for Laser Energetics (UR/LLE) and GA. There are three major ICF facilities where this work is performed: the OMEGA glass laser at UR/LLE, the Z pulsed-power facility at SNL, and the National Ignition Facility (NIF) at LLNL. These facilities are supplemented by LANL's Trident laser, LLNL's Jupiter laser and other smaller lasers.

General Atomics' Inertial Fusion Technology (IFT), a division of GA within the Energy and Electromagnetics Systems (E&EMS) concentrates on producing the targets and doing the R&D for the targets for experiments that are carried out at the above facilities. Through target fabrication, GA supports the ultimate goal of the ICF Campaign to develop laboratory capabilities to create and measure extreme conditions of temperature, pressure, and radiation density, including thermonuclear burn conditions and achieving HEDP conditions. As in prior years, for this effort, GA supports all four of the strategies of NNSA's ICF Campaign to accomplish this long-term goal:

1. Achieve ignition in the laboratory and develop it as a scientific tool for stockpile stewardship.
2. Support execution of HEDP experiments necessary to provide advanced assessment capabilities for stockpile stewardship.
3. Develop advanced technology capabilities that support long-term needs of stockpile stewardship.
4. Maintain robust national program infrastructure and attract scientific talent to the Stockpile Stewardship Program (SSP).

GA continued its unmatched performance in FY10, bringing together a dedicated and high-quality staff, an efficient management system, an understanding of the integrated program needs, the appropriate facilities and equipment, and a commitment to the customer, to produce targets, conduct R&D for the target supply, and support the ultimate goals of the ICF, NIC, and HEDP programs.

These experiments were the first step towards support of the ignition campaign expected to be completed in FY12.

In FY10, following the initial shots in FY09 at NIF as part of the scaled hohlraum energetics and symmetry campaigns, NIF continued those experiments into the first quarter

of FY10 and GA's support was again central in the ability to field over 30 cryogenic gas filled hohlraums in that time frame. GA responded exceptionally to rapid changing needs in that period for NIF and provided all the required components as well as assisting in the final assembly and metrology of the completed targets. GA produced the majority of the central target components and sub-assemblies for the cryogenic gas filled hohlraum targets. These components included gold (Au) or gold/boron (AuB) hohlraums, germanium (Ge) doped CH capsules, capsule fill tube assemblies (CFTA) with 10 μm fill tubes, thermo-mechanical components and associated sub-assemblies required for cooling to 20 K, as well as laser entrance holes (LEH). GA continued support of NIF during the Ignition Preparation Period (IPP) by producing components for prototypes targets, targets for cryogenic layering experiments at LLNL, as well as producing inventory for shots planned post IPP. Beyond the production activities, the ongoing developmental work on capsules with graded doped ablators continued. In particular, based on the results of the campaign in early FY10, the surface finish specifications requirements for Ge doped CH shells became tighter by over a factor of 10. Hence our work in FY10 was geared towards improvements in CH capsules surface, specifically polishing of such capsules, which previously was deemed unnecessary. A team of scientists from LLNL and GA were able to develop a baseline polishing technique, which also involved laser ablation of large isolated features that improved the CH capsule surfaces to obtain a sufficiently large yield of capsules with the required surface finish. Development of Be shells also continued, with precision metrology techniques identifying an undesired non-uniform diffusion of the copper dopant. The GA-LLNL team again worked expeditiously towards a solution, which is nearly in hand. These developments will be discussed in this report. GA also supported the Cryogenic Target System (CTS) for the NIF through its LLNL-onsite engineering staff, which included the chief engineer in charge of the CTS. GA also supported fabrication of pinholes for various NIF diagnostics in FY10, based on its ability to produce and characterize such parts more readily and at higher quality than other suppliers. This latter work was supported through de-obligation of funds from LLNL.

GA continued its support of NNSA's ICF program for OMEGA by on time delivery of fully characterized target components and targets necessary to enable ICF and HEDP experiments as required by the shot schedule. The OMEGA target support accounted for the majority of components produced by GA in FY10, more than 2210 targets and components. Each shot-day or half-day generally required a completely different type of tightly specified and well-characterized target, in some cases requiring major R&D effort on a relatively short time scale. The Z facility continued to increase its shot rate in FY10 and GA continued to produce many novel and different types of components for Z, made by techniques requiring significant development. GA supported Z on almost all of its nearly 125 shots in FY10, including close interactions on the design to enable fabrication of such complex targets and all in a timely manner. GA also continued its development of next generation of targets on Z in collaboration with SNL.

Since targets are the initial conditions for the experiments, the targets and components need to be accurately measured and characterized for each shot. In providing these key components, the GA target fabrication group, an ISO 9001:2008 registered program,

maintained excellent communication with the users of the targets to ensure adherence to the required quality and quantity, while continually seeking to improve processes to increase efficiency to enhance the performance of the team. In addition to getting extensive and generally very positive feedback from its customers in FY10, the GA staff authored a number of papers in refereed journals and presented work at major international conferences. Highlights of the GA ICF technology work performed under DOE Contract No. DE-AC52-06NA27279 in FY10 comprises the subject of this report.

In Section 2, we give a brief overview of the fabrication centers within the GA's IFT group that ensure delivery of the various components needed for ICF experiments. In Section 3 we summarize the target deliveries to the OMEGA and NIF facilities by program or laboratory, and include descriptions of target deliveries of note. In FY10, as in previous years, GA worked closely with all other sites to manage the rolling specification of hundreds of targets per year required for OMEGA, through weekly teleconference and videoconference meetings under a Change Control Board. Such meetings ensured that target specifications for each facility shot-day, which is essentially a new experimental campaign, were specified well enough in advance for complete manufacture and characterization of the target to specification.

In Sections 4-6, we summarize research and development work performed in support of target fabrication or metrology. Section 4 deals with that effort for NIF, in particular, the national ignition campaign (NIC). Section 5 summarizes developmental activities for OMEGA (NIC x-ray drive target production and NIC direct drive target production) and Section 6 those for the Z facility (SNL Target Development and Production). Much of this development work has been presented to peers in the inertial fusion and HEDP community at major international conferences (e.g., the Target Fabrication Specialists Meeting in Orlando, Florida). Section 7 discusses technical developments and target fabrication that were done either on internal GA funds or through contracts other than the one that is the subject of this annual report. We present this work since much of this is anticipated to be beneficial to the NNSA effort eventually in either the ability to field new targets or for improved efficiency.

Comments and requests for further information may be directed to the GA Inertial Fusion Technology Program Manager, Abbas.Nikroo@gat.com, (858) 455-2931.

2 CAPABILITY CENTERS

2.1 Center for Capsule Production (CCP)

The Center for Capsule Production (CCP) is primarily responsible for the manufacturing of thin-wall microcapsule components and targets for experiments carried out at OMEGA, Z, NIF and other laser facilities for LLNL, LANL, UR/LLE, National Laser Users Facility (NLUF) and SNL. Capsules produced by CCP include a variety of polymer capsules with multiple layers, drop tower and "Hoppe" glass capsules.

Polymer capsules are essentially all fabricated using the depolymerizable mandrel technique, where pure CH or CD, or their doped varieties are deposited using the glow discharge polymer (GDP) coatings (Fig. 2-1) on a removable mandrel or mold to produce the final deliverable shells for the experiments. The mandrels are produced by the Foam and Materials Center discussed in Section 2.3, with the centers working very closely to ensure an appropriate supply of high quality mandrels in the required sizes to allow rapid response to requests from the labs.

Fig. 2-1. A GDP coater (1 of 9) operated at General Atomics to produce polymer and doped polymer capsules.

In addition to polymer capsules, CCP also produces high quality glass shells using the drop tower or "Hoppe" techniques. Drop tower shells are produced in large quantities by blowing glass formers into spherical shells in the range of ~ 200- 900 μm. These shells are used in many of the experiments involving neutron or proton (particularly for NLUF) generation at OMEGA. Since these shells are made in a drop tower, they suffer from larger wall thickness non-uniformity (> 0.1 μm to as much as > 1 μm) compared to "Hoppe" shells, which are made using the process described in previous years, by converting Si-doped GDP (Si-GDP) shells into glass shells. Since Si-GDP shells can be made with wall thickness uniformity of <0.1 μm, "Hoppe" glass shells also have the same level of uniformity. In

addition, the diameters of shells made in the drop tower is limited to ~ 900 μm as mentioned above, but the "Hoppe" technique has yielded shells over 2000 μm in diameter. "Hoppe" shells are made usually in batches of ~ 10 or so, and the process is more time consuming, therefore they are used for experiments needing the larger diameters, higher precision and uniformity.

CCP, in addition to developing and producing capsules, often also undertakes development of thin polymer films which involve GDP, used in experiments to study the behavior of this material in planar experiments as a predictor for the ablator behavior in spherical implosions. In FY10, this included developing and producing doped and undoped GDP foils with engineered "bumps" and in collaboration with the CPM center, precision smooth steps in GDP.

Other developments in CCP for FY10 included successfully producing capsules with ultra-thin buried Ti layers at very high Ti doping (~ 5-6 at. %) which presented a challenge due to the reactivity of Ti with air at these high doping levels.

UR/LLE cryogenic experiments on OMEGA were supported by production of thin walled strong carbon deuterium (CD) with tighter wall thickness specifications than previous. Capsules were also delivered for Fast Ignition, Shock Timing and other direct drive experiments.

NLUF deliveries included GDP capsules with a titanium doped GDP (Ti-GDP) layer for the Core Imaging campaign, drop tower glass as well as polymer capsules for the PRad campaign, and tantalum crystal assemblies for the ICE:BCC Metals campaign.

2.2 Center For Precision Manufacturing (CPM)

The Center for Precision Manufacturing is responsible for the micromachining of high precision components and the assembly of cone and shell targets. The machined components and the cone and shell assembled targets are used in experiments carried out by the National Labs, (LLNL, LANL, UR/LLE and SNL), and by Universities, (MIT, University of Michigan, Rice University, UCSD, Cornell, Ohio State and the University of Nevada at Reno) on the OMEGA, NIF, and the Z pinch facility at SNL. In addition, CPM also produces a few targets or target components for the Titan and Trident laser facilities, usually those that are more complex or require higher precision.

CPM also heavily supports the NIF effort which is discussed below in Section 2.4.1.

The components are made using very high precision machining equipment; such as diamond turning lathes like the kind used by the optics industry, high precision milling machines like the kind used by the watch making industry and a high precision EDMs like the type used in the MEMS and micro-Fluidics industry. These machines have been adapted to fabricate the very complicated and high tolerances components needed for experiments in the high power laser facility. Figure 2-2 shows a picture of the latest addition to the center, a Moore Nanotech 350 FG, a 5-axis capable diamond turning lathe.

To ensure the timely delivery of components and targets the Center for Precision Manufacturing works in close collaboration with our partners at the National Laboratories

and Universities. Planning is initiated up to six months in advance of the shot date to define specifications and component design. This advance planning is important in development, prototyping and developing new characterization techniques that are needed to fabricate and metrologize complicated targets. In FY10 the Center for Precision Manufacturing was able to deliver all the requested components and targets.

Fig. 2-2. Photograph of the newest addition to the Center for Precision Manufacturing a Moore Nanotech 350 FG, a 5-axis capable high precision diamond turning lathe.

The Center for Precision Manufacturing has fabricated, characterized and assembled several new types of targets and components in FY10 for OMEGA and Z. Examples include composite copper/gold cones and copper wedges for UR/LLE, spherical hohlraums and beryllium tubes for SNL, and lithium fluoride disks for LLNL.

In FY10, the CPM produced components varied from simple hohlraums up to multi-component targets such as the SNL Cibola II target where each target assembly had a total of eight components. The cone and shell assembled targets were used for Shock Timing and Fast Ignition experiments at UR/LLE.

2.3 Foams And Materials Center (FMS)

The Foams and Materials Center produces a wide range of components and performs R&D work towards fabricating first of a kind targets. These targets were for experiments performed by Laboratory for Laser Energetics (LLE), Lawrence Livermore National Laboratory (LLNL), Sandia National Laboratory (SNL), AWE and various universities.

The FMS center collaborates extensively with and provides support for the CCP and NIF centers through fabrication of the depolymerizable mandrels [poly-α- methyl styrene (PAMS)] for both OMEGA and NIF producing aluminum shields for indirect drive assemblies. This led to the shields becoming a reoccurring, routine order that GA has delivered. The FMS center also continued its support of the NIF direct drive campaign, by working closely with LLE to further develop 3 mm diameter foam capsules with fill tubes for cryogenic layering experiments, and fabricated and delivered many assemblies used in layering experiments at LLE.

Various developmental targets were demonstrated by the FMS group in FY10. For LLE, we were able to fabricate copper foils with very small, 1 μm wavelength pattern for the enhanced coupling experimental series (Fig. 2-3). For LLNL we were able to develop a lithographic procedure to produce gold wire backlighters (Section 5.4). For SNL we produced tantala aerogel foam targets similar to those for NIF and OMEGA RadXport campaigns, but in a hohlraum assembly design for Z. For NLUF shots on OMEGA, we were able to reduce the density perturbation due to embedding multiple features and characterize the resulting Astroshock foams. Embedded cones in foam were also produced for the NLUF PRad campaign for studying the fields at the tip of a cone relevant to Fast Ignition.

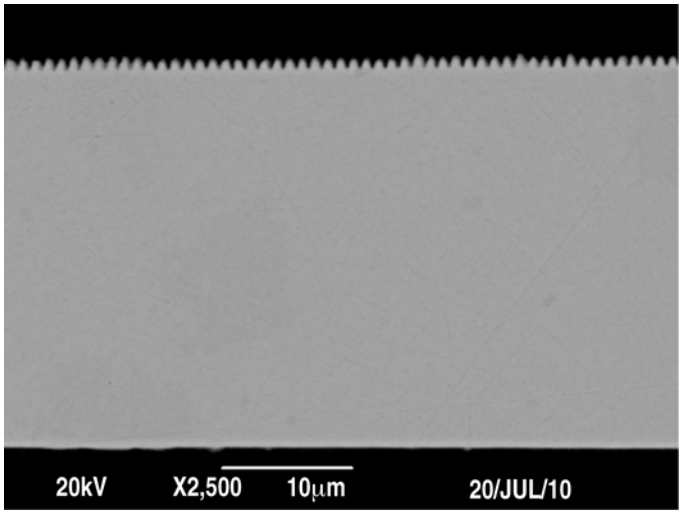

Fig. 2-3. SEM of mechanically cross-sectioned copper foil with 1 μm wavelength pattern for Enhanced Coupling series.

Also of note are various internal R&D projects, high energy density (HED) contract work and related ICF development activities. For LLNL/HED we were able to use a similar lithographic process For NIF diagnostics, a process for fabricating and characterizing deuterated polyethylene foils was developed (as described in Section 7.4). A process for mass-producing foam shells was furthered by the development of a UV cure process for resorcinol formaldehyde shells (Section 7.3) and work on electrowetting techniques (Section 7.6) for forming the precursor droplets to the foam shells.

2.4 NIF Centers

2.4.1 Center for Precision Manufacturing (CPM) – NIF Operations

As mentioned in Section 2.2, the Center for Precision Manufacturing also provides essential support for the NIF effort. CPM is responsible for the fabrication of the Thermo-mechanical Packages (TMP) and other NIF target components that are used for fielding NIF targets cryogenically. This effort involves dedicated diamond turning lathes and precision mills for NIF component fabrication as well as drawing from the general purpose equipment to allow quick response which usually is the result of a finding at NIF and changes in the component designs.

The types of NIF components being fabricated include: aluminum cans, aluminum bands, LEH inserts, window washers, gated x-ray detector (GXD) plugs, and KeyHole cones. In addition, CPM provides support to the NIF hohlraum and capsule production centers. CPM is responsible for milling out all of the features on Gold NIF hohlraum and in FY10, its laboratories were certified to conduct such operations on uranium hohlraums as well. The milled features include diagnostic holes, fill tube holes, tamping gas holes, and view holes such as the Star Burst pattern.

The staff in the Center for Precision Manufacturing is in continual contact with the LLNL NIF personnel to rapidly prototype, implement new or modifications in design and advanced planning for on time delivery of targets. This advanced planning is especially important for work involving component fabrication for the NIF.

2.4.2 NIF Hohlraum Center

The NIF Hohlraum Center is responsible for producing gold and uranium hohlraums for NIF. It has streamlined its production facility for routine delivery of hohlraums (delivered in halves to allow for capsule insertion during assembly) while simultaneously incorporating R&D efforts to support the NIC. The hohlraum center works closely with CPM and LMM for precision diagnostic features such as GXD, Starburst, and Keyhole cutouts. NIF Hohlraum center is situated in a radiation-monitored laboratory to allow fabrication, handling and processing of uranium parts. Based on GA's long time experience with handling radioactive materials, GA's health physics department regularly monitors the lab for proper operations. NIF Hohlraum Center capabilities and equipment include, Precitech NanoForm 200 precision lathe, three PVD sputter deposition systems, and two devoted PVD sputter deposition systems for Depleted Uranium (DU) coating, with a third DU coater system under construction. The facility contains a dedicated chemistry lab housing two, 10 part electroplating baths, a dedicated hood for etching and cleaning uranium and gold hohlraums, and a polisher to prepare samples for Scanning Electron Microscopy (SEM). A Z-Mike™ laser micrometer is used to check and measure tolerances of up to ± 0.3 μm. The NIF Hohlraum Center utilizes a Nikon MM400 for high magnification inspection of all parts and a Keyence VHX-600 digital microscope scope for lower magnification images. Utilizing the equipment of the ICF characterization lab, high accuracy interferometry measurements are taken, on a Wyko NT3300. The center is responsible for holding of tolerances of ± 0.3 μm

on dimensions of engineered half hohlraums as well as a surface finish below 200 nm. These dimensions are consistently met on a routine basis. Finally, residual resistivity ratio (RRR) has been reinstated to improve understanding of hohlraum thermal conductivity, which improves deutrerium-tritium (DT) ice layering modeling and understanding.

The primary focus over the past year has been to maintain Au hohlraum manufacturing capability while improving the process for Depleted Uranium (DU) hohlraums. This focus has increased both overall yield and throughput of DU Half hohlraums. In FY10, there was a total of 108 DU sputter runs on 540 half hohlraums. Included in these runs were changes in design and process to help improve yield. This is discussed in the development Section 4.1.2 of this report. This has led to an inventory of 167 DU coated half hohlraums ready for further processing to final dimensions and delivery as well as other parts for developmental activities such as identifying failure modes in order to further improve the process.

The Hohlraum Center has also continued to provide our LLNL colleagues with prototype designs and solutions for assembly failure modes. This includes a hohlraum that has a radius on the inner diameter of the half hohlraums in order to alleviate tent failures. In FY10, the Hohlraum Center delivered a total of 282 components including 20 DU half hohlraums. We pushed for validation of the AuAuB design, which from experimental data from NIF showed no significant change in styrene-butadiene-styrene (SBS) between AuAu and Au half hohlraums. This disproved the theory and increased the yield of production. From FY09 to FY10 the yield of AuAuB and Au half hohlraums increased from 50% to 80% as a family of parts. Development on the 1.2 (635) scale half hohlraums was successful and manufacturing capability was proven for a 1.2 MJ shot.

2.4.3 Center for NIF Capsule Production (NCP)

The Center for NIF capsule production is responsible for the manufacturing of capsules and capsule fill tube assemblies (CFTA) for experiments carried out at NIF. NCP produces the NIF design graded doped capsules required for NIF tuning and ignition experiments. These include both CH and beryllium shells (with Be coatings performed both at GA and LLNL). NCP utilizes the GDP process for making the layered CH capsules with the Ge dopant in four dedicated coaters within the general GDP coating lab, drawing from personnel used in the OMEGA work. Sputter coating is used for producing beryllium shells, with 3 coaters at GA and 2 coaters at LLNL. FMS Center supplies the mandrels critical for NIF shell fabrication, while NCP works closely with the CPM Center for targets that involve machined holes in the capsules such as shock timing shells.

With the results of the 2009 NIF energetics campaign pointing out the possible contribution of isolated features on CH capsules to hydrodynamic mix, NCP worked rapidly with our LLNL colleagues to institute new measures to reduce these features. First a novel polishing technique combined with laser ablation was developed to eliminate features present on the shells due to the GDP coating process. Secondly, the clean room environment used in fabrication and processing of shells was upgraded at GA to meet the anticipated class 100 levels required for NIF shells. These latter steps were coordinated closely with concomitant

improvements at LLNL . Figure 2-4 shows one of the new modular units implemented in FY10.

As in other areas, NCP works in close collaboration with our partners in the national laboratories to obtain target specifications well in advance to ensure timely delivery. This advanced planning is especially important for work involving component fabrication for the NIF. NCP scientists and engineers are in continual contact with LLNL personnel to rapidly prototype and implement new or modifications in design.

In FY10, the NCP produced a total of 112 components and targets including fabricating, characterizing and assembling several new types of targets and components in FY10, examples include: keyhole capsules 4th shock capsule fill tube assemblies, SymCap capsules (Fig. 2-5), THD capsules as well as ignition quality capsules. These have now all been used at NIF in critical tuning experiments.

Fig. 2-4. Image of Cleanroom Enclosure for Capsule Fill Tube Assembly

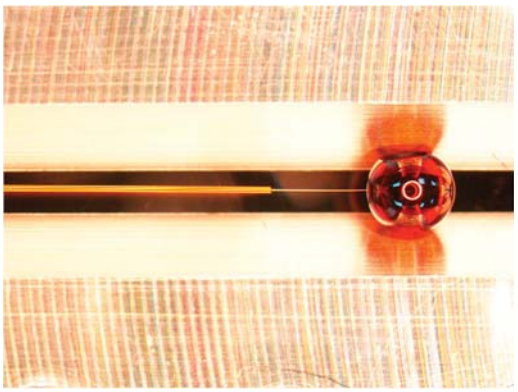

Fig. 2-5. Photo of a SymCap fill tube assembly in shipping cradle ready for shipment to LLNL for final assembly.

2.5 Laser Micromachining Center

The Laser Micromachining Center (LMM) is primarily responsible for laser drilling capsule fill tube holes for both CH and Be NIF ignition target designs for attachment of the fill tubes mentioned above in Section 2.4.3. It continued its support of NCP in that respect. In addition, production and characterization of X-ray diagnostic pinhole and attenuation arrays for the NIF became a new activity for this center in FY10 through direct LLNL support. The LMM Center also performs production of various target components for experiments performed at the OMEGA and Z facilities.

The LMM Center expanded its 532 nm wavelength laser machining capacity through the addition of a new 1600 square foot laboratory space in FY10 including addition of a second 532 nm wavelength laser work station as well as a femtosecond laser system that will provide opportunities for additional R&D. Production capability to perform unattended multiple part production runs was implemented increasing production throughput significantly. New laser machining capability was added as research was conducted to reduce production quality hole diameters from 10 μm to less than 8 μm through 75 μm thick material. The LMM Center further leveraged the CAD file to laser station milling G-Code process via 3rd party software, greatly accelerating prototyping. A significant future improvement to the LMM Center's 532 nm facility is the purchase of two higher power laser systems, expected to be operational in Q2 FY11. These systems will greatly facilitate increased production throughput as well as expand R&D efforts in support of IFE target and diagnostic component development.

The LMM Center improved its UV wavelength laser machining capacity and facility in FY10. The LMM Center is responsible for maintaining the UV laser facility as a multiple user facility within IFT. An older 248 nm Excimer gas laser was replaced with a solid-state quadrupled YAG 266 nm laser for improved operational reliability. The YAG laser was then further modified to increase the laser's shot repetition from 1 kHz to 30 kHz adding additional production throughput capability. The UV lab facility as a whole was converted into a Class 10,000 cleanroom to support NIF specifications for debris and dust mitigation. Currently the facility is regularly used to laser cut thin plastic foils (Kapton, Mylar, etc) creating custom shapes and patterns. Additionally, cutting holes into shells for Fast Ignition

targets 100 units at a time is performed. This work is in support of IFE and a demonstration of robotic assembly of targets.

Working with the CCP personnel, using the UV laser workstation, a technique was developed to remove surface protrusions from CH capsules that is a beneficial precursor to the capsule polishing. Surface protrusions, usually in the shape of truncated spherical domes on CH capsules, hinder implosion performance by causing hydrodynamic instabilities during compression. By reducing the size of such domes, the capsules are smoother and the probability of successful ignition is increased. We have developed a process to remove the deleterious larger domes (~600+ nm height, 20+ μm width) from the capsule surface by laser ablation. This process combined with a polishing method co-developed by GA and LLNL to reduce the remaining material and smaller domes, will render capsules for appropriate ignition experiments.

For work on pinholes, working with the NIF capsule metrology personnel, a characterization process was developed to apply virtual fitting and data summarization to these pinhole/collimator diagnostic arrays. The process includes application of existing IFT capabilities towards small feature measurement, including contact radiography metrology and optical coordinate measuring machine (OCMM) automated microscopy with the addition of custom data analysis (and summarization), providing LLNL with virtual fitting information to match X-Ray pinhole arrays with collimator pairs.

In FY10 the LMM Center produced more than 500 components in over 30 separate orders via 266 nm and 532 nm wavelength laser workstation systems utilizing unique capability to create very small diameter features, order 10 μm, as well as drill high aspect ratio holes. In addition, the LMM Center provided characterization for an additional 200 LLNL produced pinhole and collimator components.

2.6 Onsite Work

As part of the effort provided by GA and its subcontractors, a number of personnel assist in various target fabrication work onsite at the ICF laboratories including SNL, LLNL, LANL and LLE. These personnel are mainly involved in assembly activities, as well as cryogenic system engineering and some fabrication work. These personnel include Schafer Corp. (our subcontractor) personnel as well as General Atomics personnel as summarized in Table 2-1. The following briefly discusses the activities involved at each site.

Table 2-1
Onsite Personnel Break Down

Onsite @	LLNL	LANL	SNL	LLE	Total
GA	14	0	3	2	19
Schafer	3	1	4	0	8

2.6.1 SNL

SNL onsite work includes many assembly activities related to shots on the Z facility. Also, some of the classified target production operations now take place onsite at SNL, through the transfer of technology from GA including assistance in some of the facilitization. This is expanded upon in Section X,

2.6.2 LLE and LANL

Two onsite GA personnel assisted in fabrication and assembly of targets, including those for NLUF experiments, at LLE. These personnel assisted in planning and processing of a subset of targets assisting and complementing LLE target fabrication personnel in that task, as well as detailed assembly of targets either for LLE or for the NLUF program. At LANL, a technician through Schafer Corp. assisted both in assembly and fabrication activities including machining tooling and parts (primarily for the Trident laser).

2.6.3 LLNL NIF and OMEGA Assembly

The LLNL onsite assembly team has three divisions which work within LLNL to support three distinct areas in support of LLNL NIF and OMEGA target fabrication. One division is integrated with the NIF cryogenic target assembly team where GA personnel work to prototype, assemble, and metrologize targets for the NIF. One task is integrated with the NIF Cryogenic Target Systems, where GA personnel work on design, analysis, fabrication, assembly and test of cryogenic target delivery systems for the NIF as well as performing other appropriate engineering work. The third team works primarily on targets for various scientists at LLNL in support of NIF and HED target campaigns on the OMEGA Laser system. This team also fabricates targets for other lasers, as well as non-cryogenic targets for shots on NIF.

The focus of the cryogenic target assembly group is to produce targets used for various development tasks and used in experiments on the NIF. In FY10, this team produced 65 different targets. This work is done in a 3000 square foot Class 100 clean room at LLNL (Fig. 2-6). The clean room houses the production line as well as the tools used to develop new assembly and metrology methods. The assembly line consists of component incoming inspection, subassembly fabrication, cleanliness interrogation, final integration, assembly bonding, and proofing. GA personnel participate in each stage of the assembly process. The work is managed by LLNL staff and is in support of the National Ignition Campaign.

The target fabrication team at LLNL supported over 60 shots on the OMEGA laser system, which ranged from foil experiments to gas filled hohlraums with various packages. The support team also produces Be sputtered capsules. While these targets have not been requested as deliverables for the NIF laser system yet, some capsules are produced for shot campaigns on the OMEGA laser and the support team is working to modify coating techniques to minimize copper diffusion. The NIF Cryogenic Target Systems (CTS) is supported by an engineering team that is responsible for fielding cryogenic targets in the NIF laser. Over the past several years, the team has developed and commissioned a cryogenic system for the existing NIF target positioner (TARPOS). During FY10, the team installed and

commissioned a new target positioner, the cryogenic target positioner (CryoTARPOS), which is now used to field cryogenic targets with fully characterized ice layers inside the capsule in the NIF chamber.

Fig. 2-6. NIF Cryogenic Target Final assembly machine in the final assembly clean room area at LLNL.

3 DELIVERY SUMMARY

3.1 OMEGA Deliveries

GA supplied approximately 2210 target components, assemblies or sub-assemblies to LLNL, LANL, UR/LLE and others in FY10 for the DOE/NNSA contract for NIC, LBS, and NLUF campaigns. In addition, roughly 700 components or sub-assemblies were delivered to various labs in support of HED, Fast Ignition and AWE campaigns conducted at the OMEGA/EP facility. Bringing total deliveries to 2933 for experiments on OMEGA or EP. As NLUF targets became more sophisticated this year, the number of required components decreased while their sophistication increased. Capsules and micromachined components comprise the majority of the components built at GA in support of this work. Figure 3-1 shows the deliveries in FY10 by laboratory or program on a quarterly basis. Table 3-1 summarizes these deliveries by major component types: capsules, hohlraums and "packages" that included foam components, assemblies, and flat plates with various precision-machined surface perturbations. A "special" components section includes precision cone in shell assemblies, buried cones, and cone and wire assemblies for fast ignition; direct drive capsules with file tubes for ice layering studies; and cones buried in foams for proton radiography. All of which require more than component fabrication but also delicate and precision assembly and metrology to inform the PI about the target.

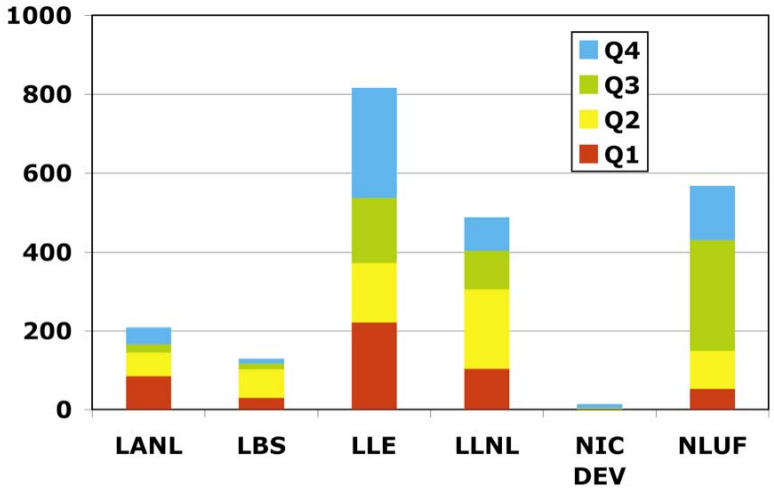

Fig. 3-1. FY10 deliveries by laboratory per quarter.

Table 3-1. FY10 DOE/NNSA Deliveries by Laboratory and Types of Components

Lab	Capsule	Hohlraum	Package	Special	Grand Total
LANL	136	36	27	10	209
LLE	643	0	53	121	817
LLNL	63	54	278	94	489
NLUF	121	98	250	99	568
LBS	51	15	0	63	129
Grand Total	1014	203	608	387	2212

3.1.1 Capsule Deliveries

3.1.1.1 Capsule Support for UR/LLE

The capsule center coordinated delivery of 643 targets in 2010 to UR/LLE. While a number of different targets were delivered, the majority of the effort was focused on capsules for cryogenic shots on OMEGA.

Cryogenic OMEGA shots primarily used thin walled strong CD capsules layered with DT and shot cryogenically. The requested capsule wall thicknesses spread (from shell to shell) tolerance was much tighter in this past year and was a challenging 9.25 ± 0.25 μm thick wall, compared to ± 0.5 μm in previous years. Metrology of these capsules was essential to ensure specified wall uniformity required for the layering process as well as outer surface finish. In addition, as in prior years, buckle pressure of sample capsules from each batch was measured to ensure survival during the fill process at LLE. In addition to "OMEGA" size capsules for cryogenic shots, 3 mm diameter CD capsules were delivered for use in cryogenic layering research.

The capsule centers supported a number of additional shot campaigns on OMEGA. Table 3-2 illustrates the variety of the various types and the experiments they supported.

We also supported LLE by producing a number of precision planar targets made of GDP to study ablator material properties. These included 20-50 μm planar GDP and germanium doped GDP (Ge-GDP) foils in support of the Ablator EOS campaign experiments.

Table 3-2
LLE Campaigns Requiring Different Capsule Types

Capsules Design	Thickness	Experiment
CD	9 μm	Cryo
	20 μm	Preheat
	40 μm	Shock Ignition
CD/CH	Various/1 μm	Shock Timing
		Fast Ignition
CH	15-40 μm	Neutron diagnostic dev
	24 μm	Mass equivalent
	20-27 μm	HXRDist
	9 μm	LattScat
	24 μm	MIFEDS
	24- 27 μm	PDHiConv
	20 μm	Reference
	27 μm	TPDCoherence
Glass	2 μm	MIFEDS
	14 μm	Hoppe

3.1.1.2 Capsule Support for LLNL

Our group coordinated delivery of 63 targets in 2010 to LLNL plus others in support of LLNL LBS experiments. Both Be and GDP capsules were delivered for CapAdiabat experiments. CompRad, IronComp, LattScat, ICELaue, and PhaseKin experiments were supported with the delivery of single-layer GDP capsules of various thicknesses. Multi-layered CH capsules with a polyvinyl alcohol (PVA) permeation barrier and a krypton gas fill were produced for MBop shots, each shell was analyzed for gas permeation rate. Tantalum foils were coated with GDP and Al and attached to a collimator for ICELaue shots.

3.1.1.3 Capsule Support for LANL

Our group coordinated delivery of 136 targets in 2010 to LANL. GDP foils with measured steps and "bumps" were developed and delivered for CHaRM experiments to study the effects of capsule wall perturbations. Two orders were delivered for HiZ shots, for the second a thin high atom % Ti (0.5 μm, 6%) inner layer was developed. Defect Implosion Experiment (DImE) capsules with a measured "trench" perturbation and Al permeation barrier were again delivered. Krypton filled multi-layered capsules with a PVA gas barrier were delivered for NIF5 experiments. In addition, Al coated GDP capsules with measured DD half-lives were delivered.

3.1.2 Micromachining Deliveries

3.1.2.1 LLE

In FY10 the Center for Precision Manufacturing supported LLE by machining of cones and capsules and the assembly of these into cone and capsule targets. For the Integrated-FI series of fast ignition shots 48 targets were delivered. A process to fabricate a target with a cone with a copper tip and a gold body was successfully developed. A picture of such a cone is shown in Fig. 3-2. For the SphShT series of shock timing shots 64 targets were made with two different capsule thicknesses, 5 and 9 μm. In addition copper wedges were fabricated to study high intensity laser plasma interaction in wedge-shaped cavity targets. Figure 3-3 shows one of the wedges, as a reference, the width and length of the wedge is 300 μm and the included angle of 34°.

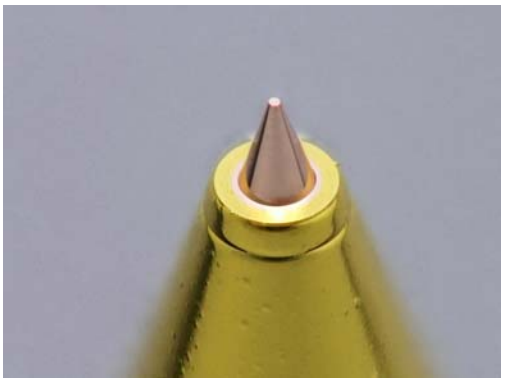

Fig. 3-2. A copper cone, replacing the usual gold cone, was made for fast ignition experiments.

Fig. 3-3. Picture of Cu wedge 300 μm long.

3.1.2.2 LANL

In FY10 the Center for Precision Manufacturing supported LANL by fabricating hohlraums for the CHaRM campaign and by providing gold electroplating support for the NIF-5 campaign. In addition the Center for Precision Manufacturing provided indirect support through the Capsule Center by machining channels on the equator of capsules for the

DImE campaign and machining known spacing steps on flat GDP foils in support of the CHaRM campaign.

3.1.2.3 LLNL

In FY10 the Center for Precision Manufacturing supported 10 OMEGA campaigns. Gold hohlraums, epoxy hohlraums, gold half hohlraums and gold tubes were made for Capseed, Hydro, InnerSRS, MBop, RelTS, XRSD and the Viscosity campaigns. Truncated cones were made for the CapAdia shot series. For the RelLPI series of experiments 22 cone and wire targets were fabricated and assembled. For this campaign two types of cones were fabricated, gold cones and aluminum cones.

The Center for Precision Manufacturing working in collaboration with the Precision Machining group at LLNL transferred the technology for machining brittle materials and this was successfully implemented in the machining of the LiF package for the D2/CH Therm experimental campaign. Figure 3-4 is a photomicrograph of one of the LiF disks with a 20 μm deep trench.

Fig. 3-4. Micromachined LiF disc

3.1.3 Onsite LLNL Assembly Support

The LLNL onsite assembly team works primarily on targets for various scientists at LLNL in support of NIF and HED target campaigns on the OMEGA Laser system. This team also fabricates targets for other lasers, as well as non-cryogenic targets for shots on NIF.

The target fabrication team at LLNL fabricated 689 targets for various experimental campaigns on the OMEGA laser system. These targets ranged from simple mounted foil experiments to gas filled hohlraums with complex angles and various packages (Fig. 3-5).

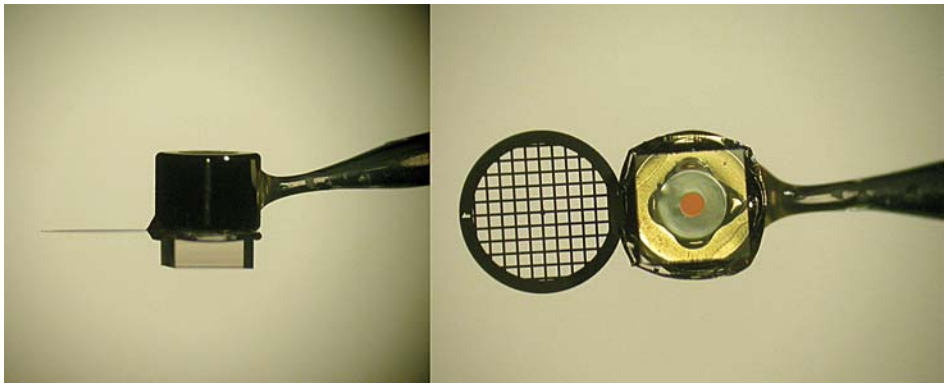

Fig. 3-5. A fully assembled target for the OMEGA laser system, with a half hohlraum, a resolution grid, and a target package.

The support team also fabricated over 50 targets for use on the NIF laser. These targets also range in complexity from simple grids to align the laser, to complex targets with multiple alignment angles and components (Fig 3-6). Our team also supports research and development tasks to solve problems in a very dynamic fashion. Scientists using the NIF laser have about 60 times more energy to work with than with any previous laser system. As with any emerging technology, unanticipated problems arise. The target fabrication team is often asked to help develop solutions. For example, the unconverted light in the target chamber was being reflected by various components and bouncing back into the laser system, where it was damaging the laser optics. A number of techniques were proposed to diffuse the light in order to mitigate the damage. Our team worked to make prototype components that were tested in the laser system. This work has led to the development of the dimpled shields which are now routinely used on cryogenic target assemblies.

Another effort that the LLNL target assembly team supports is the development of beryllium sputtered capsules. Over the course of the last year, we set out to quantify the amount of copper diffusion that occurred as a result of our processing methods. It was known that the copper diffused radially, but it was observed that the copper also migrated azimuthally; creating non-uniformities that are not acceptable in the anticipated NIF design plan. We are now testing various methods of fabrication that will prohibit or minimize the non-uniform migration of copper. This work is more fully discussed in Section 4.1.7.

Fig. 3-6. A pressurized, thin walled hohlraum mounted for a NIF laser experiment.

3.2 FY10 Support For Sandia National Laboratory

3.2.1 Onsite Support

In FY10, Sandia's Z machine had a productive and innovative experimental program that advances in areas such as Dynamic Material Properties and ICF research. To support these efforts there were 7 onsite personnel: 1 production planner, 1 chemist, 1 characterization specialist, 2 machinists and 2 target assemblers. They supported 105 Z shots and 20 NLUF OMEGA shots. This effort required the management of 2,462 target components, 219 of which were fabricated onsite. There were two types of components fabricated onsite, foams and micromachined components (Fig. 3-7). The large majority of the parts were of the Micromachined type. This capability was brought from the GA San Diego facility in FY09 and the need has continued to grow rapidly. At this point, two Precitech machines are operating almost daily allowing the majority of SNL targets to be entirely fabricated onsite.

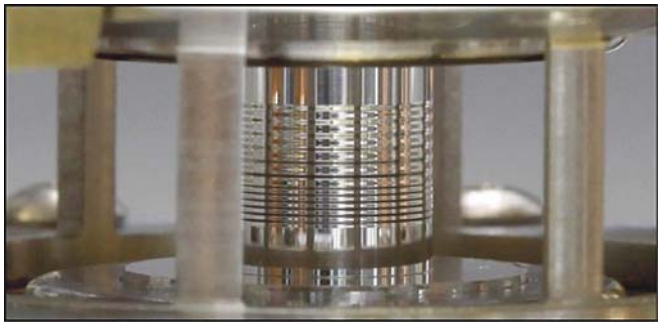

Fig. 3-7. An aluminum Magneto-Rayleigh-Taylor target fabricated by General Atomics onsite at SNL.

3.2.2 GA San Diego Support – Developmental Deliveries

Complex parts, whose specifications exceed the onsite capabilities, were supported by GA resources in San Diego. In FY10 GA San Diego supplied 109 target components for SNL that required either micro-milling, single-point diamond turning of beryllium, specialized aerogels, and/or sputtered or electroplated coatings. The most notable components were micromachined beryllium cylinders. While it is common to use beryllium filters and current return cans, the beryllium targets had stringent dimensional and surface finish tolerances that

required a significant R&D effort to achieve. In addition, GA San Diego machinists have been trained to fabricate all SNL targets so that San Diego can relieve heavy fabrication demand periods at SNL. The combinations of onsite target support coupled with GA San Diego support has resulted in quality, on-time target deliveries for SNL operations.

3.2.3 GA San Diego Support – Micromachining Deliveries

SNL. In FY10 the Center for Precision Manufacturing supported five of SNL campaigns. Machining of beryllium tubes supported the Lincoln and Union campaigns. Through continuous improvements the surface finish of machined beryllium tubes was improved by almost a factor of two. For the Cibola campaign the Center for Precision Manufacturing made 13 different types of components. Noteworthy is the spherical hohlraum. Figure 3-8 shows one of the spherical hohlraums with five machined diagnostics.

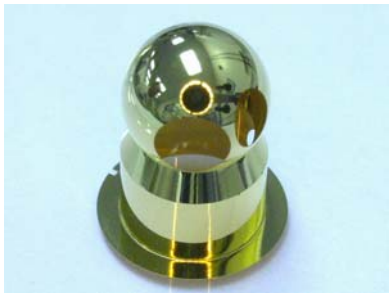

Fig. 3-8. Hohlraum machined to be driven by Z machine for Cibola experiments at SNL.

3.3 NIF Deliveries

3.3.1 Overview

We continued our effort for NIF in FY10 by delivering over 1900 components or subassemblies (see Table 3-3) for the NIF assembly effort at LLNL. These parts were essential for both developmental assembly activities as well as actual target assembly efforts towards fabricating full cryogenic targets for the tuning campaign on NIF, which resumed in August of 2010. The components delivered ranged over a wider selection of targets and experiments including key tuning experiments such as shock timing, re-emit and convergent ablator experiments, as well as refined SymCap experiments at higher energies (exceeding 1 MJ). In addition, components for the first ever THD layered cryogenic shots were fabricated and delivered. We continued our close interaction with the NIF team and to enhance it implemented weekly production meeting with LLNL production staff to ensure priorities and inventories were met and consistent. Sharing of databases was also implemented so that full analysis of changes could be made. Visibility of raw inventory, work in process and finished components was also implemented.

Table 3-3- NIF Deliveries

	Qtr 1	Qtr 2	Qtr 3	Qtr 4
Capsule Fill-Tube Assembly	29	20	14	49
Cone	0	21	0	20
Diagnostic Band	20	27	49	29
Hohlraum	46	80	46	110
Laser Entrance Hole (LEH)	23	40	100	60
Unconverted Light Shield	0	0	0	198
Thermo Mechanical Package	0	48	66	50
TMP Sub-Assembly	50	4	0	0
Window Washer	40	140	200	322
Sub-Total[a]	208	380	475	838
[a]The above table sums to Qty 1901.				
Specials & sub tier suppliers	90	160	106	222
Total[b]	298	540	581	1060

[b]Including specials, table sums to Qty 2479.

3.3.2 NIF Micromachining Deliveries

The Center for Precision Manufacturing delivered over 1100 micromachined target components in support of ignition for NIC. The components are part of the TMP and include Al cans and diagnostic bands, Au LEH inserts, Al window washers, GXD plugs, Au cones. In addition the Center for Precision Manufacturing provides support to the hohlraum fabrication group by milling features on Au hohlraums and U hohlraums. The milled features include the fill tube hole, tamping gas hole, view holes, StarBurst pattern and diagnostic holes. The Center for Precision Manufacturing also provides support to the capsules group by machining large holes on capsules for the KeyHole targets, which are cone and capsules targets used for shock timing experiments. Figure 3-9 shows one of the assembled KeyHole Targets. The Center for Precision Manufacturing also supported the Unconverted Light Shield fabrication group by micromachining the molds used to shape the unconverted light shields.

Fig. 3-9. **A keyhole target assembly used in shock timing experiments at NIF**

In FY10 a total of 69 different types of TMP components were made, this includes 12 types of cans, 14 types of bands, 2 types of LEHs, 25 types of hohlraums, 8 types of cones, 4 types of capsules, 2 types of window washers and 2 types of special components, ShockCom inserts and MV^2 spheres. The good working relationship with LLNL and dedicated equipment has allowed for quick turn around of parts as a result of design changes or the need of test parts, as can be seen by the number of different types of components machined. With continuous component fabrication improvements and the TMP design maturing the center is evolving into a production facility that would be able to produce the hundreds of components per year needed to ensure the success of NIF.

3.3.3 Sub-Assembly Deliveries

We delivered 187 thermo-mechanical package (TMP) subassemblies to LLNL. A TMP subassembly consists of the TMP Shell mounted to the Si cooling arm. A number of sensors, heaters, and a wiring harness are then connected. These subassemblies were used for NIC experiments including Ignition Layering, Re-Emit, SymCap, Convergent Ablator, ITPS, and Shock Commissioning targets.

3.3.4 Au and DU Hohlraum Deliveries

A total of 282 half hohlraums were delivered across 17 part numbers (designs) using three materials. Of these components, 224 were Au half hohlraums, 36 were AuAuB half hohlraums and 20 were depleted uranium (DU) half hohlraums (Fig. 3-10, Table 3-4). These components were used to support the NIC experiments including ignition, layering, vacuum experiments, and symmetry campaigns. Precision diagnostic features used to observe the implosion are milled into each half hohlraum via collaboration with CPM and LLM centers. Additionally, these half hohlraums had a large flange added to them electroplated with Au and micromachined to lie flat on the TMP can surface to provide a large gluing surface which increases production time by a day. Production times range from 3-5 weeks from date of order. Implementation of a new design generally takes 6 weeks. A prototype may be available earlier, but regular production takes programming of mandrel design, back machine design

and milled features to get underway, this usually takes up to two weeks to ensure that all programs are working properly.

Significant improvement in cleanliness was undertaken in FY10. Cleanroom products were used consistently with recommendations from LLNL cleanliness team. Particle counts are taken and analyzed weekly, and inspection has moved into a cleanroom environment.

Significant focus was applied to the tent side of the flange. Debris, sharp features, burrs, and scratches were documented with greater frequency compared to FY09 because the LLNL Tiger Team specifications lowered (tightened) the specification by a factor of 3. Implementation of semiconductor cleaning processes to remove debris and contaminants has proven successful in removing organic and plastics.

Shipment in Vertrel was implemented in order to quantify cleanliness of shipments. Through NMR spectroscopy LLNL can analyze the liquid for contaminants to ensure that parts are clean when they arrive at LLNL.

Close collaboration with LLNL scientific and design teams continued throughout FY10 enabling quick turn prototyping of designs because discussions were happening weekly.

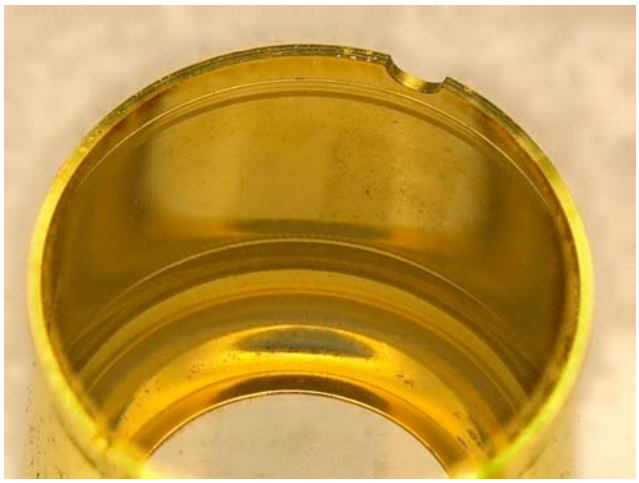

Fig. 3-10. DU SymCap half hohlraums with flange.

Table 3-4
Half Hohlraum Component Deliveries by Material and Design

Hohlraum Deliveries FY10				
Material	**Design[a]**	**Upper Half hohlraum**	**Lower Half hohlraum**	**Total**
Au	ConA_544	13	13	26
	IgLT_544	11	11	22
	Key1-4_544	23	23	46
	Remt_544	0	3	3
	Remt_544_Slot	3	0	3
	Remt_544_Win	11	11	22
	Sym_544	20	20	40
	THD_544	12	12	24
	THD_544_170	12	12	24
	THD_544_902	3	3	6
	THD_544_913	4	4	8
Au Total		112	112	224
AuAuB	ConA_90	5	5	10
	ITPS_913	4	4	8
	Sym_544	5	5	10
	Sym_90	5	3	8
AuAuB Total		19	17	36
DU	Sym_544	3	3	6
	Uranium R&D	8	8	16
DU Total		11	11	22
Total		142	140	282

[a]Nomenclature for design is as follows: Shot Type_Hohlraum Scale_Starburst Size or Diagnostic Hole Type

3.3.5 Laser Machining Deliveries

In FY10 the LMM Center coordinated delivery of more than 500 components in over 30 separate orders via 266 nm and 532 nm wavelength laser workstation systems, see Fig. 3-11.

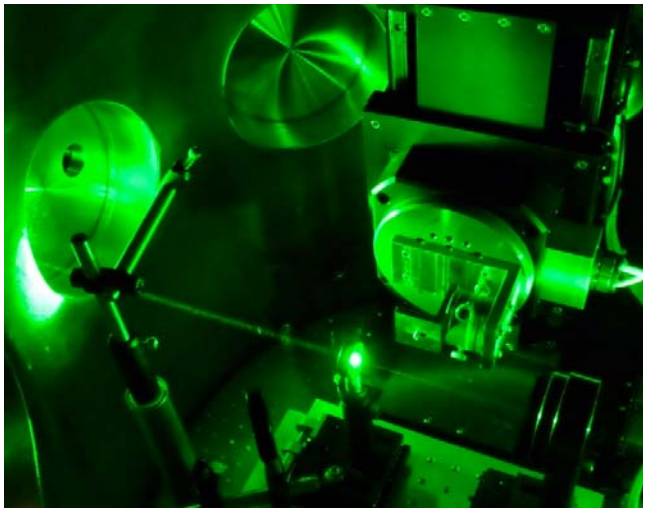

Fig. 3-11. Looking inside a 532nm wavelength laser workstation during an alignment step.

The LMM Center's production effort is categorized into three primary areas: Diagnostic arrays, backlighters and attenuators in support of NIF/OMEGA ignition experiments, beryllium and CH capsule hole drilling as part of the NIF target fabrication production process, and fabrication of various target components in support of ICF experiments on the OMEGA and Z facilities at LLE and SNL respectively. The LMM Center also provides associated characterization for all fabricated components utilizing documented, established metrology techniques and equipment from across the IFT organization, detailed in Section 7: Other Developments.

3.3.5.1 Diagnostic Arrays, Backlighters and Attenuators

The LMM Center employs a patented laser machining technique to create extremely small feature sizes while maintaining a high aspect ratio and cut quality through the material. Nominal feature size for these arrays, see Table 3-5 for a summary of various diagnostics arrays supplied to the NIF in FY10, spans 7 μm to 300 μm in diameter through 25 μm to 500 μm thick material. Material of choice is typically Ta, although Ti, Al, Cu, Ag, Au, Pt and SST have all been machined in FY10. A completed diagnostic pinhole array is sandwiched between two collimators that have larger feature sizes of the same pattern. While larger feature sizes are easier to control dimension wise, our technique enables fast material removal rates as well. Please see Figs. 3-12 through 3-14 for a sample of parts fabricated in FY10.

Table 3-5 - Diagnostic arrays/back-lighters/attenuators: Delivery Types FY10

Design Descriptor	Thickness Range	Associated NIF/OMEGA Diagnostic	Production (includes Characterization) and/or Characterization Only Orders
3 and 4 hole arrays, 25, 45, and 100 μm diam. holes	100 μm	SXI	Production
12 hole arrays, 100 μm diam. holes	50 to 100 μm	SXRI2	Characterization Only
18 hole arrays, 10, 100 and 300 μm diam. holes	50 to 100 μm	Gas Pipe	Both Production and Characterization Only orders
153 hole arrays, 10, 200, and 300 μm diam. holes	75 to 500 μm	hGXI	Production
186 hole arrays, 7, 10, 150, 300 μm diam. holes	75 to 500 μm	GXD	Both Production and Characterization Only orders
6400 hole array, 50 μm diam. holes	25 μm	Dante	Both Production and Characterization Only orders
25, 30, 150 and 250 μm wide slots	100 to 500 μm	Snout Assembly	Characterization Only
235 hole dual arrays with multiple slots, 10 to 150 μm diam. holes	75 to 500 μm	hSXRS, 5-Zone	Characterization Only, Planned Production in 1QFY11
Square feature arrays	12 to 50 μm	High energy back-lighters	Production

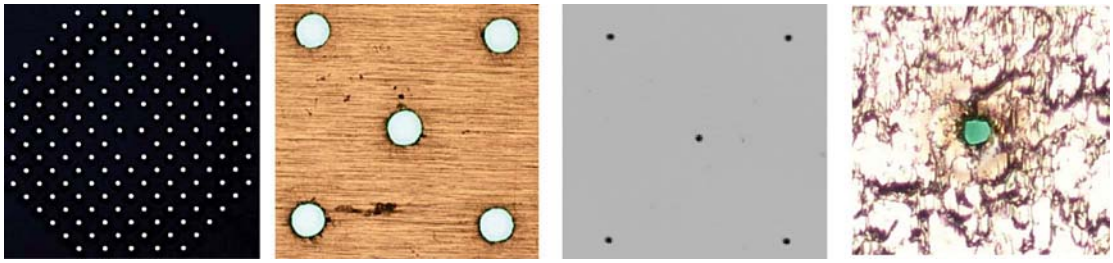

Fig. 3-12. hGXI THD Snout Assembly Pinhole and Collimator Parts. From left to right: Backlit collimator with 153-300 μm holes through 500 μm thick Ta, close-up of same collimator array, digitized image of matching pinhole part with 153-10 μm holes through 75 μm thick Ta, close-up of same pinhole array.

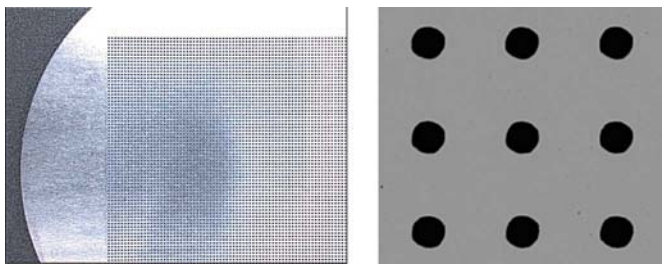

Fig. 3-13. Dante attenuator array. From left to right: 6,400-50 μm diameter holes through 25 μm thick Ta, digitized close-up image of same.

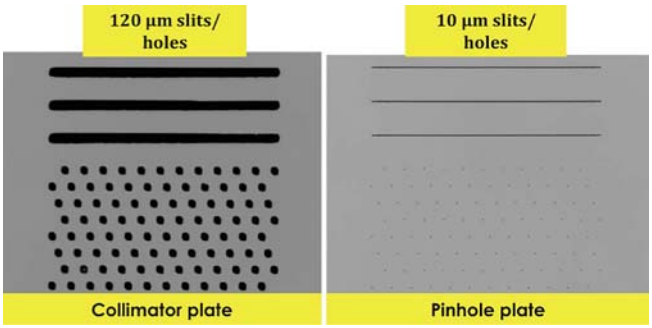

Fig. 3-14. hSXRS Dual slot and hole array test part, digitized images.

Capability to perform unattended multiple part production runs was implemented increasing production throughput significantly. A primary contributor to this throughput improvement was the further leveraging of tightly integrated 3rd party software that enables CAD file to laser workstation milling G-Code. This was the fruition of a collaborative effort between the LMM Center and the software vendor during the first half of FY10 to optimize the post processer, see Fig. 3-15. The process enables not only quick prototyping, but also easily creates large multipart CNC files. Typical production run times were increased from 1 part-1 production run to 24-hour production cycles as needed.

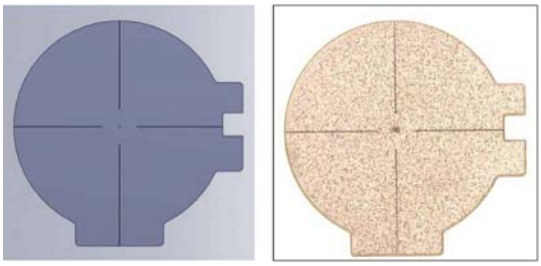

Fig. 3-15. We start with a CAD model and through optimized 3rd party software can quickly develop laser workstation machining code to produce a part.

3.3.5.2 Beryllium and CH Capsule Hole Drilling

The LMM Center has continued to perform high aspect ratio hole drilling in both beryllium capsules, utilizing our patented double pulse format laser processing1, and in CH capsules utilizing our AVIA 266 nm wavelength system. See Fig. 3-16 for recent drilling results to produce NIC fill tube attachment holes. In addition, we have employed several other laser processing techniques to produce a variety of holes in capsules including employment of a trepanning system to effect hole taper, sacrificial foils to mitigate surface recast, and optimized the hole drilling process with multistep shot sequences to effect hole profile.

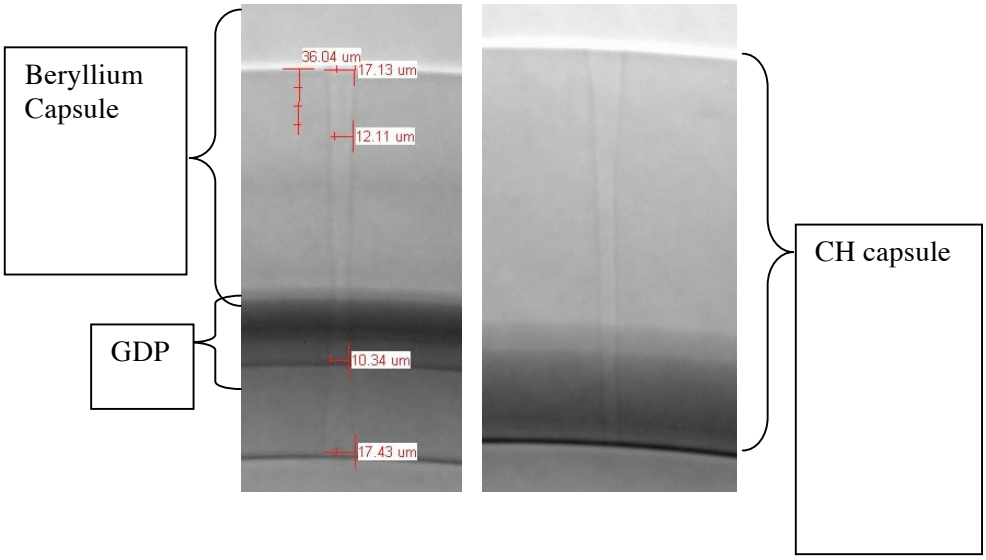

Fig. 3-16. Recent Be and CH hole drilling results. The CH capsule has 17.4 μm entrance and 6.0 μm exit hole diameter.

We have in the past produced a variety of laser drilled holes in Be capsules: thru-holes ranging in diameters from ~5-50 μm for pyrolysis tests, counter-bore fill tube holes for capsule fill tube attachment testing, and funnel shaped fill tube holes that are at or near NIC ignition design specifications, see Fig. 3-17 for a sample of hole cross sections we have fabricated.

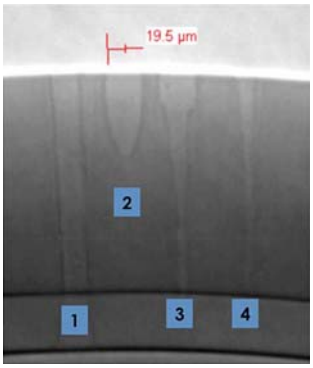

Fig. 3-17. 1) Thru hole, 2) Blind hole, 3) Counterbore, 4) Funnel.

3.3.6 Capsule and Capsule Fill Tube Assembly Deliveries

We delivered more than 112 ablator components in support of ignition for the NIC. The components are part of the capsule, capsule fill tube assemblies and machined capsules.

A good working relationship with LLNL and dedicated equipment has allowed for quick turn around of part requests as a result of design changes or the need for test parts. With continuous component fabrication improvements and the capsule design maturing the center

is evolving into a production facility that will be able to produce hundreds of components per year to ensure success of the NIF.

During FY10 several types of CFTAs were made including; Scale 0.7, Scale 0.9 SymCap, Scale 0.9 IgLT, Scale 0.9 ConvAbl, Scale 1.07 SymCap, Scale 1.07 KeyHole, Scale 1.07 4th Rise, and Scale 1.07 Re-Emit.

Collaboration between GA and LLNL resulted in the successful completion of many DOE Milestones. The list of milestones are as follows – 1) a successful assembly of a THD layered target, 2) a successful assembly of a 4th rise shock tuning target, 3) a successful assembly of a convergent ablator target and 4) a successful assembly of a Re-emit target.

In addition, the CCP Center assisted in providing 2 mm diameter Hoppe glass capsules that were produced and individually permeation tested for use in NIF Exploding Pushers experiments. Capsules were DT filled at LLE as discussed in Section 4.1.6.

3.3.7 Onsite Deliveries

The cryogenic target assembly group produced targets used for various development tasks and used in experiments on the NIF. In FY10, this team produced 65 different targets. This work is done in a 3000 square foot Class 100 cleanroom at LLNL. GA personnel participate in each stage of the assembly process. The work is managed by LLNL staff and is in support of the National Ignition Campaign. These targets were used for Ignition Layering, Re-Emit, SymCap, Convergent Ablator, ITPS, and Shock Commissioning experiments.

3.4 NLUF Deliveries

During FY10 the IFT team continued to fabricate components and assemblies and full targets for the second year of the NLUF funding cycle. The La Jolla site supported 17 shot dates with 580 assemblies and or component deliveries. GA's onsite support staff at UR\LLE supported over 75% of the NLUF shots with target assembly, mounting, and/or final characterization. NLUF targets were fully assembled in most cases by the GA team. In addition, some minor assembly was completed at SNL by GA support staff. This assembly capability was replicated and demonstrated at GA's La Jolla site. Figure 3-18 depicts the range of components and assemblies requested for the FY10 NLUF experiments.

The complexity of the NLUF targets continued to increase after the FY09 campaigns as the PIs tweaked or redesigned their experiments and targets. Characterization continued to be a substantial portion of the fabrication and delivery process as investigators required not so much precise designs but knowledge of what the critical features were, with high confidence of the values reported.

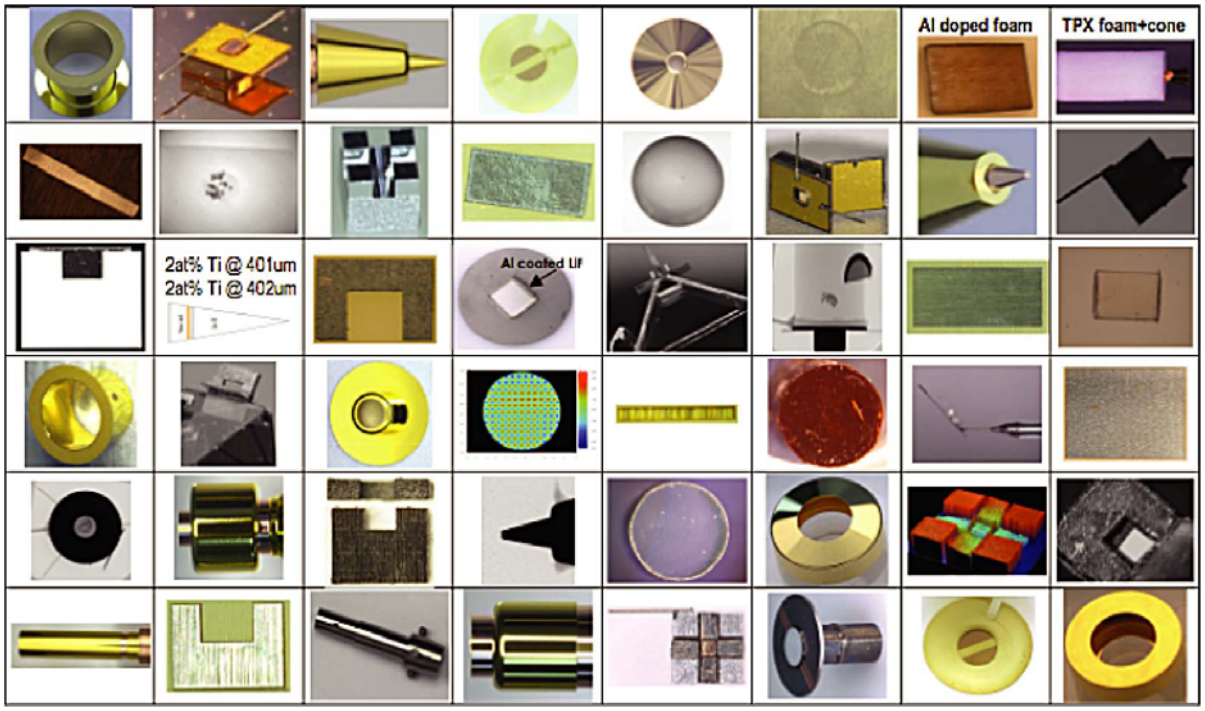

Fig. 3-18. Collage of components, assemblies, & metrology used in FY10 NLUF experiments.

Foam components were fabricated for the AstroShock, eXport, PRad-EP, and BCCMetals campaigns. Developmental efforts to match foam densities in an assembly was key to the astrophysical experiments so that the interior foam sphere was nominally the same density, allowing just the perturbations of the 0.1 mm ruby spheres to be studied. For the eXport campaign, electron transport targets were fabricated with 15 wt% aluminum oxide dopant ($3.5x10^{20}$ atoms/cc). This represent a 3.5x increase in dopant level and required research into techniques to uniformly disperse this amount of aluminum oxide during the foam cure process. Several trials were necessary before an acceptable process was refined. The quick turn around between foam fabrication trials and metrology via contact radiography enabled multiple iterations in a short period of time. The key aspect here was the metrology and close collaboration with the PI and experimenter regarding the metrology technique, the resulting data, and interpretation of the results. GA also used the history with these targets to expedite and improve assembly techniques. Improvements in the laser cutting of the Au shields improved assembly time.

PRad-EP experiments required a gold cone embedded into a TPX foam cylinder. Two key criteria were 1) good foam to cone contact at the tip. And 2) minimal density perturbation due to a) the insertion of the cone and b) wicking of the glue into the open cell foam. GA leveraged the Fast Ignition cone design to aid the assembly. The step in the cone increased surface area for the glue and cone to interact prior to foam penetration, minimizing glue wicking to the cone tip. A lesson learned after target shipment was the need for a supporting fiber on the underside of the foam to prevent the foam "sagging" under its own weight in this highly cantilevered design. This only became apparent once the target was mounted to the stalk at UR/LLE. Again the close communication of the NLUF assembler at UR/LLE, GA

and the PI enabled a workable solution to be determined and implemented in time for the shot day.

GA continued to fabricate a set of novel targets for the PRad campaign consisting of gold and silver disks with radiating holmium and dysprosium wires embedded into the surface of an aluminum block. Precision package assembly has also become part of GA's repertoire as demonstrated in the BCC Metals targets, again where critical Metrology was a key deliverable. This capability is being leveraged by other campaigns outside of the NLUF experiments. Capsule deliveries to NLUF experiments consisted of GDP capsules with a titanium doped inner layer for Core Imaging, and polymer capsules and spheres for Proton Radiography. For Core imaging the metrology required to differentiate between 1 μm dopant layers was a critical requirement for the PI. GA scientists evaluated and implemented an ion exchange process which increases gas retention in drop tower glass shells commonly used as backlighters, thereby improving the yield of the Drop Tower Glass process. These shells have been used successfully in multiple campaigns, including PRad, in FY10.

GA staff members are co-investigators in several NLUF experiments, providing detailed target fabrication insight for the experimental designs and requirements, along with cost cutting measures, which still retain the physics value of the experiments. Where GA is not a co-investigator, this thorough understanding of the physics involved allows GA staff to propose target design modifications that improve or enable manufacturability without losing the physics value. All the above has led to an integrated, robust, and successful target fabrication for NLUF PIs as evidenced by their feedback on the targets and the process:

- Farhat Beg of UCSD commented on e-Xport targets, *"I am very much impressed with the target fabrication group at GA. They make complex targets for us with good accuracy. We appreciate it very much." Farhat went on to say, "(GA has) an excellent target fabrication team. Coordination has been very good. … (I am a) very satisfied customer."*
- Chikang Li of MIT included GA co-authors on his science paper on proton radiography and said, *"I am very satisfied with GA's responses whenever we need help. Frequent communication with GA really helps us and is greatly appreciated."*
- Roberto Mancini of University of Nevada, PI on Core Imaging remarked, *"I am very happy with the work that you and your team have been doing to support our experiments. Keep it up!"*
- Melissa Douglass of LANL commented on astroshock targets, *"I wanted to tell you how much I appreciate the efforts you put into these targets. I realize they are difficult to make, and am so impressed by the target fab at GA. You guys are amazing!"*
- Ray Smith of LLNL, studying Structural Phase Transformation Kinetics stated, *"Everything we have asked of GA for our NLUF campaigns has been delivered in a timely manner and has a high level of quality. As our understanding of the target physics has improved there has been a lot of flexibility shown to facilitate changes in the original request. This is very much appreciated. We look forward to our continued collaboration with GA with the goal of producing high quality Science."*

- Patrick Hartigan of Rice University, conducting Astrophysical research avowed, *"As PI of several NLUF research projects conducted at OMEGA over the past several years, I'd like to compliment the team at GA on the target manufacturing and support they have provided our team. During that time our astrophysical research has driven us to pursue several completely new target designs, each of which required extensive R&D to bring to fruition. Our studies of deflected supersonic jets required both precise alignment of the target components to create the jet, and precise positioning of the obstacle to study the hydrodynamics of the deflection. An equally challenging task was to manufacture a target that contained multiple clumps in such a way that the clumps were suspended in a matrix without touching. In all cases, GA was able to meet our frequent deadlines and has delivered quality targets for us. As a result we have been able to publish several papers on this research and have more in various stages of development. In our new NLUF program we will be exploring several designs to study Mach stems, and the support of GA frees us to consider options that would be impossible without their expertise in manufacturing."*

In addition, in FY10 the Center for Precision Manufacturing supported the University of Michigan on a NLUF sponsored experiment. The components made were the rippled packages used in the Super Nova Rayleigh Taylor (SNRT) type experiments. This experiment was shot for the first time using the OMEGA EP facility so the package was much thinner than the standard OMEGA rippled package. The thinner package required the development of a new technique to hold the package during machining to achieve the desired dimensions and tolerances.

We supported a number of NLUF experiments by providing 121 capsules of different varieties including: As mentioned above, GDP capsules with a titanium doped inner layer for Core Imaging, polymer capsules and spheres for Proton Radiography, and complex stacked assemblies with tantalum crystals for the ICE:BCC experiments. In addition the development of a process to improve the gas retention of drop tower glass shells has increased the availability of capsules with permeation rates in the appropriate range for backlighters for Proton Radiography.

4 NIF TARGET DEVELOPMENT

4.1 Indirect Drive Targets

4.1.1 NIF Capsule Fabrication and Metrology Development

In FY10, the focus of capsule fabrication development continued to be on germanium doped CH. Improvements were needed in the production mechanism of these components to fulfill the needs of the national laboratories for the NIC.

4.1.1.1 Update in NIF Capsule Production Mechanism

The current process for fabricating a CH:Ge-CFTA starts with a micro-encapsulation process to produce capsules made from poly-alpha-methyl styrene. The plastic mandrel gets coated with a crossed linked polymer called glow discharge polymer (GDP). The mandrel is then removed through pyrolysis. A 10 μm diameter hole is then laser-drilled through the capsule, into which a fill tube is attached with a uv-curing adhesive. Capsules are fully characterized using the following: phase shifting diffractive interferometry (PSDI), atomic force microscopy (AFM), contact radiography (CR), scanning electron microscopy (SEM), Xradia, energy dispersive x-rays (EDS), x-ray fluorescence (XRF), precision radiography and x-ray absorption spectroscopy. The characterization process flow can be seen in Fig. 4-1.

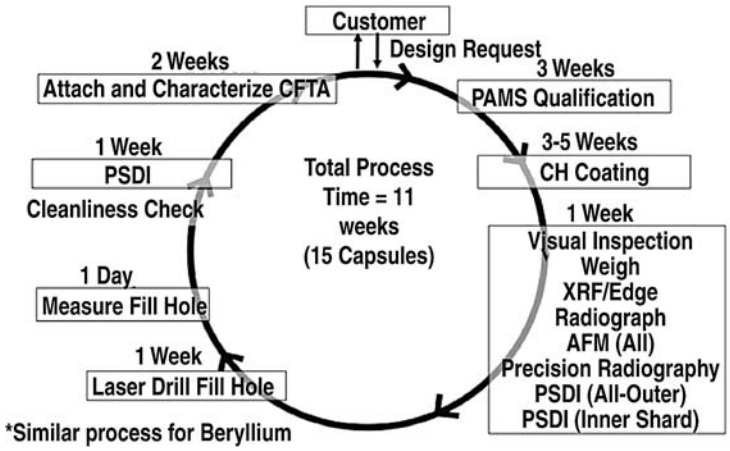

Fig. 4-1. Flow chart of NIF capsule production.

Changes to this process include performing the PSDI analysis (measuring the isolated defects) both before laser drilling and after laser drilling as compared to previously when it was only performed before laser drilling. Bright spots seen in implosions during early symmetry shots at NIF in fall 2009, indicated that isolated defects, such as domes or debris, may contribute to the observed features. Since the shell orientation was not recorded during assembly, it was difficult to match the bright spots with a particular defect. PSDI analysis was added as a final inspection step after the laser drilling and before attaching the fill tube to allow proper mapping in the final assembly, with the fill hole as a fiducial, and to potentially find any debris that was added to the capsule due to handling.

The coating process alone can take up to six weeks. Due to that coating rate, more coaters were required to maintain the production needs for the hohlraum energetics campaigns. Two additional coaters were added to the NIF-production coaters. Special steps were taken to qualify two new coaters to NIC standards. The steps include changing the agitation mechanism to a rolling technique, installing a fine mass-flow controller on the Ge inlet, and implementing a clean air hood over the coater to maintain cleanliness. Many coating runs were performed to validate the coating results before implementing the new coaters into NIC-production. The addition of these two coaters has produced a production rate of 30 capsules per month. This rate will help guarantee an adequate number of capsules for the ignition experiments.

4.1.1.2 Metrology Tools and Procedure Improvements

The specifications for the capsule fill tube assembly (CFTA) can be separated into two groups: capsule data and attachment data. The capsule data can be further defined in three sub areas: surface roughness data, dimensional data, and chemical composition data. The suite of tools that is used has not changed dramatically, but our understanding of the specifications and how to analyze the data has improved. The early hohlraum energetics campaign showed that the data that was produced from these tools needed to be further investigated by all parties (including the principal investigators and designers of the experiments) and a better understanding of the data was needed.

4.1.1.2.1 Surface Roughness Data Reporting Improvements

The surface roughness of each capsule is measured using an atomic force microscope (AFM) and a phase shifting diffraction interferometer (PSDI). These instruments are used together to fully characterize the surface: the AFM is used to measure the shape of the capsule (low mode roughness) where the PSDI is used to measure the isolated defects (high mode roughness). The way that the data from these two measurement techniques is analyzed has changed since previous publications.

The first important modification was that modal groupings were set for the AFM data. This was achieved through communication between the primary designers and the target fabrication team. The root mean square roughness of four different mode groups (modes 2–6, 7–12, 13–25, 26–150) are averaged together and compared to the NIF surface specification to obtain a factor for each mode group (Fig. 4-2). This improvement to the data analysis has allowed for more straightforward communication between the target fabricators and the primary investigators on the NIF experiments. It became obvious that the quality of the capsule shape needed to be represented in a few numbers that could be used to rank the capsule for experiments. More than one group was necessary because the importance of different modes needed to be weighed when deciding which capsule to move forward with. It was also important to allow a capsule that may have a large spike in one mode to not be removed from production as the other modes could improve the quality.

As mentioned above, in the early hohlraum energetics campaign, bright spots were observed in the GXD during the implosions that indicated some of the Ge was getting into

the core during the implosion. The Ge getting into the core during the implosion is a means for cooling the central core and quenching the fusion reactions and minimizing the yield. This unexpected observation was linked to possibly isolated defects. Isolated defects could mean large domes formed during coating or dust that collects on the capsule surface during handling. The isolated defect specification that existed before the early hohlraum energetics campaign was tightened by an order of magnitude as a result of the Ge penetration. Defects that were originally acceptable now drive the capsule out of specification. The yield took a major hit from 100% of capsules meeting the isolated defect specification to only 20% of the capsules meeting the specification. This yield hit also showed the importance of having more coaters to allow sufficient capacity to meet the demand of capsules for NIF.

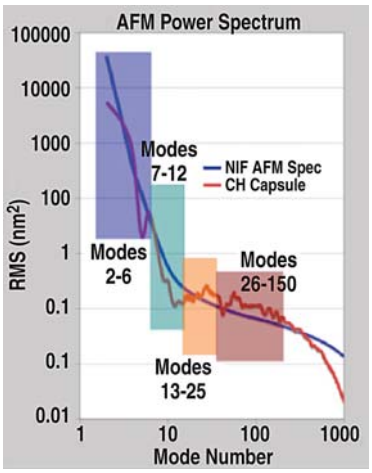

Fig. 4-2. AFM data is now grouped into several mode bands to determine quality of shell using fewer parameters than the full 1000 modes.

An investigation into the cleanliness of the CFTA production process resulted in substantial improvement to the number of isolated defects. One of the most significant changes is that all production steps for the CFTA now take place in a class 1,000 clean room or better. Also a new metric was developed by LLNL and implemented to verify the quality of the capsule surface. This figure of merit rolls up the AFM data and the PSDI data. It is called the expected ignition threshold factor for the surface. Also a 2D map of the isolated defects was developed to allow proper mapping when building the final assembly at LLNL.

4.1.1.2.2 Dimensional Data Improvements

Outer diameter, wall thickness and layer thicknesses are measured using a film-based contact radiography system. A recent design change to the capsule resulted in the first two layers of the ignition capsule being 5 μm thick. These layers are too thin to resolve in standard film processing due to phase contrast effects. A secondary means of measuring these layers was developed. A sample from each batch is measured using scanning electron microscopy (SEM) to determine the layer thicknesses. No yield change was observed. The error in the coating rate has never been greater than 20% causing only a 1 μm possible error in the 5 μm layer which is within the 2 μm specification).

The fill hole dimensional measurement has also changed. We now measure the hole in two orthogonal views to account for any ellipticity. Now both major and minor axes of the hole are captured. This allows confidence in the ability to fit a 10 μm fill tube in the hole.

4.1.1.2.3 Dopant Characterization Improvements

The atomic percent of the dopant in each layer is measured through contact radiography – gray scale analysis. In the past, a complex simulation was used to verify the absorption profile of the capsule and then calculate the amount of absorption due to the dopant. This process has been automated. The average process time has gone from 2 hr/capsule to 15 min. This has allowed analysis of every capsule in a batch as opposed to just a batch statistic. This improves the data accuracy on every capsule.

It also became apparent that variations in the exposure amounts varied depending on the placement of the sample on the film plate. A standard is now placed near every production sample to remove this variation. With this correction, the error on the atomic percent of the dopant went from 20% to 3%.

4.1.1.2.4 Improvements in Meeting Fill Tube Attachment Requirements

Once the capsule is fully characterized and laser drilled, a fill tube is attached to the laser-drilled hole with a minimal amount of glue (Fig. 4-3). The amount of glue allowed on the fill tube to capsule joint is specified to be <2.5 ng (Fig. 4-3B). The procedure has been to use a 10 μm diameter dispensing tip to apply the glue. This has resulted in a 20% yield. With a larger dispensing tip it is impossible (due to physical interference) to get close enough to the fill tube to minimize the amount of glue that wicks around the fill tube. The dispensing tip was modified to a 5 μm diameter tip and a yield of 95% was observed.

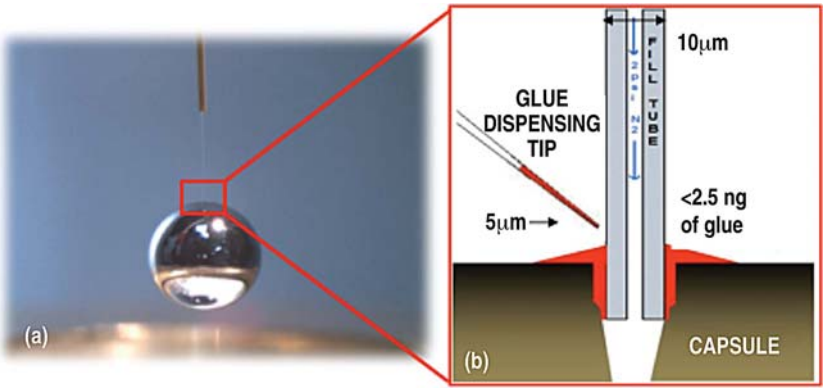

Fig. 4-3. A– Optical image of a capsule attached to a fill tube; B– Cartoon representation of dispensing the glue to create joint

The rate of fabrication has also improved. On average the rate has increased to two CFTAs per day when only a year ago it was one CFTA per day. A second CFTA station has been made to facilitate an even higher throughput for the expected NIF shot plan. This additional station will facilitate an increase of the production rate to 4 CFTAs a day. Also a more robust cradle design has been made to improve cleanliness and handling failures. The

biggest changes in the cradle design are removing any screw. The screwing process could produce dust/debris from the grinding of screwing in and out. Also there is no longer a loop of the transition tube that posed issues for the final assembly team when trying to remove the CFTA from the cradle. In many instances the capsule would be jarred greatly when releasing the loop of the transition tube resulting in the capsule falling off of the fill tube.

4.1.2 Hohlraum Development and Fabrication

Development in FY10 was focused on increasing output and yield of Depleted Uranium (DU) hohlraums. NIF shots are still on hold for DU hohlraums as the proper controls and safe guards are being implemented to handle radioactive material. Furthermore, GA has invested internally to improve the uranium coating and production facilities to allow increase of production output to allow bringing a third DU coater online in early FY11 to further respond to the anticipated short lead time demands for NIF shots. The DU hohlraum fabrication process is a nine-step process outlined in Fig. 4-4. Hohlraums as shown in Fig. 4-4 are made in two parts, i.e. two hohlraum halves or half hohlraums. The NIF Hohlraum Center has shown the successful fabrication of DU half hohlraums for all NIF target designs and has started preliminary R&D for FY11 to further increase control over the process.

In FY10 developments were made to increase output, improve the process and gain further control over the process. Improvements regarding increased coater capacity, decreasing equipment related issues, adhesion of uranium coatings to mandrels for higher yield, surface finish, automation of data recording and reconfirmation of environmental results are discussed below.

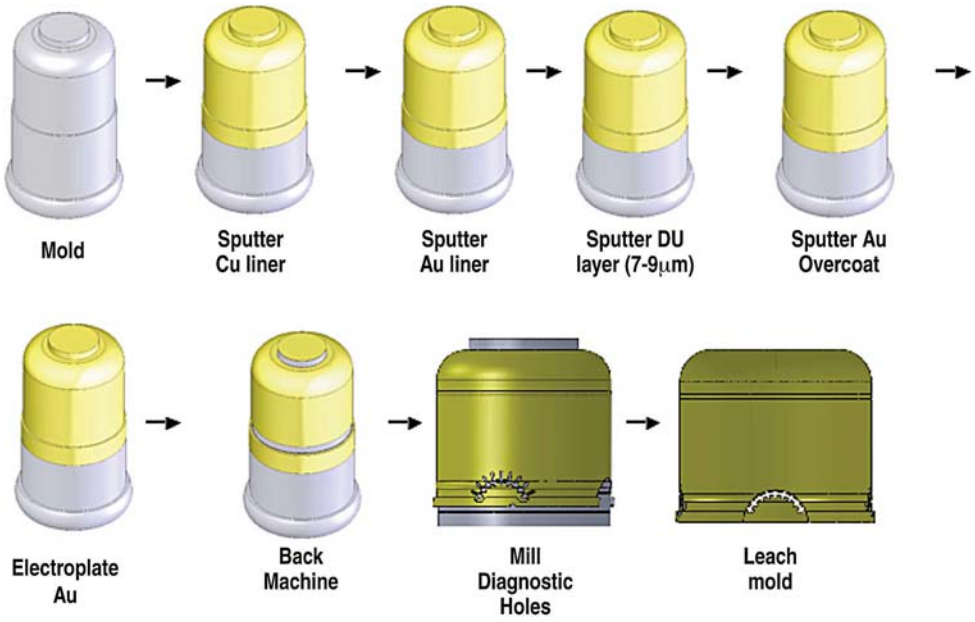

Fig. 4-4. Uranium Hohlraum Process

During FY09 the DU coating operation was still mostly in the R&D phase. Each coater had the capacity to generate two parts per run. In FY10, there was a major effort to increase

the capacity of each coater. Currently, in the production setup, there is capacity for five parts per run. This gives an output of up to twenty DU half hohlraums per week, as compared to a maximum of ten parts per week, a two-fold increase to allow supplying parts for nearly 5-10 shots per week at a fabrication yield of 25-50%. To further increase our yield (~ 10-20% previously), many improvements were made to equipment as well.

The major fabrication yield hit for FY09 was due to equipment malfunction. On a regular basis parts would fail due to rotation issues, poor electrical contact, and shorting of bias rings. Through preventative maintenance, discovery and minimization of problem areas where electrical shorts were most common, equipment failure has dropped considerably (Fig. 4-5). After reducing equipment failures substantially the next challenge was to identify the failure point for an issue related to the DU coating itself, i.e. de-lamination from the mandrel.

De-lamination is an issue that is problematic for DU half hohlraums as it exposes the DU to oxygen and increases the oxide layer. After investigation and analysis of the data it was shown (Fig. 4-6) that the adhesion of the Cu liner used in the process was poor in one of the deposition systems used for that step compared to the other. Utilizing the better of the two deposition systems we could ensure that the Cu liner was well adhered and the setup was duplicated to allow for a secondary system to be on-hand for increased demand capabilities. Improvement of this process aspect improved adhesion of coatings to the mandrels. This allowed improvement of the outside surfaces of the half hohlraum and pointed the way towards reducing mechanical failures at the back machine step.

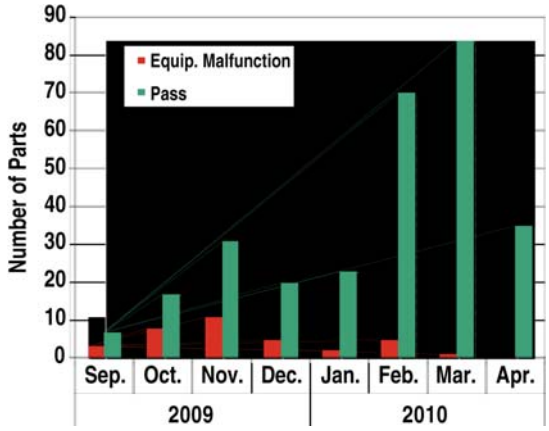

Fig. 4-5. Equipment failures were an issue in early FY10, accounting for almost 30% of failures and were remedied in April FY10

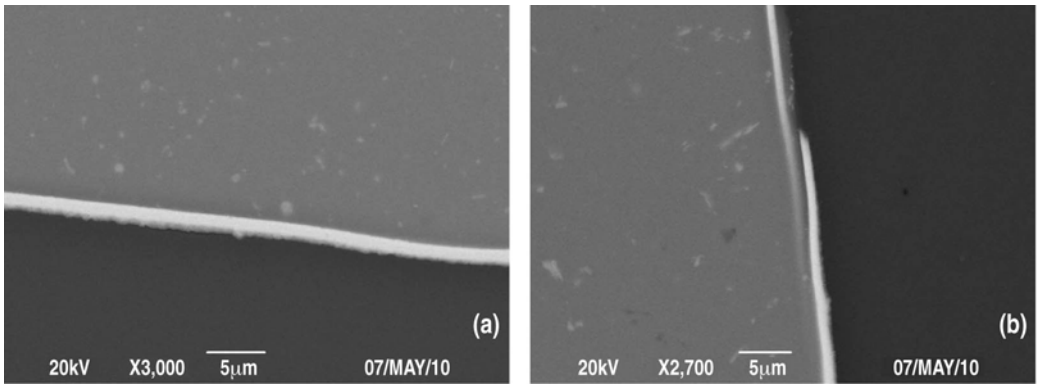

Fig. 4-6. (A) Cu layer from the production deposition system. The cu liner is fully intact with no gaps. (B) Cu layer from secondary deposition system (before modification). Gap at the interface between Al stock and Cu layer.

The back machine step, required to cut hohlraum length and flanges to shape, was normally only done on the flange surface and the Laser Entrance Hole (LEH) surface. This resulted in a very rough and uneven surface on the exterior of the hohlraum, which could cause issues when inserting the hohlraum into the Al can [Fig. 4-7(a)]. The improved adhesion allowed implementation of a full back machining of the entire hohlraum outer surface as is usually done for gold parts, removing nodules on the hohlraum barrel associated with the plating process on the usually rough DU coated surface [Fig. 4-7(b)]. This allowed consistent insertion of the hohlraum halves into the TMP cans without any obstruction. However this change exacerbated the exposure of DU on the top LEH surface (Fig. 4-8). After performing SEM cross section analysis it was determined that the DU thickness in this area is approximately three times the thickness of our measured DU thickness on the barrel [Fig. 4-9(a)] as expected given the required coating geometry for DU deposition. Therefore, in full back machining the hohlraum half to the required 30 μm thickness a DU coating of > 10 μm would result in a coating > 30 μm in the LEH area causing an exposure upon back machining. Limiting and controlling our coating thickness to 7-10 μm alleviated this issue (Fig. 4-9b).

We also added new equipment to catch potential failures. Both current DU deposition systems now utilize integrated real time data capture. This improvement allows us to identify potential failed parts well before the leach process (where the final yield is determined) saving valuable production time that would otherwise be wasted on a failed part. The data capture also allows for analysis of potential differences between gun and part positions, which can then be remedied to ensure the half hohlraum product is consistent from part to part.

The environmental storage of DU hohlraums was reestablished this year. If the Au liner is intact the oxygen content is well below the NIF standard. Oxygen is detrimental to NIF experiments as it decreases energy gain from the DU layer. DU half hohlraums have a survivability of up to 5 months with the oxygen percentage and structural integrity intact (Fig. 4-10).

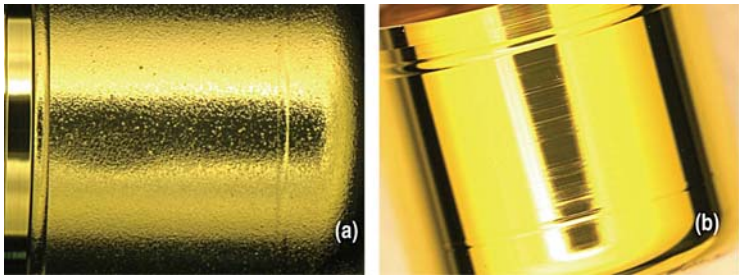

Fig. 4-7. (A) DU half hohlraum with nodules that can impede insertion in TMP (B) DU half hohlraum clean of nodules using full back machine possible with improved adhesion of coating to mandrel.

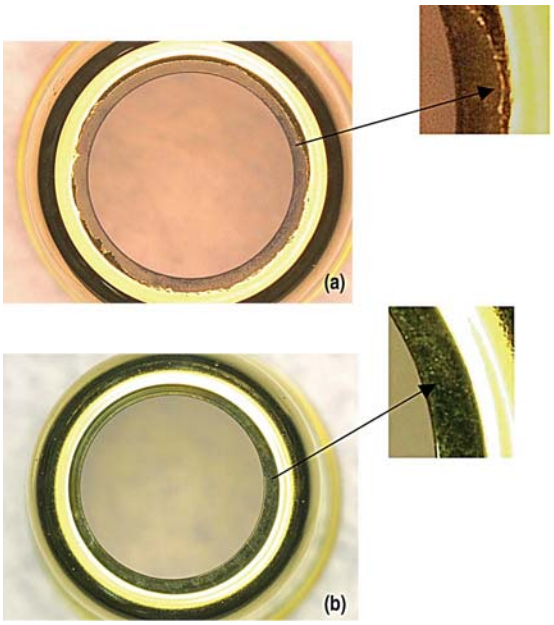

Fig. 4-8. (A) DU Half hohlraum with exposed LEH, DU thickness >10 μm (B) DU Half hohlraum with pristine LEH, DU thickness 7-9μm.

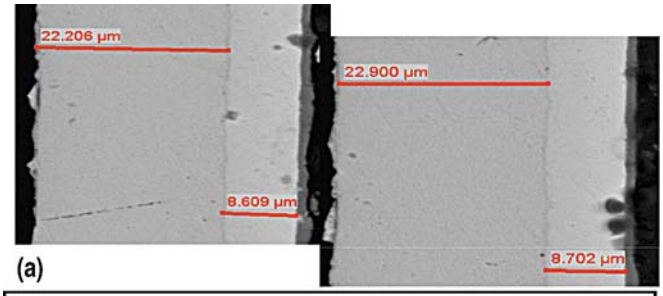

Part Number	Avg Thickness SEM (Micron)	Expected Thickness Z-Mike (Microns)	Difference (Microns)	% Change
14073	9.25	8.57	0.68	7.93465578
14151	6.6	7.1	-0.5	-7.04225352
14144	8.5	8.56	-0.06	-0.70093458

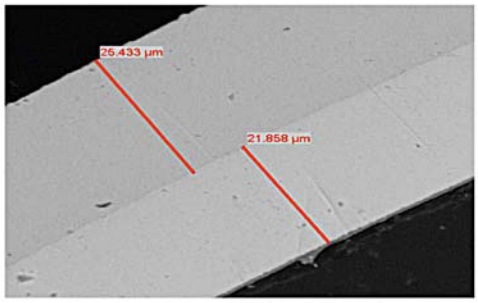

Part Number	Radius/LEH Avg	Radius to Barrel Difference	% Change
14073	25.175	15.925	185.822637
14151	18.39	11.79	166.056338
14144	19.459	10.959	128.025701

Fig. 4-9. (A) SEM images of DU half hohlraum. Shows barrel thickness over three different parts (B) DU Half hohlraum SEM image of the LEH radius, thickness can be up to 185% greater than the measured barrel thickness.

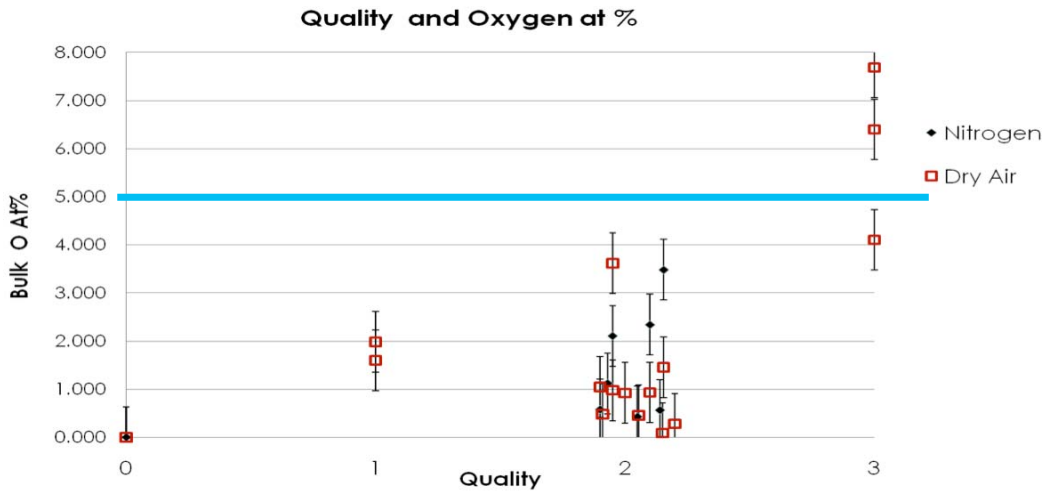

Fig. 4-10. The Oxygen percentage is below NIF spec for all parts with the Au liner intact (0-1 Quality), and can go above the NIF spec when the Au liner is compromised (Quality 3)

The Hohlraum Center in conjunction with CPM and LLM center has successfully milled all NIF designs including the most complex THD Starburst design (Fig. 4-11). By the end of FY11 the Hohlraum Center will have three DU deposition systems, which will enable full support to NIF for DU hohlraum demand.

Preliminary R&D efforts for FY11 has shown that depositing half of the Au liner in the same deposition process as the Cu liner will improve yield as well as give better control over the Au liner thickness by utilizing QCM technology. Other R&D efforts for FY11 will include control and measurement of the Au liner to ± 0.05 μm.

A

B

Fig. 4-11. (A) DU Half hohlraum with THD starburst window cut by LLM. (B) Half hohlraum with THD window cut by CPM.

4.1.3 Cryogenic Target Systems

General Atomics personnel assigned onsite at LLNL are participating in the assembly, test and commissioning of the NIF Cryogenic Target System (CTS). This work was performed under the direction and management of LLNL staff, and is part of the National Ignition Campaign (NIC).

The CTS team focused on three distinct tasks during FY10. The first task was to support and upgrade the cryogenic target capability of the existing NIF target positioner (TARPOS). The second task was to develop an off-line test facility to allow the proofing of ignition targets before they are installed in NIF. The third task was to continue the fabrication, assembly, installation and test of hardware required to field ignition targets on the NIF laser.

4.1.3.1 Target Positioner (TARPOS)

The original NIF target positioner is referred to as the TARPOS. During FY09, the CTS group added the Ignition Target Inserter Cryostat (I-TIC) to the TARPOS to allow the fielding of cryogenic targets. The I-TIC, shown in Fig. 4-12, is designed to cool targets to cryogenic temperature and deliver them to the focus of the 192 laser beams. The I-TIC is designed to be used on either the TARPOS or the new cryogenic target positioner (CryoTARPOS).

The CTS effort early in FY10 was highlighted by the fielding of ignition-scale targets at the center of the NIF Target Chamber. The targets were cooled to temperatures as low as 20 K and the targets shot at laser energies up to 1.1 MJ.

In late FY10, the CTS group upgraded the cryogenic shrouds for the upcoming keyhole target campaign. These targets include a large cone that extends out from the hohlraum wall. To maintain the cryogenic temperature of the target and to limit condensation, a unique shroud design was required. The keyhole shrouds have been fully assembled with temperature sensors, heaters and windows and have been installed on the I-TIC.

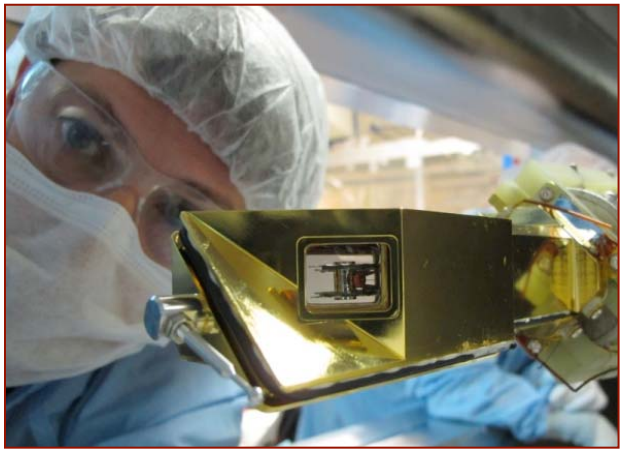

Fig. 4-12. Inspection of a target encased in the I-TIC shroud.

4.1.3.2 Ignition Target Proofing Station (ITPS)

The second major task for FY10 was to develop an off-line test facility to allow the proofing of ignition targets before they are installed in NIF. This system, called the Ignition Target Proofing Station (ITPS), is designed to cool an ignition target down to cryogenic temperature, fill it with hydrogen isotope fuel, layer the fuel and take x-ray images of the frozen layer.

In early FY10, CTS received and assembled the Ignition Target Proofing Station major components and integrated them with the control system and tritium system plumbing. Next, commissioning tests of the ITPS x-ray imaging system was begun. This system consists of three axes of microfocus x-ray sources, charge-coupled device (CCD) cameras, shutters and shielding components.

The CTS team next installed the Ignition Target Proofing Station helium compressor skid in preparation for cryogenic acceptance tests and demonstrated that the cryogenic system meets all thermal performance specifications. The target gripper was cooled down to 6 K and the cold shield to 45 K, meeting performance specifications.

The initial fielding of a NIF target on the ITPS was first done in April 2010. This effort involved cooling the target down to cryogenic temperature (~20K) and filling the capsule with isotopes of hydrogen gas. The target was then imaged in three orthogonal axes using the ITPS phase contrast X-ray imaging system. The ITPS, shown in Fig. 4-13, has been fully commissioned and turned over to the Target Layering Group and is now routinely used to proof ignition targets.

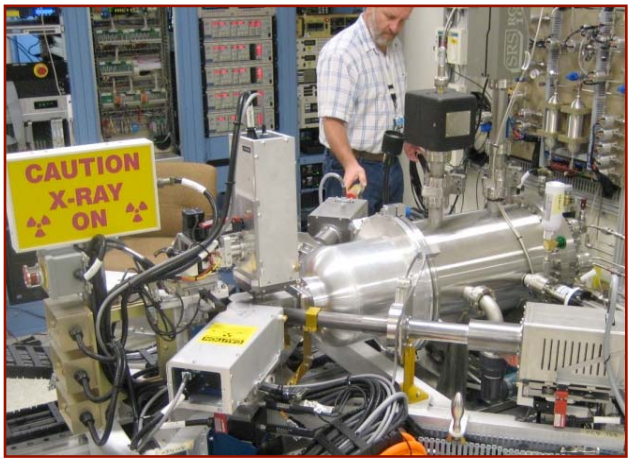

Fig. 4-13. The Ignition Target Proofing Station is fully operational.

4.1.3.3 CryoTARPOS

The third major area of focus during FY10 was the continued development of the NIF Cryogenic Target Positioner (CryoTARPOS). This device includes an x-ray imaging system and contamination control to allow the fielding of layered ignition targets on NIF. The CryoTARPOS was first assembled and tested in the off-line Integrated Test Facility before being moved into the NIF Facility.

During the first quarter of FY10, the CTS team focused on final assembly and test of the CryoTARPOS. These efforts included integration of the I-TIC with the CryoTARPOS, initial x-ray operation, demonstration of the contamination control ventilation system, and operation of the target positioning system.

The tasks complete during the second quarter of FY10 included getting the NIF Facility ready to receive the CryoTARPOS. The large structural stand that supports the CryoTARPOS vessel was installed in the NIF Target Bay. Other modifications required in the Target Bay included the installation of utilities, such as electrical, compressed air, vacuum, controls, and ventilation systems.

Late in the second quarter, the CryoTARPOS vessel was mated to a custom sixteen-wheel cart that was used to transport it to the NIF Target Bay. The CTS effort in March was highlighted by moving the CryoTARPOS assembly from the CTS Integrated Test Facility to the NIF. The 20,000-lb CryoTARPOS was lifted by crane onto the second floor of the NIF Diagnostics Building and transported into the Target Bay, as shown in Fig. 4-14.

The tasks completed during the third quarter of FY10 included confirming the vacuum integrity of the CryoTARPOS vacuum vessel after its move to the NIF Target Bay. The CTS team then integrated the CryoTARPOS with the NIF Target Bay utilities, as shown in Fig. 4-15. Once the CryoTARPOS was operational, the CTS team began the process required to hand the equipment off to the NIF Operations Group. This process involved formal Initial Qualification and Operational Qualification tests. These tests were divided into functional areas and included the vacuum, positioning, ventilation, cryogenic and x-ray systems.

During the last quarter of FY10 the CTS team assisted in developing the CryoTARPOS into an operational device. The transporting and handling of targets filled with hazardous materials was successfully demonstrated. These tests included moving a mock target between test labs, the DT fill building and the NIF facility and installing the target in the CryoTARPOS vessel. Many NIF milestones were obtained over the summer including the first cooling of an ignition target to cryogenic temperatures, the first fill of hydrogen isotope fuel into a target, the first x-ray images of the hydrogen isotope ice layer. The year was closed out by the successful first laser shot of a NIF cryogenic ignition target with a symmetrical ice layer.

Fig. 4-14. The CryoTARPOS vessel being moved into the NIF Facility

Fig. 4-15. The CryoTARPOS installed in the NIF Target Bay

4.1.4 Aluminum Shield Development

During FY10 General Atomics developed a process and began routine deliveries of aluminum shields to LLNL (Fig. 4-16). The aluminum shields were required by designers at LLNL to mitigate problems with unconverted light reflecting off the silicon target arms. These shields were precisely cut, coated with plastic and aluminum, and dimpled into a 3 dimensional shape. LLNL began by producing the first simplified prototypes in house, but the need for a precise control of the plastic coating and sufficient manufacturing throughput for shots were issues. As a result, LLNL approached several vendors at the start of Q3/FY10 to demonstrate the capability to produce the targets. In the end, General Atomics was the only turn key supplier that could demonstrate every part of the fabrication process and successfully produce complete components. The speed at which GA was able to bring up the process was such that by the end of FY10 GA had shipped 200 units across 6 part numbers.

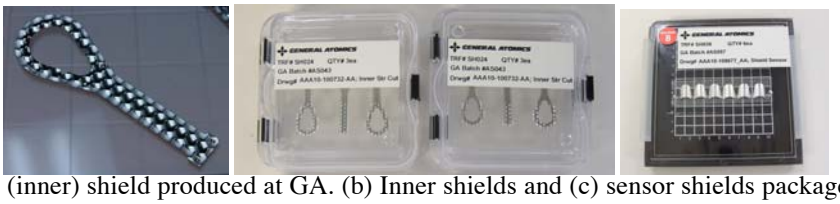

Fig. 4-16. (a) Al (inner) shield produced at GA. (b) Inner shields and (c) sensor shields packaged and ready for shipment.

GA (and other potential vendors) benefited from the initial development done at LLNL. Staff at LLNL had demonstrated a dimpling process with a machined mold and had been able to make simplified prototypes. The additional requirement of a precise 1 mm margin to the plastic coating (Fig. 4-17) was an issue, however. GA utilized its extensive capabilities to develop the process and do all the fabrication steps in house. This was a distinct advantage compared to other possible sources that would have required substantial post processing requiring the use of LLNL staff and resources.

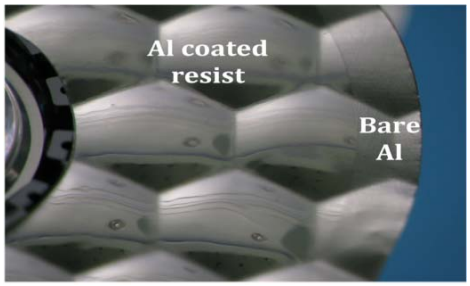

Fig. 4-17. A GA made shield in the initial stage of assembly at LLNL. The 1 mm bare Al margin (dull surface) can be seen next to the shiny Al coated resist.

We were quickly able to address the challenge of plastic deposition to produce a bare Al margin around the part (Fig. 4-17). Using photolithography, it was possible to precisely control which areas of the part were coated and which were left bare. Using inexpensive plastic photomasks on plastic film, we quickly prototyped parts to prove the principle and select the best photoresist. Different commercial photoresists were tested, and SU-8 3010 seemed to work best. This resist needed relatively short exposure times (good for high throughput), good adhesion to aluminum, and was stable at relatively high temperatures (good for Al coating). After the initial proof of principle stage, chrome on quartz masks were acquired with an accuracy of better than 1 μm. This resulted in improved edge quality, from 10-20 μm previously, to 1 μm.

Simply dimpling the resist-coated aluminum, however, produced problems with cracking and de-lamination of the plastic resist layer. We developed a heat pressing technique that softened the resist enough that it could be pressed into the dimpled shape as needed. Although this is well below the glass transition temperature of 200 deg C, the heat pressing made the resist pliable enough to eliminate cracking evident in the early lithographed prototypes.

During the development, we spent engineering time to refine the process to both reduce cost and maximize throughput. Cutting the shield blanks was accomplished at LLNL by both wire EDM and laser cutting. We demonstrated laser cutting with equipment in house, but quickly developed a die cutting routine to cut the parts. The die cutting process enabled GA to cut more parts, and make the process more cheaply scalable. By buying a few more inexpensive dies and extra pneumatic cutting presses, this part of the process can be scaled as needed if demand for the parts increases.

We were also able to scale up the process using a large capacity aluminum coater to coat the shields. The electron beam evaporative coater had difficulty at first getting coatings that strongly adhered to the resist. By using a plasma pretreatment step, adhesion was improved so that parts would survive without de-lamination of the aluminum.

In the end, we were able to produce prototypes quickly in Q3, and by Q4 we were making deliveries of target ready components. These parts are now standard, recurring deliveries integrated into the GA NIF ordering system and are continuing in FY11.

4.1.5 Metrology Uncertainty for Ablator Capsule Measurement

Delivering targets whose parameters are repeatable within specifications is critical to a successful ignition campaign. We developed a wide range of metrology instruments (Contact Radiography, Energy Dispersive Spectroscopy, X-ray Absorption Edge Spectroscopy, Precision Radiography System, Spheremapper, and Phase-Shifting Diffraction Interferometer, etc.) to measure capsule specifications in five broad categories: (1) Dimension (2) Composition (3) Homogeneity (4) Surface Finish (5) Point Defects. Knowing the repeatability of the metrology techniques and determining the random error bars is central in achieving this goal. For example, small error bars in the diameter measurement (Fig. 4-18 (a)) enable easy culling of production batches for sample delivery (Fig. 4-18(b)). Similarly, the wall thickness can be measured to a tight tolerance of ± 0.5 μm.

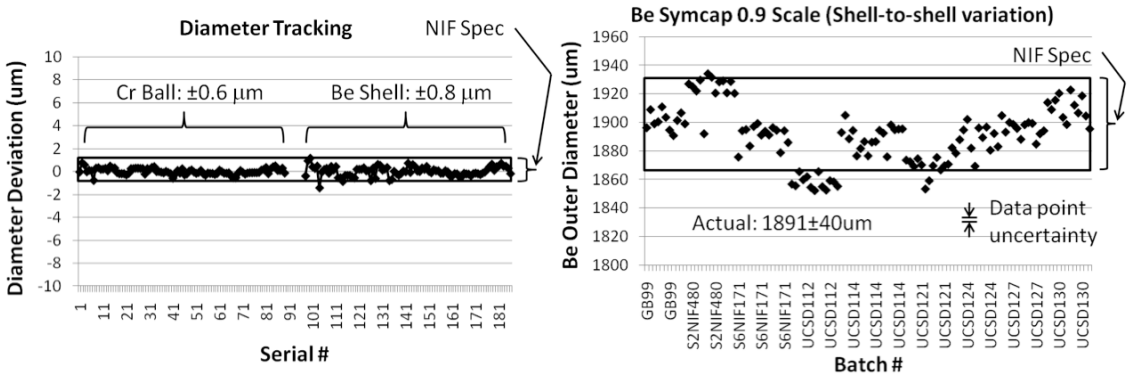

Fig. 4-18. (a) Contact radiography produces shell diameter measurements with sub-micron repeatability for a) a Cr steel ball and b) a beryllium shell. The entire plotted range represents the overall NIF diameter tolerance whereas the boxed area represents the required measurement precision. The measurement precision is slightly better than the specified measurement error of 1.0 μm, and a factor of 10 better than the allowed variability of ±10 μm. (b) SymCap (0.9 Scale) capsule diameter tracking. The boxed area indicates the NIF tolerance. Because the measurement error is smaller than the dots representing the data points, this graph can be used to select the good capsules.

Contact radiography is used to measure single dopant profile to a repeatability of ±0.05 at. % (Fig. 4-19), however, it is incapable of distinguishing multiple dopants such as Ar and Cu in a beryllium shell. We developed a Energy Dispersive Spectroscopy (EDS) method to measure multiple dopant profiles with a repeatability of ± 0.12 at. % on layers containing 1.0 at. % copper dopant (Table 4-1). Absorption Edge Spectroscopy (Edge) can be used to characterize overall dopant to ± 0.02 at. % without profiling capability.

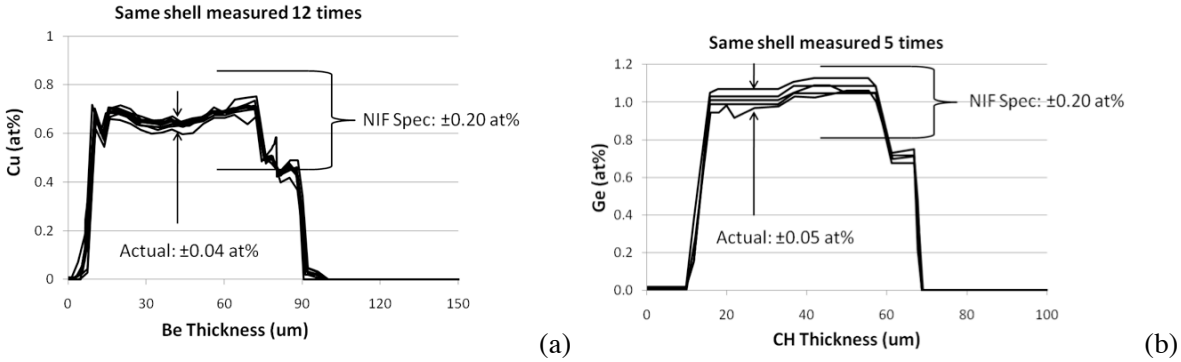

Fig. 4-19. Measurement repeatability for (a) Cu doped Be shell (b) Ge doped CH shell. The bracketed width is the overall NIF tolerance on shell variability whereas the required measurement precision is 2x tighter.

Table 4-1
EDS Statistics for Select Shells. Cu at. % Doping Levels for Layer #3 are Presented

Shell ID#	Cu (at%)	# Measured
UCSD111	1.18±0.13	68
UCSD113	1.10±0.14	17
UCSD123	1.13±0.10	11
S6NIF111	0.69±0.08	20
S6NIF168	1.53±0.18	10
GA223	0.64±0.09	6

Precision radiography (PR) is used to measure lateral inhomogeneity in a sample. Given time, the measurement can be infinitely precise as the noise floor goes down linearly with time (Fig. 4-20(a)), however, partial sampling of a shell surface could introduce ± 40% orientation-dependent variations. For beryllium shells, better statistics can be obtained by sampling the full shell surface with two orthogonal measurements. For CH shells, the x-ray exposure damages the chemical bonds, leading to an oxygen-absorption-induced x-ray opacity increase. This makes the measurement on a second orbit impossible. In practice, the measured power spectra are weighed against the computed NIF power spectrum based on surface and wall thickness roughness specification, and further reduced to a single Quality Control (QC) factor for pass-fail purpose [Fig. 4-21]. A QC factor above 1 means the shell on average has higher inhomogeneity than called for in the NIF specification. Large PR QC factor on CH capsules are caused by isolated defects, whose presence is adequately

characterized by PSDI. A polishing step is used to remove the localized defects. The underlying coating appears to be sufficiently homogenous to meet the NIF requirement.

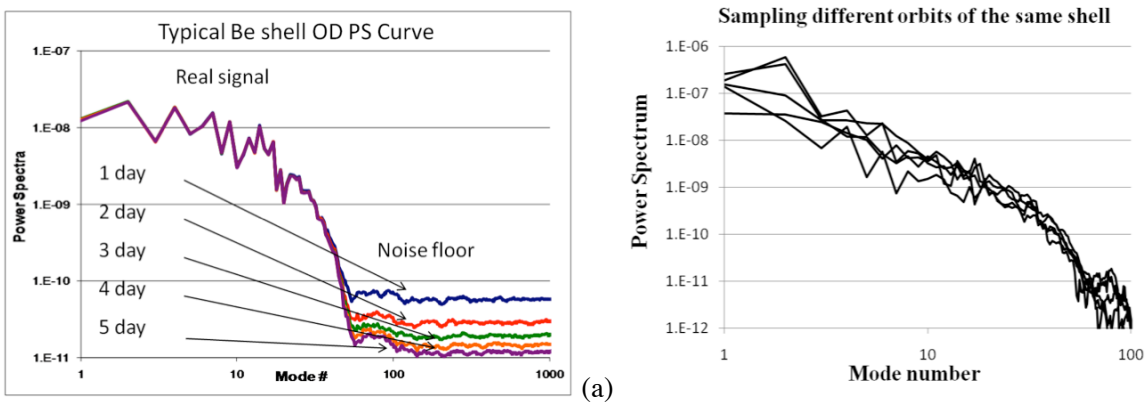

Fig. 4-20. (a) The noise floor of precision radiography measurement goes down linearly with time. (b) The detectors sample a 1mm wide band on a 2mm sample, the results are affected by the shell orientation. This incomplete coverage of a randomly oriented sample is the leading cause of measurement uncertainty.

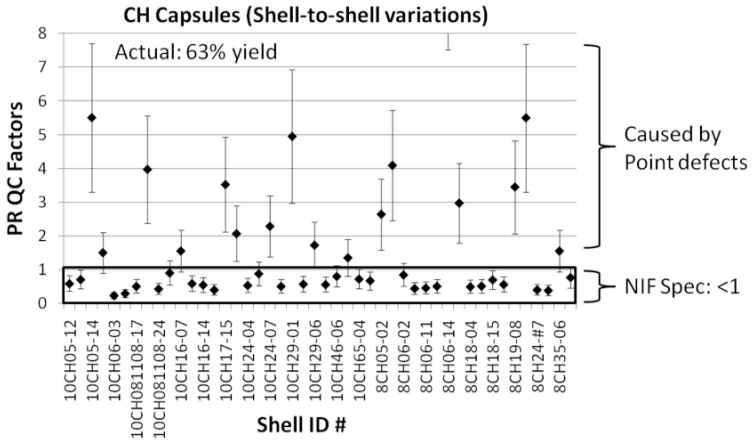

Fig. 4-21. Precision radiography power spectra are converted to a single Quality Control (QC) factor per shell for pass-fail purpose. The boxed area is the range allowed by the NIF specifications. Large QC factors are typically caused by isolated defects.

Surface shape is measured by a Spheremapper, an AFM adapted instrument to measure surface height variations. The accuracy of the height measurement is calibrated against the surface curvature of a known sphere (Fig. 4-22(a)) to ± 7% accuracy. Like precision radiography, the sampling error due to shell orientation dominates the error budget. Recently, a 19 orbit process was introduced to control the orientation dependence to ± 25% level.

Point defects are measured by a combination of Phase-Shifting Diffraction Interferometer (PSDI) and dust inspection microscope. This area is under rapid development. A summary of metrology capability for various instruments is found in table 4-2.

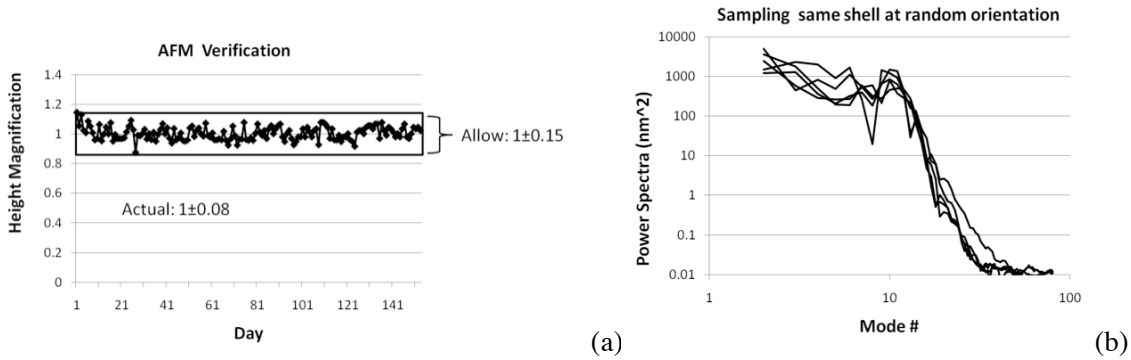

Fig. 4-22. (a) The surface curvature of a sphere with known radius is used to verify Spheremapper low-mode measurement on a daily basis (b) The metrology uncertainty is limited not by the intrinsic capability of the instrument, but rather, by the limited sampling of a shell with unknown orientation.

Table 4-2
Metrology tools and their measurement repeatability as compared to the NIF specifications.

Target Parameter	Method	Metrology (2-σ)	NIF Spec
Diameter	CR	±0.8 μm	±1 μm
Wall Thkn	CR	±0.5 μm	±1 μm
Ge Profile	CR	±0.05 at%	±0.1 at%
Ar, Cu Profiles	EDS	±0.12 at%	±0.1 at%
Average Ge, Ar, Cu	Edge	±0.02 at%	±0.03 at%
Homogeneity	PR	±0.40	<1
Surface figure	AFM	±0.50	<1
Point defects	PSDI	±0.20	<1

"Please note NIF specs can require much tighter measurement precisions than the overall allowed variations in the capsules. For example, for the shell diameter, the specs say ±10 μm is allowed. However, for a given shot, the diameter must be measured to a ±1 μm precision in order to understand the effect of diameter variation to the shot performance. The NIF specs listed in this table pertain to the required measurement precision."

4.1.6 High Aspect Ratio Hoppe Glass Capsules Development for NIF Diagnostics Experiments

Large (>1400 μm diameter) glass capsules are routinely used for neutron diagnostic development experiments for NIF as well as experiments studying mix in relatively high neutron yield shots. In particular, 1550 μm diameter by 4 μm wall glass shells were required for the early neutron diagnostic experiments (exploding pushers) on NIF. The SiGDP conversion process, commonly known as the Hoppe process, is currently the only route to manufacturing glass capsules of this size. The diameter and wall thickness range of glass capsules that have been successfully made using the SiGDP conversion method is shown in Fig. 4-23. The gray area depicts the range of shells made previously while the red stars represent the high aspect ratio glass shells recently made for the first diagnostic development shots on NIF. While the drop tower technique can produce shells in large quantities (hundreds to thousands per day) it can only make shells in the range of <1000 μm, with wall thicknesses of < 3 μm at that diameter. Of course, the yield of high quality drop tower shells is small (~ <10%) and requires much metrology. Hence, the Hoppe process is indeed needed for the exploding pusher experiments designed to generate neutrons to calibrate neutron diagnostic equipment of various sorts. However, the Hoppe process produces shells at a much slower rate of ~ 30 shells per batch, and one completed batch per ~ one month, however with multiple batches being processed at the same time every several days. But nonetheless, the production rate is much slower than the drop tower process. Hence, it is crucial that the yield of the process be sufficiently high to meet the shell demand for the neutron diagnostic experiments.

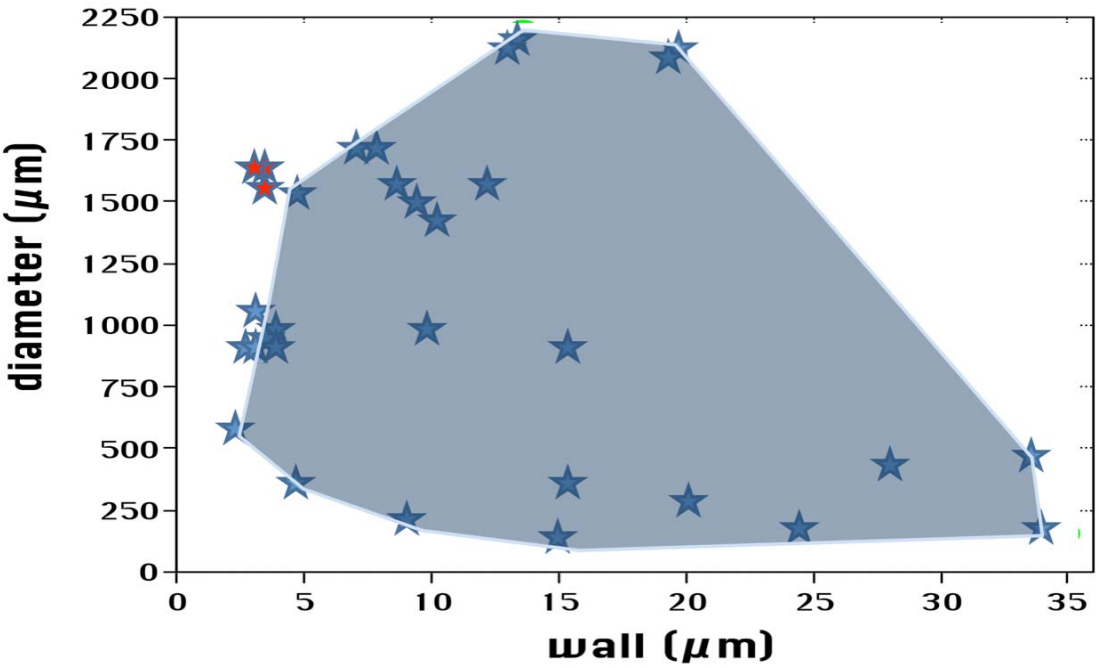

Fig. 4-23. Diameter and wall thickness range of glass capsules made by the SiGDP process.

The Hoppe process can suffer from wrinkling of shells and dimple formation in shells when large diameter glass shells are made. These dimple defects are thought to occur principally as a result of the shells staying motionless in their ceramic dishes during the long, high temperature conversion process. The silicon content of the doped GDP prior to conversion may also be critically important with respect to wrinkle formation since the lower the silicon content the more shrinkage that occurs during conversion. This issue is quite common for thin-walled glass shells (<5 μm) that were required for the NIF experiments and results in very low yields (<10%) of shells with absolutely no dimples or no wrinkling. Figure 4-24 shows common defects observed on these high aspect ratio glass capsules. However, the degree of wrinkling or dimples in these shells can vary over a large range also indicated in Fig. 4-25. Note that not all these high aspect ratio glass capsules have visible wrinkles or dents and optically look very good as shown in Fig. 4-25. However, even these shells still show some minor wrinkling when measured by more sensitive techniques such as spheremapping (Fig. 4-26) and compared to the ignition specifications for NIF. Nonetheless, the yield of shells with such shallow dimples is on the order of 50%, allowing a large enough inventory of shells to be made using the Hoppe process for the NIF neutron diagnostic shots if such features do not affect the neutron yield. Therefore, a representative set of shells were made for a series of OMEGA shots designed to study neutron yield sensitivity on the suggestion of target fabrication. The results showed excellent performance of the lightly dimpled/wrinkled shells which allowed the selection of such shells at NIF and increasing the fabrication yield over 5 fold.

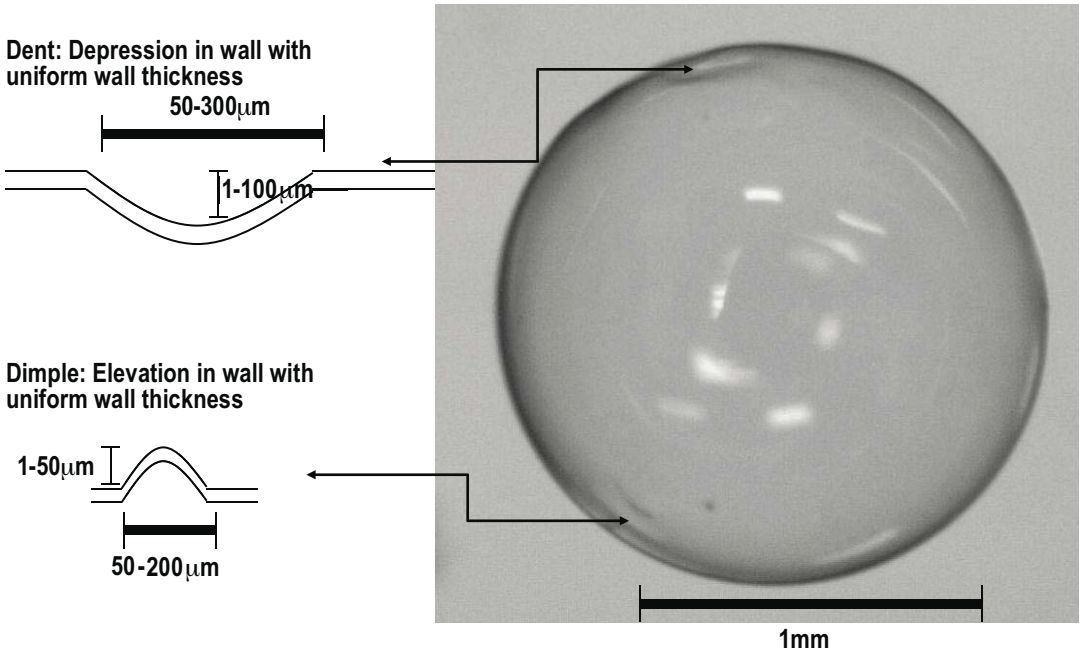

Fig. 4-24. Common defects observed on glass capsules.

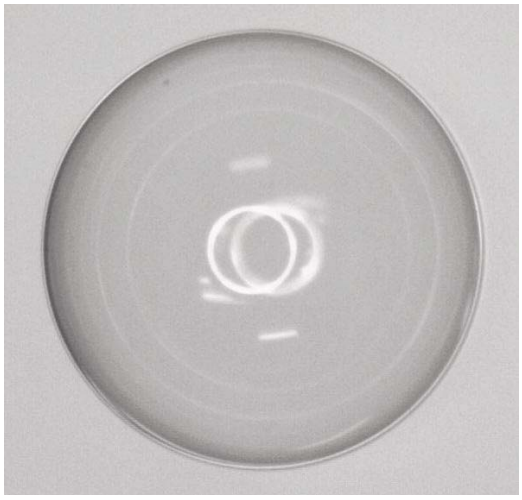

Fig. 4-25. Example of optically good quality glass shell (~1600x4μm).

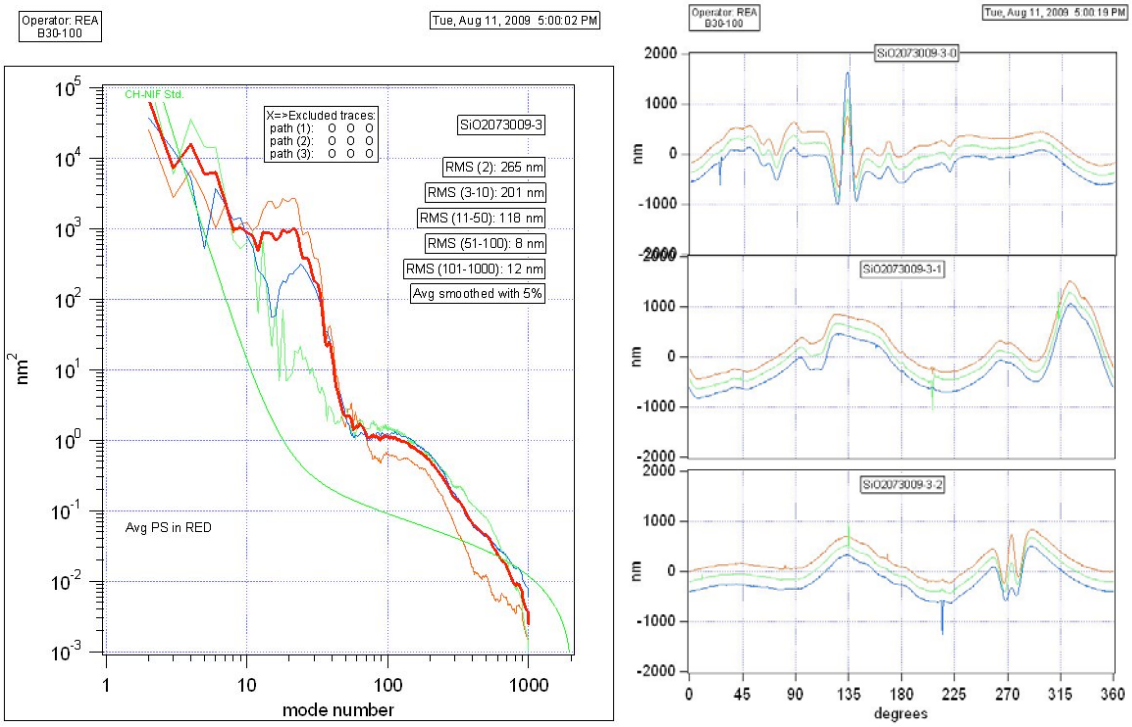

Fig. 4-26. Surface quality by spheremapping of one of the better large diameter glass capsules.

These types of Hoppe shells were used at NIF with neutron yields that were in phenomenal agreement with the calculations and they are planned to be used as a workhorse for experiments testing effects of neutrons on diagnostics as NIF facility neutron yield limits are increased.

4.1.7 Cu Diffusion in Beryllium and Mitigation

Beryllium capsules are produced by sputtering beryllium onto a plastic CH mandrel. The mandrel is then burned out in a high temperature pyrolysis process. The 425°C/48-hour pyrolysis process causes the beryllium to diffuse radially, which leads to a blurred copper interface that is shown as a grayscale contrast in Backscattered Electron (BSE) imaging (Fig. 4-27). Copper diffusion in sputtered beryllium exhibits two anomalous behaviors: (1) the length scale is ~15x longer than extrapolated from the bulk beryllium data (~3 μm vs. 0.2 μ m) and (2) the diffusion is highly heterogeneous, leading to plume-like extensions into the undoped region. Tilting the sample in SEM does not lead to any visible change in the pattern (Fig. 4-27(b)), proving the contrast is based on composition instead of crystalline orientation. More direct proof of compositional contrast can be obtained through Energy Dispersive Spectroscopy (EDS) where copper concentration is mapped using the characteristic Cu-L emission (Fig. 4-28). The typical azimuthal copper variation near the copper interface is ~± 0.06 at. %. As shown in Fig. (4-29), the copper profiles on the two sides of an interface are anti-phased, a strong indication that the compositional variations are due to copper diffusion in which the total amount of copper is conserved.

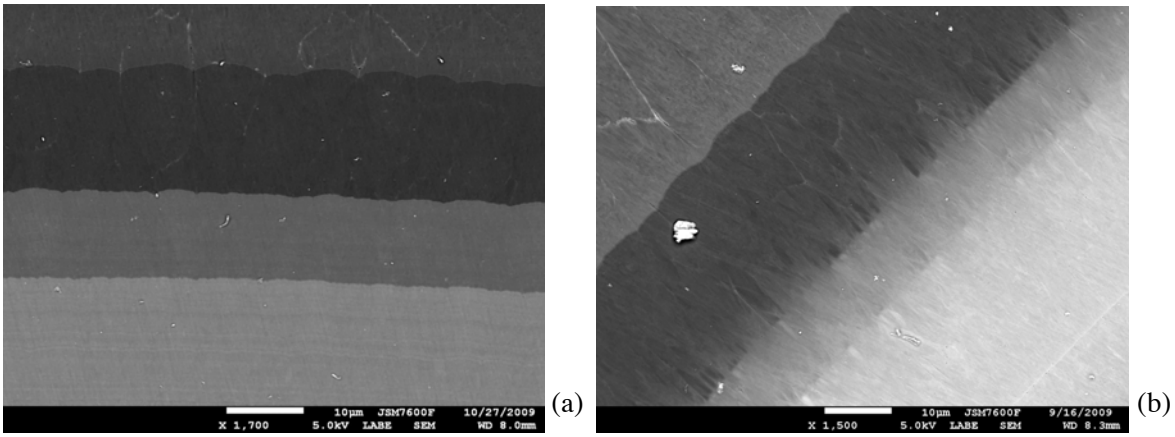

(a) (b)

Fig. 4-27. Backscattered electron (BSE) images of (a) pre-pyro (b) post-pyro sample cross-sections. The grayscale is modulated by the atomic Z contrast. Regions with higher dopant concentration increase the BSE production and therefore appear whiter. The pre-pyro copper interfaces are sharp, whereas the post-pyro interfaces are non-uniformly fuzzy due to inhomogeneous copper diffusion.

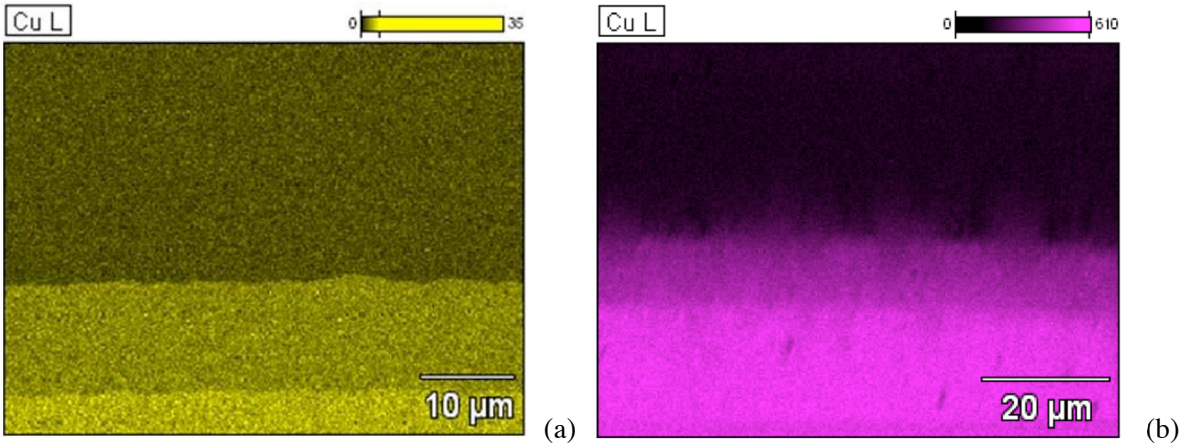

(a) (b)

Fig. 4-28. Copper element maps on (a) pre-pyro (b) post-pyro sample cross-sections. The pre-pyro copper interfaces are sharp, whereas the post-pyro interfaces are non-uniformly fuzzy due to copper diffusion.

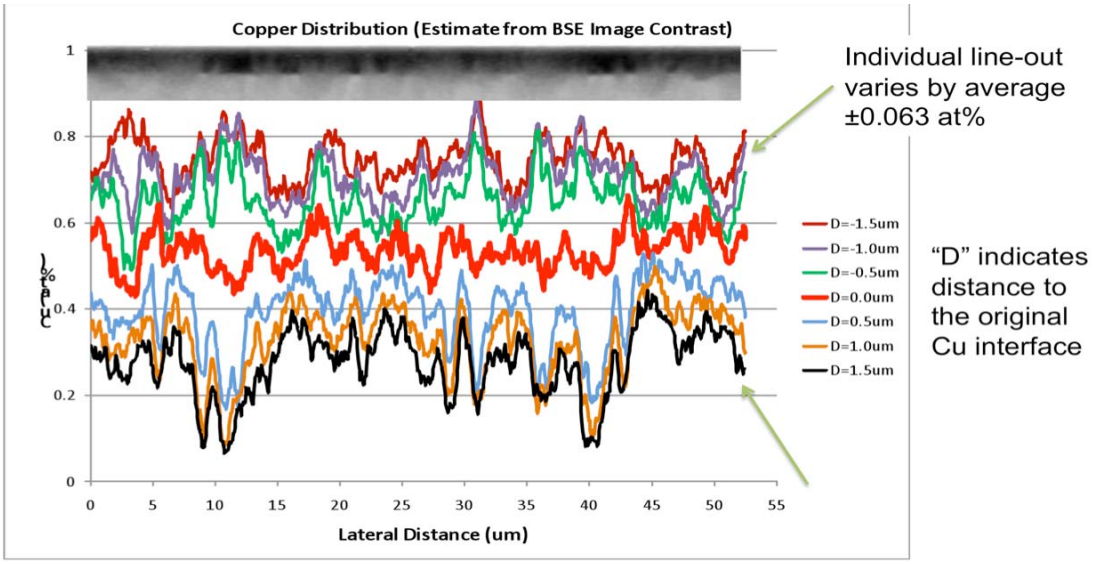

Fig. 4-29. Typical azimuthal copper variation is ~±0.06 at. % near the original copper interface.

By measuring a shell from the outside rather than on a cross-section, we can conclusively prove the compositional pattern was due to copper diffusion rather than polishing smear. We coated a beryllium shell with 1 at. % copper, followed by a 4.5 μm undoped beryllium layer. The external surface was polished to remove any surface topology, and verified to contain no copper contrast. After pyrolysis, the shell was measured again and the non-uniform copper was visible both by BSE and by EDS line scans (Fig. 4-30(a)). Cu at. % increased with the depth from the surface, proving conclusively that the copper source was from the shell interior and that non-uniform diffusion had occurred (Fig. 4-30(b)).

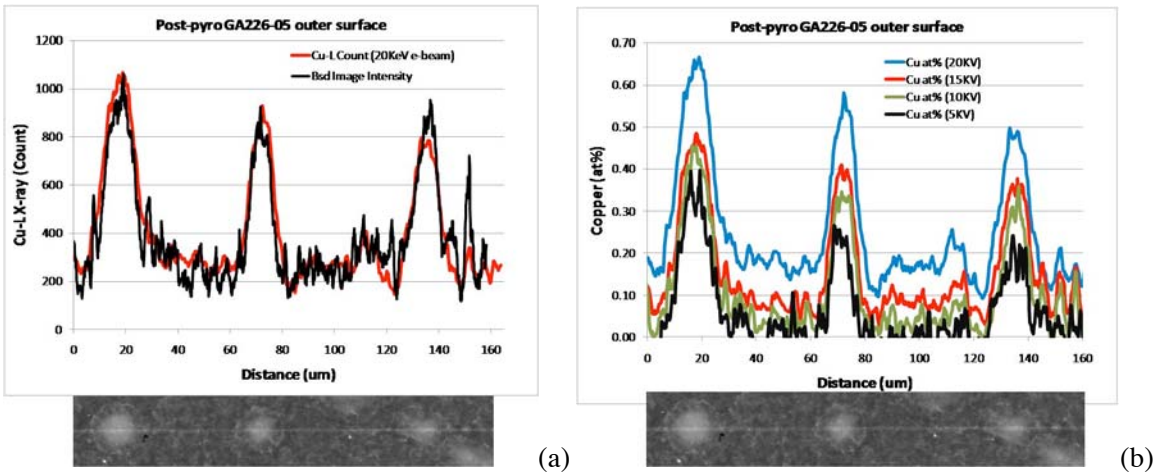

Fig. 4-30. Surface SEM measurement of a post-pyrolysis shell that contains a 4.5 μm undoped final beryllium layer. No contrast was visible prior to pyrolysis whereas prominent contrast showed up after pyrolysis. (a) Line-scans based on Cu-L x-ray emission and backscattered electron intensity both agree that the non-uniform post-pyro copper distribution. (b) As the e-beam energy is increased from 5, 10, 15 to 20KeV, the maximum EDS probing depth is increased from 0.4, 1.5, 3.0 to 5 μm. The increased Cu at. % sampled by more energetic e-beams (with larger interaction volumes) proves that copper is from an interior source and the diffusion is not uniform.

Sputtered beryllium layers forms a columnar grain texture with a typical cross-section between 0.1 and 1 μm. These grains form the normal 2-5 μm clusters that produce nodular textures on the as-deposited surface. On occasion, large clusters up to 15-30 μm in sizes are formed, which forms super nodules (large "bumps") on the coating surface. The center of the super nodules, which shows up as white blobs in the BSE images in Fig. 4-30, experiences accelerated copper diffusion. A TEM study of the grain structures (performed at LLNL in collaboration with their researchers) indicates the accelerated diffusion is likely due to a grain boundary diffusion mechanism, which occurs where the grain sizes are smaller and the structure more porous (the "bump" region in Fig. 4-31 or the white-dot "super nodule" region in Fig. 4-30). Non-uniform copper distributions on ion-beam cleaned cross-sections have also been confirmed by a variety of other instruments such as TEM, Auger Electron Spectroscopy (AES) (Fig. 4-32(a)) and Time-Of-Flight Secondary Ion Mass Spectroscopy (TOF SIMS) (Fig. 4-32(b)). Most recently, a synchrotron-based x-ray microscope was used to directly measure the copper variations in whole shells.

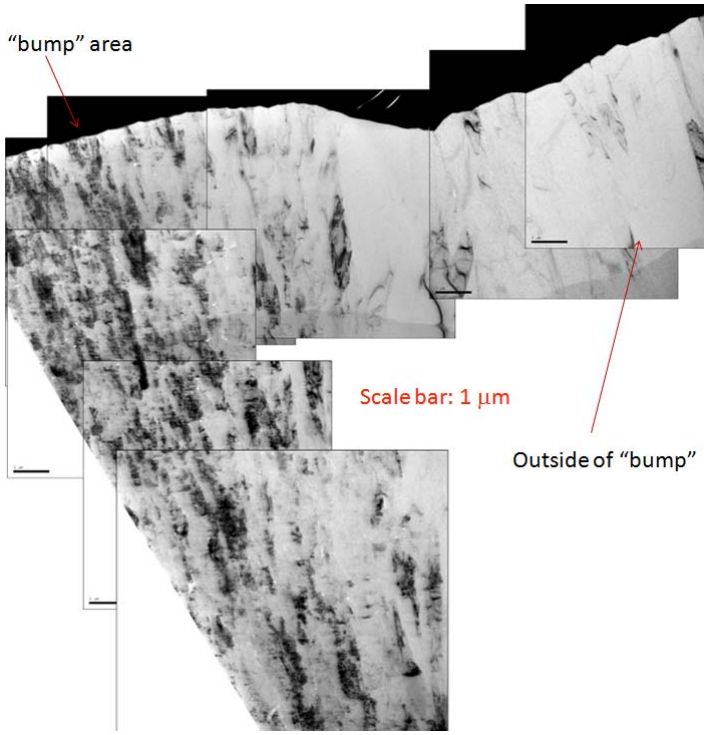

Fig. 4-31. A composite TEM image of a Focused Ion Beam (FIB) lift-off contains the center of a super-nodule ("bump") and the surrounding area outside the nodule. The super-nodule region has much smaller grain sizes and more complex structure with many nano-voids, as compared to the normal region outside.

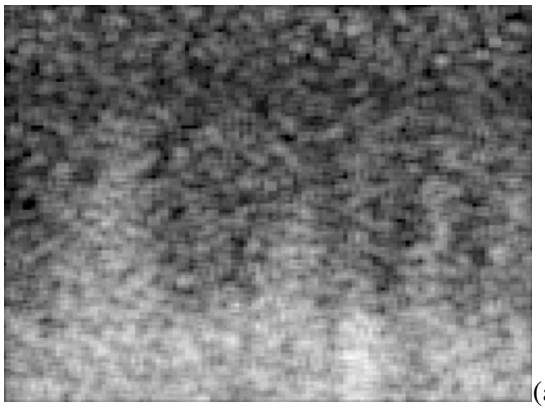
(a)
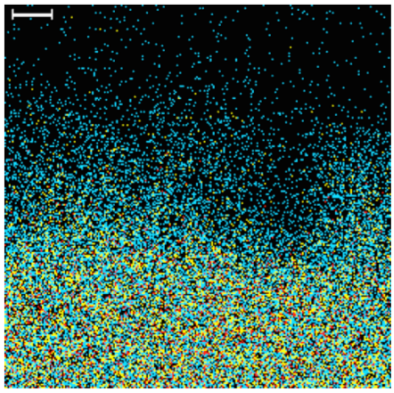
(b)

Fig. 4-32. Non-uniform copper distribution on post-pyro cross-sections near the original copper interface. (a) By Auger Electron Spectroscopy (AES) (b) By Time-Of-Flight Secondary Ion Mass Spectroscopy (TOF SIMS).

While the radial diffusion data has been known since the beginning of the Be work, the azimuthal non-uniformity of that diffusion was not quantified until this year, and the analysis work has been a joint effort between LLNL and GA. The azimuthal non-uniformity could impact the implosion uniformity and is therefore very undesirable. Three methods of mitigating copper diffusion have been proposed and are subjects of research in FY11 as shells exhibiting the Cu diffusion at the length scale reported here are planned to be shot on NIF to examine the importance of this issue. The first method requires a change in the ablator design from that with a stepped copper profile to that with a graded profile. The lateral dopant variation is a fraction of the concentration gradient over the diffusion length. By spreading out the dopant gradients over many microns, the effect of dopant diffusion would be greatly reduced. Figure 4-33(a) shows that the measured copper profiles are not much different between pre-pyro and post-pyro for a shell with a graded design. The second method requires the introduction of an oxide layer as a diffusion barrier. We have demonstrated that any oxide with more than a few nanometer thickness, be it natural beryllium oxide or an Atomic Layer Deposition (ALD) coated Al_2O_3 layer, is sufficient to stop the copper diffusion. In Fig. 4-33(b), a NIF point-design shell with a three-step copper dopant profile was fabricated with two thermal oxide layers (formed by 6 and 24 hours at 250°C respectively in an air furnace) that bound both sides of the copper doped region. After pyrolysis, copper diffused between the non oxidized interfaces between layer #3 (higher Cu doped) and the layers #2 & #4 (lower Cu doped), but both of the interfaces that bound the Cu doped region are sharp because the oxide stopped the diffusion. Preliminary data shows that there are two competing requirements to balance in this approach: From the perspective of not disturbing the ablator performance, a thin oxide is preferred; from the perspective of not having layer de-lamination, a higher temperature oxide (therefore thicker) might be preferred. We are currently experimenting with the temperature and the duration to optimize the oxidation process.

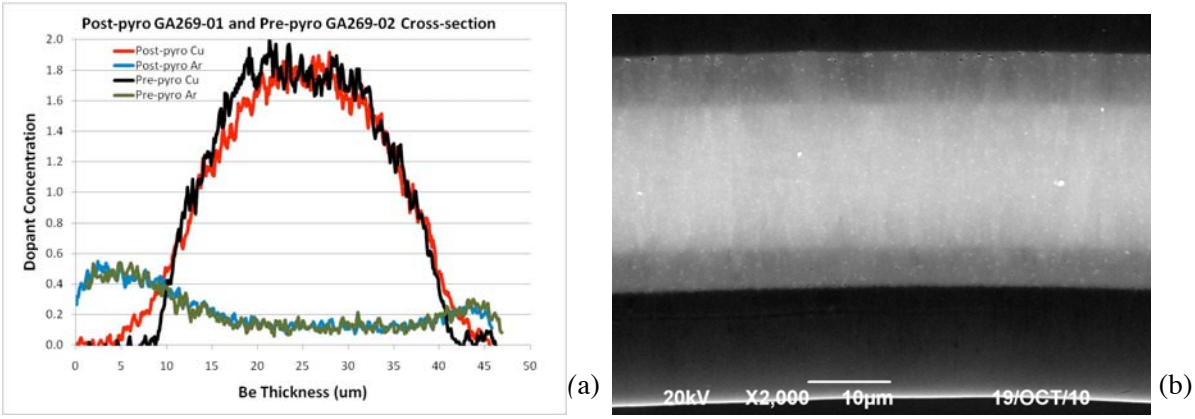

Fig. 4-33. Copper diffusion mitigation methods (a) A continuously graded dopant profile minimizes the impact of copper diffusion. The copper profile difference before and after pyrolysis is quite small. (b) A cross-section SEM image showing the presence of two oxide layers (invisibly thin) that bound the copper-doped (whiter) region effectively stopped copper diffusion into the undoped (darker) region, whereas the lack of oxide within the copper doped region led to strong inter-diffusion between the three sub-layers with varied copper concentration (fuzzy interfaces).

A third method to halt diffusion is to perform the pyrolysis of the beryllium capsule before the copper layers are coated onto the shell. We drilled a 5 μm hole into a 14 μm thick beryllium shell and pyrolized out the plastic mandrel. We over-coated this mandrel with the specified Cu layers and coated with an additional 113 μm of beryllium, as specified by the current design. After that, we drilled through the entire shell and leak tested the capsule using a fill tube assembly. The overcoated beryllium mandrels are not leak tight. We are testing a carbon plug in the 14 μm thick shell before overcoating to determine if we can effectively produce beryllium targets that do not suffer from Cu diffusion using this method.

4.1.8 FINAL ASSEMBLY METROLOGY

4.1.8.1 Introduction

Inertial confinement fusion (ICF) experiments at the National Ignition Facility (NIF) require cryogenic targets at the 1 cm scale to be fabricated, assembled, and metrologized to micron level tolerances. During assembly of these ICF targets there are physical dimension metrology steps to be made of the components, sub-assemblies, and completed targets. Metrology is primarily completed using optical coordinate measurement machines that provide repeatable measurements with micron-precision, while also allowing in-process data collection for absolute accuracy in assembly.

A NIF cryogenic target is comprised of a number of components that form two main subsystems, the base and the target. The base provides the target interface to external gas handling and electrical systems as well as to the cryogenic cold head (Fig. 4-34). The target is composed of two distinct subsystems, the thermo-mechanical package and physics package. The thermo-mechanical package (TMP) consists of TMP shells, diagnostic band, various windows and cooling arms. This package has an engineering purpose to allow for

precision repeatable assembly, while accommodating changing attributes of target components and maintaining thermal symmetry of the target.

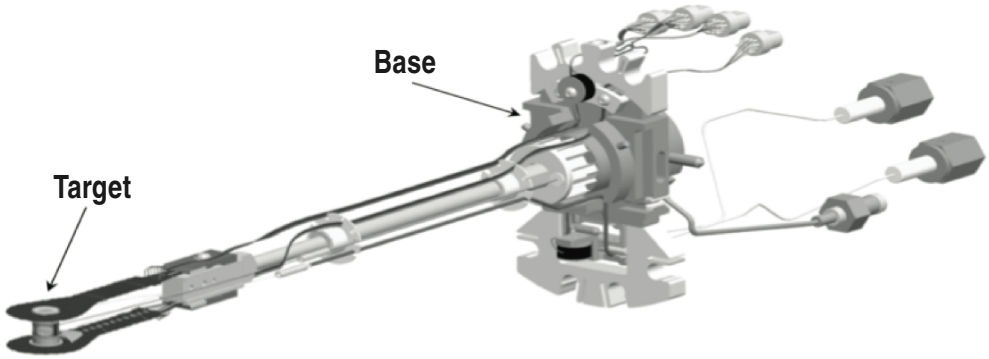

Fig. 4-34. Energetics Campaign NIF Cryogenic Target Attached to Base Model.

The physics package consists of the hohlraum, laser entrance hole (LEH) inserts, tents, and the capsule fill tube assembly (CFTA) (Fig. 4-35). The physics package meets the specifications set forth by the physics experimental requirements. Assembly tolerances are derived from physics flow down requirements, fabrication tolerances, and metrology capabilities. Table 4-3 below lists the primary final assembly requirements and tolerances. The TMP and physics components and subassemblies are assembled into a completed target at the "final assembly" step in the production process. This step includes threading the CFTA into the diagnostic band, capturing the capsule in the tents of the TMP/hohlraum subassemblies, and attaching the target to the base.

Fig. 4-35. Target Physics and Engineering Packages.

Target components and subassemblies are designed with features specifically for metrology purposes. Notches in the TMP shell, flats with defined surface roughness and parallelism, and clean burr free edges are examples of metrology features designed into target components. Without these purpose built metrology features the quality and uncertainty of the measurements would be negatively affected.

Following final assembly, over 400 dimensional measurements are made and over 70 values are reported per target.

Table 4-3
Portion of Target Assembly Dimensional Requirements Table

Category	Description	Specifications
TMP Subassembly	Hohlraum to TMP Can Clocking (deg)	7 ± 1 degree
	LEH Insertion Depth (mm)	0.350 ± 0.011 mm
	Hohlraum Insertion Depth (mm)	1.770 ± 0.006 mm
Capsule Position	Capsule Axial Position from Nominal wrt Target Center in Z (μm)	0 ± 10 μm
	Capsule Radial Position wrt LEH (μm)	0 ± 12 μm
Diagnostic Line of Sight	GXD Line of Sight, phi (deg)	315 ± 0.5 degree
	GXD Line of Sight, theta (deg)	90 ± 0.5 degree
	Hohlraum GXD Notch Upper to Lower Angular Alignment (deg)	90 ± 0.25 degree
Hohlraum Gaps and Length	Gap (z) between hohlraum halves (μm)	20 ± 8 μm
	Gap between hohlraum and LEH, upper/lower (μm)	23 ± 6 μm
	Nominal Hohlraum Inner Length, total (μm)	10052 ± 20 μm
Target Location wrt Base	Target Pitch Offset, Rx, relative to Base Datum (deg)	0 ± .250 degree
	Target Roll Offset, Ry, relative to Base Datum (deg)	0 ± 1 degree
	Target Center Offset, X/Y, relative to Base Datum (mm)	0 ± .500 mm
	Target Center Offset, Z, relative to Base Datum (mm)	0 ± .500 mm
Fiducial Surface	Upper/Lower Fiducial Surface to LEH Midplane (mm)	5.426 ± .010 mm
Fiducial Surface to LEH Concentricity	Upper/Lower Fiducial Surface ID Location wrt LEH axis, x/y (mm)	0 ± .005 mm
Shield Location	Shield Location at x and y (mm)	0 ± 0.250 mm

4.1.8.2 Metrology System

The metrology system used for these measurements has four main requirements. First, the system has to make all of the pertinent measurements via non-contact methods due to the fragility of the targets. Second, the system has to work over the entire volume of a target mounted to a base and embedded in the assembly hardware. This volume is approximately the size of a shoebox. Third, assembly tolerances are typically in the 5–20 μm range and therefore the goal for the measurement system was to be 10 times better or in the 1–2 μm accuracy and repeatability range. Finally, it was also critical to have the ability to metrologize targets being produced at a rate of 1–2 targets per day.

The metrology tool in use for dimensional measurements of NIF cryogenic targets was the Quest series OCMM by Optical Gaging Products (OGP®). The OGP® OCMM met the measurement system requirements including measurement volume, various non-contact measurement methods, accuracy and repeatability, and production rate requirements. The OCMM has a datasheet accuracy value in x and y, of 1.5 μm. The z-accuracy is 1.5 μm to

10 μm depending on the hardware configuration of the OCMM. Longer working distances allow room for assembly hardware during the assembly or metrology processes. The working volume, of the OCMM models in the production facility, is large enough for assembling a target with a base with all of the necessary assembly hardware in place.

The machine software, MeasureMind® 3D, allows the user to record measurement routines and automate the measurement process. Automating the process removes as much operator error as possible.

4.1.8.3 Results

Dimensional metrology is shown for key measurements taken during the metrology step following final assembly of the Energetics Campaign targets. The data is presented via moving range process control charts. Control charts are used as a tool to monitor the assembly processes during production with the intent of discovering trends early and making process adjustments before any non-conformance issues occurred. The x-axis shows the target number in chronological order of the assembly date. Each plot shows the metrology data, data average, upper/lower specification limits and upper/lower control limits. The control limits are equal to the data mean plus or minus 3 times the moving range average and are used as indicators as to whether a process is in control. A process is considered in control if the data points are randomly distributed and within the control limits. Error or uncertainty estimates are made by calculating the root sum square of the datasheet accuracy values where available and relying on experience where there is a void of information.

There are hundreds of measurements made during the final stages of target assembly and not all of the data is discussed here. The methodology, estimated uncertainties, and results are discussed for the diagnostic port angular alignment, target location with respect to the target base, and capsule position with respect to target center.

The diagnostic port angular alignment with respect to the target base is measured on each target. (Fig. 4-36). The angular alignment specification is a nominal value dependent on the primary experimental diagnostic location ±0.250°. This alignment was imperative so that the diagnostic could align to the target and record experimental results.

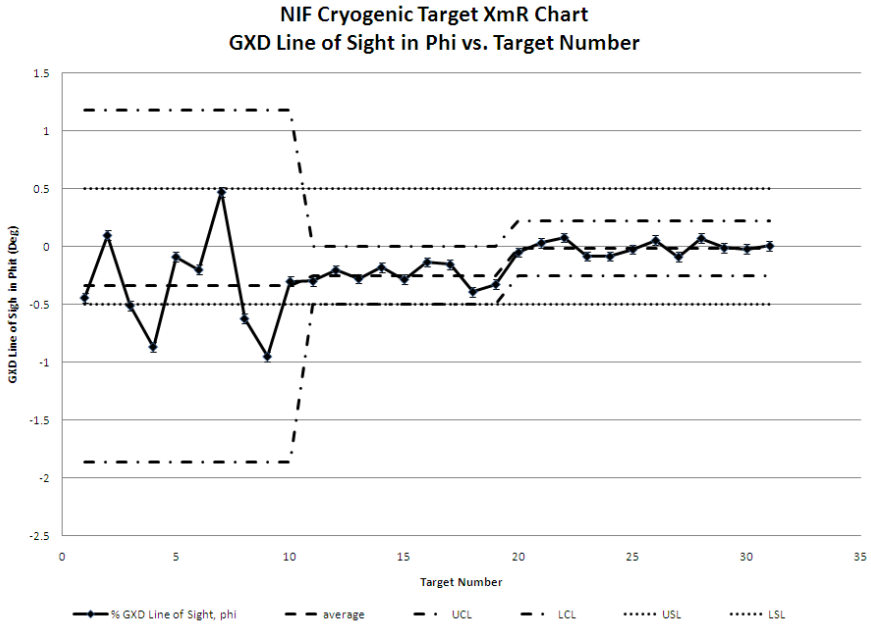

Fig. 4-36. GXD Port Angular Alignment vs. Target Number Graph.

Diagnostic port alignment process improvements were made during the production run. During the early stages of the production run it was evident that the assembly process approached or exceeded specification limits. Two changes were made at the Hohlraum Insertion Station that allowed the operator greater access to the component alignment features. The resolution and magnification of the station microscope was upgraded and portions of the assembly station were modified to allow the operator a more detailed view of the process. Following the upgrades the process variability improved and the control limits tightened. However, there was still a bias error between the assembly and metrology stations. This error was due to differences in the automatic measurement routines. A standardized routine was deployed, which corrected the difference toward the later stage of the production run. The remaining outliers shown in the plot were due to off-normal events such as parts with predicted interference fits.

The target location with respect to the base was required to be within nominal position in x, y, z to within ±0.500 mm. Roll, rotation about the y axis, of the target had to be within ±1.0° and pitch, rotation about the x axis, within ±0.250° of the nominal values. These requirements are necessary so that systems including the target positioner, alignment systems, and diagnostics can function properly. The target location in x/y is the measured distance between the center of the upper LEH insert and the datum features on the target base. The following Fig. 4-37 details the target position in x, y, and z coordinates relative to the base. For the x and y locations the processes before target #13 were much more variable. During this time better measurement methods for assembly and metrology were developed. A change was then made to standardize the measurement methods between the assembly and

metrology machines. After the measurement methods were standardized, the target x and y positions improved and were consistently within specification limits.

The z-position was measured via the Through The Lens (TTL) laser with a 0.45X or 0.50X magnification lens as the distance from the top of the TMP shell and the target base datum features perpendicular to the xy-plane of the target. A change was made by target #5 during the base assembly step to improve the base assembly process and verify that the bases were within specification prior to final target assembly.

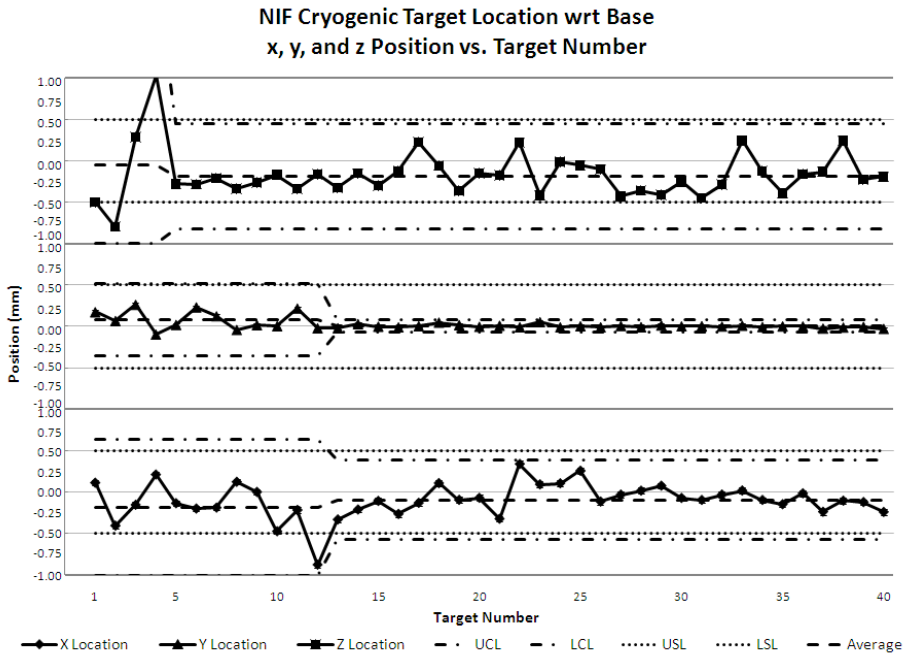

Fig. 4-37. Target Location Relative to Base Graph.

Rotation of the target relative to the base was measured by fitting planes to z-measurement data (Fig. 4-38) on the TMP shell and base datum features. The rotation about x and y shows a similar trend to the target location in z. The same assembly improvement at the base assembly step positively affected the pitch of the target relative to the base at target #5 and thereafter.

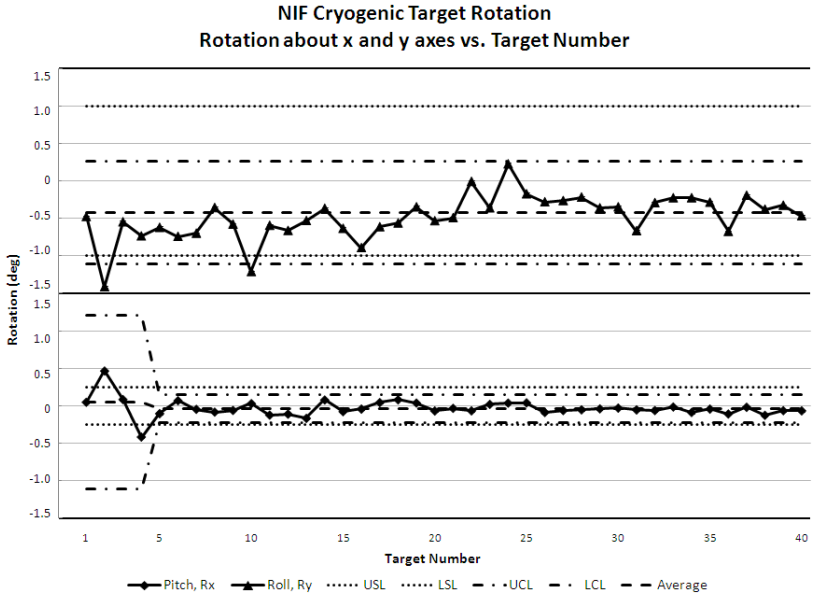

Fig. 4-38. Target Rotation Relative to Base Graph

The rotation about the y-axis, or roll of the target, has a relatively large tolerance of ±1°. This is because the target positioner can adjust in this direction more than the other directions. The assembly and measurement processes did not change for this parameter. Note that the parameter was within specifications most of the time but consistently biased in the negative direction. This was due to the assembly procedure and fixture that does not correct for a torque that is applied when attaching the long extension arm of the base to its mounting hardware.

During the Energetics Campaign, the capsule had to be positioned in the target center within ±20 μm axially and ±25 μm radially. Radial measurements are made via concentricity measurements of the capsule outer diameter relative to the LEH insert inner diameter. The axial capsule position was calculated using multiple measurements including: target axial length, LEH insertion depths, LEH insert thickness, capsule radius, and the measured distance from the top of the capsule to the top of the TMP shell.

Figure 4-39 shows the capsule radial positions in the x and y directions. The y-direction is nearly in-line with the base extension and fill tube. Both of these processes appear in control and within specification limits. However, the average data point/trend in the y-direction is biased in the negative direction at approximately 20% of the tolerance limit or 5 μm.

During the production run the process was changed such that the capsule was not centered but rather biased or positioned off-center during assembly. The capsule was positioned approximately 5 μm in the positive y-direction to see if there was an effect on the capsule position post-assembly. The biasing during assembly had the predicted effect such that for a small sample of targets the capsule radial position average improved.

Figure 4-39 also shows the capsule axial position with respect to the center of the hohlraum. The calculation is based on the target length, LEH insert thickness and insertion depth and capsule position with respect to the TMP shell. This data is shown within the control limits and specification limits.

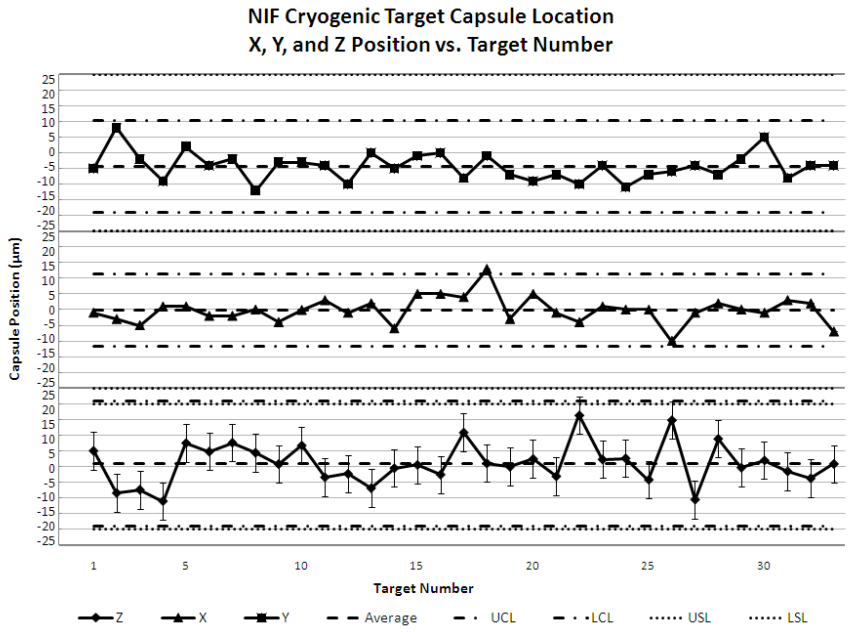

Fig. 4-39. Capsule radial position and axial position graph.

Using control charts as real-time production tools yields actionable information that can both increase production yield and throughput. The information can also be used to focus process improvement resources. Tracking of measurement values and other production related items were a work-in-progress during this first campaign. Looking forward, the systems are now in place to monitor each process and base decisions on real time information. This same information can be used for predicting yield based on future specification changes.

Automation of the metrology routines resulted in a more than 10 times metrology throughput improvement as well as increased measurement repeatability. Initially, these time-consuming measurements were performed manually for each target. With time, standard measurement routines were developed that both decreased measurement time and standardized the measurements so that the process was not as dependent on the operator.

The OCMM has proven to be a reliable, accurate, and necessary system to make measurements of complex targets for NIF. OGP® OCMMs are now in use for multiple assembly machines as well target metrology, and resulting measurement data has been collected for each NIF cryogenic target to date.

Early predictions of measurement uncertainties based on datasheet values were validated through post campaign analysis of small data samples. Many targets were measured multiple times using the programmed routines. In most cases the repeatability information gained

from these measurements yielded uncertainties that were smaller and the same order of magnitude as the estimates derived from datasheet accuracy values.

4.1.9 Debris Identification

Capsule cleanliness is a primary concern for experiments on the NIF. The NIF specification states that no single particle of dust greater than 4 μm diameter sphere of 1g/cc shall be in contact with the capsule surface. The specification extends to quantify numbers of particles of smaller sizes. For this reason a number of processes and capabilities have been developed to inspect for and quantify debris both on the capsules and the target tents.

4.1.9.1 Tent Inspection

Tents are used to support the capsule and maintain its position within the hohlraum. The tent is in direct contact with the capsule. Therefore the cleanliness of the tent is imperative. A method was developed using the OGP® OCMM and custom LabVIEW software to find particles on the tent and record their size and location. Depending on the size and location of these particles tents were either rejected or used in the next stage of the assembly process.

The OCMM is used to take a series of images spaced evenly in a grid pattern 16 across and 20 images high. Each image has a field of view of approximately 640 X 480 μm. The grid was designed such that each image overlapped so that information was not lost. At each step the TTL laser was used to focus on the tent surface, and an image is taken with oblique top light and then with transmitted light. The OCMM routine was programmed to run automatically after performing an initial setup and would complete the inspection routine in less than 45 minutes. Each tent inspection generates 640 images and position data associated with each image.

LabVIEW image analysis code was developed to analyze the tent inspection images generated at the OCMM. The code processes each of the images and records size and location of each particle. This data is then graded against specifications for particular regions of interest on the tent. Histograms are also generated showing particle counts vs. size. Based on specifications for size and location of particles, tents are rejected or sent to the next stage in the process.

This tent debris inspection and analysis method was characterized using control samples or spheres of known sizes. Tent yield based on debris inspection results is approximately 85%.

4.1.9.2 Capsule Inspection

Capsule inspection is currently performed using two inspection methods. A Keyence digital microscope is used to capture a series of images that are then processed to generate a map of known defects for each of 4 hemisphere views. These maps are then overlaid onto capsule hemisphere images. The capsule is transferred to the OGP OCMM and using the Keyence microscope overlay map the OCMM operator finds and determines the size of the features.

The OGP OCMM and Keyence microscope system finds and laterally sizes particles. However, these systems are inadequate for determining debris height. Currently, if the debris was added late in the assembly process it is difficult to determine the particle height. If the debris existed prior to attaching the capsule fill tube the Phase Shifting Diffraction Interferometer (PSDI) is used to quantify the height of the debris. The measurement using the PSDI is only possible on a capsule and not after the fill tube has been attached.

The particle size and location information is then used by the NIF scientists to predict the effect of the debris prior to running an experiment. If the results show the debris to be an issue the capsule is not used in a target assembly and a suitable replacement is chosen.

Development is focused on methods to improve existing inspection capabilities and capsule cleaning.

4.2 Direct Drive NIF Target Development

4.2.1 Fill Tube Development for OMEGA, NIF and Fast Ignition Experiments

The current design of the direct drive NIF target requires a fill tube. In FY09, the direct-drive fill tube design went through a series of dramatic changes in order to field targets for cryogenic D_2 fill experiments at LLE. In FY10, the collaboration between GA and LLE target fabrication groups focused on improving the direct-drive targets for more uniform D_2 ice layers and better survivability. Figure 4-40 shows how the assembly has evolved during this time. Also during this year, fast ignition assemblies with a fill tube and reentrant gold cone were fabricated and sent to LLE for similar layering experiments.

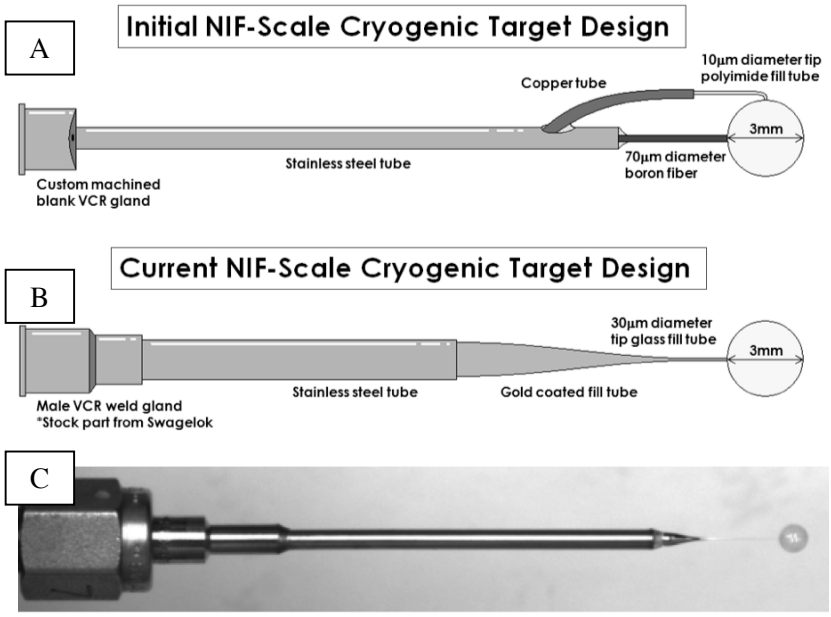

Fig. 4-40. (A) Comparison sketches (not to scale) of the initial target design in early FY09 and (B) the current target design. (C) An optical image of an actual target of the current design.

A production process for successfully attaching fill tubes was previously developed for indirect-drive NIF capsule fill tube assemblies (CFTA). The fabrication of direct drive targets

began as an extension of that original work, but adapting to the direct drive configuration had unique challenges. Some of the challenges were that the CFTA must be freestanding, robust, and rigid. The initial fill tube design had a number of issues that contributed to the non-uniformity of the deuterium (D_2) ice layer and low fabrication yield of targets. Redesign of the entire target has significantly improved the D_2 ice layering by reducing thermal perturbations. One of the iterations done was to extend the glass tube longer so that no metal components were in the radius of the layering sphere (Fig. 4-41). This required the glass fill tubes to be custom fabricated in house at GA. A series of different fill tube tapers were investigated until one was chosen with the best rigidity and strength. The latest development in FY10 was to apply a sputter coating of gold to the fill tube in order to reduce the IR absorption. The changes can be seen in Fig. 4-40. These design changes also made a more robust target that can survive the handing required in fabrication and testing.

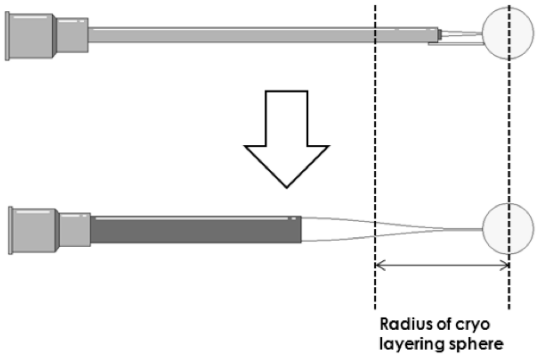

Fig. 4-41. Main emphasis for changing the target design was to eliminate all metal materials inside of the layering sphere.

In FY10 gold-coated fill tube targets were delivered and cryo-layered. The improvement can be seen in Fig. 4-42. Layering attempts with the early generation targets in FY09 had thermal issues were the SiC supporting stalk attached to the capsule (Fig. 4-42A). As the design changed in FY09 to a capsule supported only by the fill tube, the uniformity of layering attempts improved (Fig. 4-42B). (Another critical changed that happened at this time was that the glass tubing was extended so that the metal tube did not extend into the layering sphere) IR absorption of the glass fill tube still was creating a thinning of the ice layer near the fill tube, however. In the targets delivered in FY10, gold coatings were applied to the fill tube to mitigate the IR absorption of the glass. The improvement can be seen in the image (Fig. 4-42C).

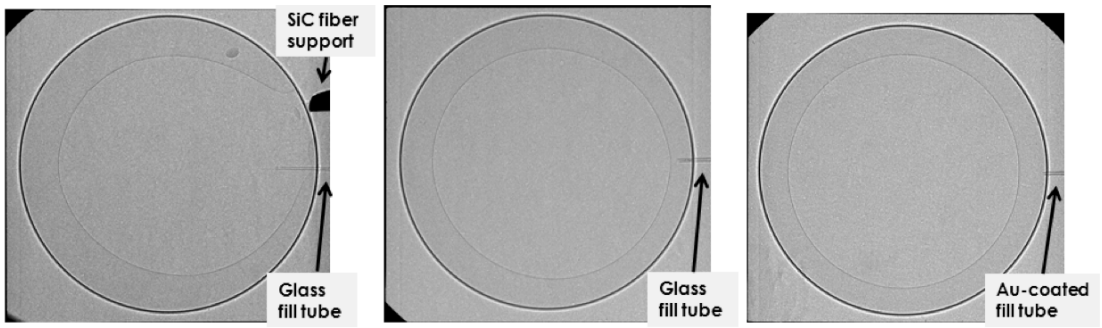

Fig. 4-42. In this phase contrast image, the uncoated glass fill tube thins the ice layer near the attachment point. Phase contrast image of a successfully layered target with a gold-coated fill tube, which was also cycled several times. *Images courtesy of LLE.*

However, a set of challenges remains with regards to survivability and yield. Several targets have been successfully fabricated and cryogenically layered, and in some cases cycled several times at LLE. Many other targets have suffered catastrophic failure or small leaks after fabrication and successful leak testing that render the target unusable. It will be important to address the causes of these losses in FY11 as work transfers to DT systems, were dependability of the target is critical.

In related work, during FY10 fast ignition assemblies with a fill tube and reentrant gold cone were fabricated and sent to LLE for similar layering experiments. Images of one of these targets can be seen in Fig. 4-43.

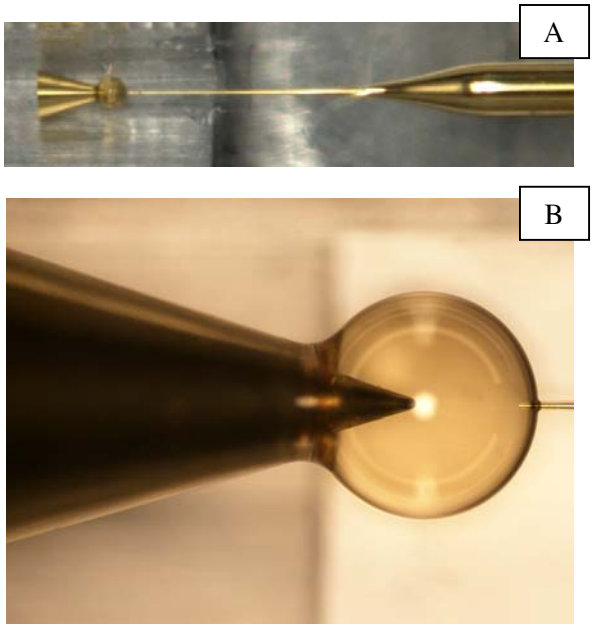

Fig. 4-43. A fast ignition CFTA with a gold cone, an 860 μm diameter capsule, and gold-coated glass fill tube. (B) A magnified image of the same target.

4.2.2 Resorcinol Formaldehyde NIF Size Shells

GA has developed a fabrication process to fabricate shells with a diameter range from 900 μm to 4500 μm. Fig. 4-44 shows the different sizes that we can fabricate. The

development of a process to fabricate NIF-Scale resorcinol formaldehyde (R/F) foam shells was first reported in the 2008 IFT Annual report in Section 4.2.2. This work discussed the development of a process to fabricate a high yield of intact NIF-Scale shells. These foam capsules are part of a design for future direct drive targets at the National Ignition Facility (NIF), which calls for a 3.5 mm diameter resorcinol formaldehyde (R/F) foam shell with a 100–200 μm wall. For the near term, these NIF R/F foam targets are needed at LLE for cryogenic layering experiments. Ultimately, the foam capsules will be used in direct drive experiments on NIF. Though the yield of intact shells was high (90%), the yield of shells that met the wall uniformity specification was low (5%). Wall uniformity is a critical specification for these targets because wall non-uniformity adversely affects the implosions. The specification for the mode 1 wall uniformity for these R/F foam targets is usually quoted in terms of non-concentricity (NC), defined by Eq. (1).

$$\%\mathrm{NC} = \frac{\Delta\ \text{Wall Thickness}}{2(\text{Avg. Wall Thickness})} \quad (1)$$

The current NC requirement for these targets is similar to the OMEGA R/F foam shells, which is ≤ 5%. The work presented here is an extension of this work in investigating ways to improve the wall uniformity of these shells.

In these experiments the R/F precursor solution was not altered from the previous work. The only parameter that was altered was the additives that were added to the outer oil phase (O2) in the fabrication process. In the previous work, a styrene-butadiene-styrene (SBS, Kraton Polymers) was added into the outer oil phase, which increased the interfacial tension (IFT) between the emulsion components in hopes of improving the wall uniformity of the shells. This helped improve the yield of shells that meet the wall uniformity from <2% to 5%. Working on this concept we investigated other types of polymer additives that could replace or possibly be added to the outer oil solution with the SBS to help increase the IFT more which would possibly lead to improved wall uniformity. This method was used to improve the wall uniformity of the OMEGA sized R/F shells, and a similar method was also found to help the sphericity and wall uniformity of the full density PαMS shells [2,3]. The beneficial effect on NC when the O2 phase is changed is purely empirical at this point. Despite several attempts by various authors [4-6], there is not a complete theory of the physics affecting NC in the complicated systems used to cure shells. Hence these results though empirical, clearly provide a hint for future theoretical work and provide a practical guide for increasing yield of shells with low NC. The polymer additives that were investigated in this work were Alkyl Ketene Dimer (AKD, Hercules, Inc.) and Polybutadiene (PBD, Sigma Aldrich). The interfacial tension of the emulsion system was measured by an interfacial tensiometer (Future Digital Scientific OCA-15) via the pendant drop method.[14] This allows measurement of interfacial tension to ±0.10 dyne/cm. Viscosity of the O2 solution can increase when using these additives. If too much of the polymer additive is added it could increase the viscosity (≥45 cps at room temperature) and could affect the stability of the emulsion that would lead to a low yield of intact shells. Because of this the viscosity of the O2 solution was monitored. The viscosity of the oil solutions was measured with a rheometer (Bohlin Instruments,

CVO050). The viscosity and IFT affects of these polymers and combinations of these polymers are shown in Fig. 4-44.

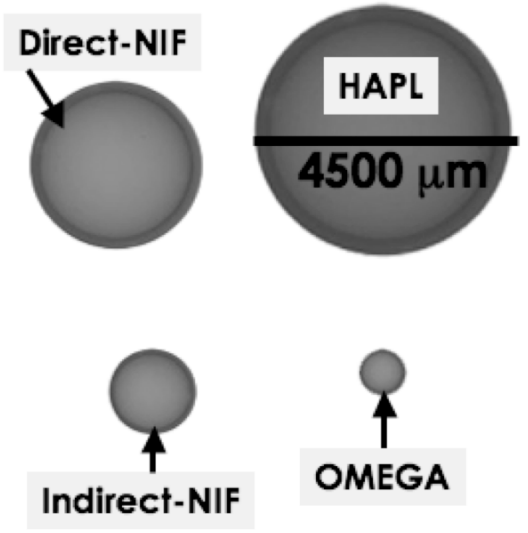

Fig. 4-44. Shows the size difference between a variety of size ranges of R/F shells that can be fabricated. This can range from OMEGA (900 μm) to NIF (1500-3000 μm) to High Average Power Laser (HAPL) scale (4500 μm) R/F foam shell.

PBD was first investigated as a possible SBS replacement. When added to the O2 at the same weight % of 0.60 the IFT only increased to 2 dynes/cm, but it's viscosity increased to 35 cps. When NIF Scale R/F shells were made with this O2 the yield of shells with an NC <5% was still <5%, but the yield of shells that had an NC of <10% was only 15%. These results show that maybe viscosity is not a major contributor to the wall uniformity of these shells, and that the IFT needs to be higher than 2 dynes/cm to make an impact on wall uniformity. The amount of PBD was also increased to 0.80wt% in order to increase the IFT higher than 2 dynes/cm. Though this increased the IFT to 3 dynes/cm, it also increased the viscosity to 45cps, which caused the emulsion to be unstable, leading to a low yield of intact shells. From these results we then combined PBD (0.12 wt%) with SBS (0.50wt%) in an O2 solution. The IFT of this increased to 7 dynes/cm with a viscosity of 35 cps. The combination of the two polymer additives produced a synergistic effect on IFT. The results on shells fabricated with this O2 showed improvement at both the 5% and 10% NC specification. The yield at 5% increased from <5% to 25% and for an NC of 10% the yield improved from 15% to 50%. These results can be seen in Fig. 4-45 along with the other experiments that were done on wall uniformity.

IFT & Viscosity Studies of Various O2 Polymer Additives

Additive 1	Additive 1 Wt%	Additive 2	Additive 2 Wt%	Span 80 (yes/no)	IFT (Dynes/cm)	Viscosity (cps)	Shells produced (Yes/No)	If No, Why ?
STD (None)	NA	None	NA	No	13	12	No	Shells Aglomerate
STD (None)	NA	None	NA	Yes	1	12	Yes	
SBS	0.6	None	NA	No	21	12	No	Shells Aglomerate
SBS	0.6	None	NA	Yes	4	20	Yes	
SBS	0.7	None	NA	Yes	5	20	No	Shells Aglomerate
PBD	0.6	None	NA	Yes	2	35	Yes	
PBD	0.8	None	NA	Yes	3	45	No	Emuslion not stable
PBD	0.12	SBS	0.5	Yes	7	35	Yes	
AKD	0.6	None	NA	Yes	8	35	No	AKD Re-Precipitated, led to unstable emulsion
AKD	0.3	SBS	0.5	Yes	13	35	Yes	

Fig. 4-45. Results of the IFT and viscosity of the variations O2 solutions that were investigated to improve the wall uniformity of the NIF Scale R/F foam shells. Despite results showing that IFT can lead to improved wall uniformity, factors such as having no Span 80, too much of an additive, or increasing the viscosity of the O2 solution to ≥ 45 cps can affect the outcome on the yield of intact shells.

AKD was another polymer additive that was investigated as a possible SBS replacement. Just as in the PBD experiments the AKD was added to the O2 at the same weight % of SBS at 0.60 wt%. The IFT increased to 8 dynes/cm and the viscosity increased to 35cps. The shells produced with this O2 had complications with the fabrication process because the AKD precipitated out of solution over time, and affected the yield of intact shells. These results led us to decrease this amount of AKD and combine it with the SBS. The combination that worked best without precipitating out of solution was an O2 formulation that had 0.30 wt% AKD and 0.50 wt% SBS. The IFT increased to 13 dynes/cm while the viscosity was at 35 cps. Again the synergistic affect of IFT was observed similar to the results from the PBD/SBS combination. Like the results from the PBD/SBS combination, the results on shells fabricated with this O2 showed improvement at both the 5% and 10% NC specification. The yield at 5% increased from <5% to 50% and for an NC of 10% the yield improved from 15% to 80%. These results of can be seen in Fig. 4-46.

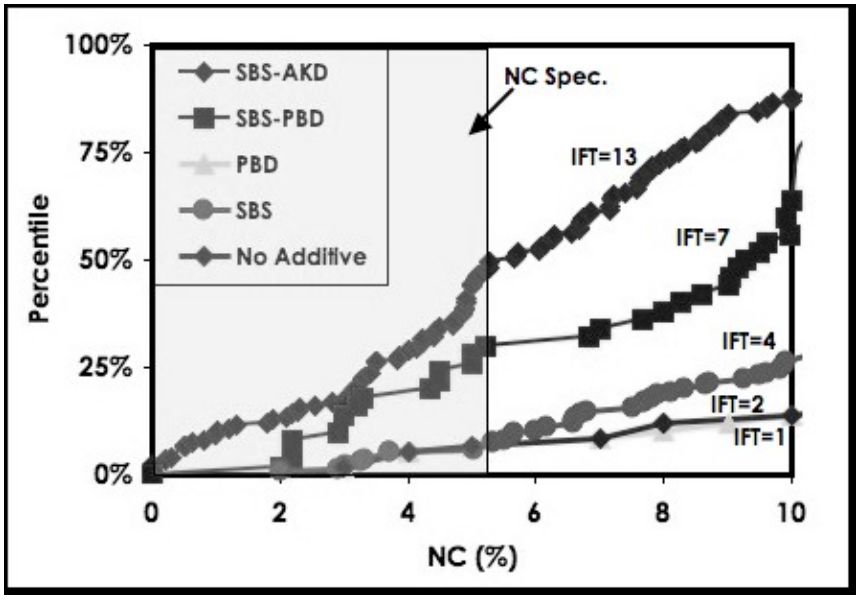

Fig. 4-46. The Percentage of shells that meet the NC wall uniformity specification based on the O2 solution that was used. Higher IFT resulted in shells with better wall uniformity.

Though this improvement to the wall uniformity of the shell may be sufficient for the initial cryogenic NIF-Scale ice layering experiments and future direct drive and indirect drive ICF experiment on NIF, further improvement of the wall uniformity is needed in order to field the necessary amount of shells (1Million/day) for a future power plant design. Future work on improving the wall uniformity of these NIF R/F foam shells will include: optimizing the O1/W1 density mismatch for NIF size shells, as well as testing new types of oils, and polymer additives in order to increase the interfacial tension of the compound droplet. Alternative methods to center the double emulsion droplet to fabricate foam shells such as Dielectrophoresis (DEP) are also being investigated [7-9]. The work on DEP has also led to investigating and altering the R/F synthesis so that it could be compatible for this work. This will be discussed in Section 7 of this report.

References for Section 4.2.2.

[4.2.2-1] R.R. Paguio, et al., "Improving the Wall Uniformity of Resorcinol Formaldehyde Foam Shells by Modifying Emulsion Components," Fusion Sci. Technol. 51, 682 (2007).

[4.2.2-2] A. NIKROO, *et al.*, "Fabrication & Properties of Overcoated Resorcinol-Formaldehyde Shells for OMEGA Experiments," *Fusion Sci. Technol.* 45, 84 (2004).

[4.2.2-3] M. TAKAGI, *et al.*, "Decreasing Out-of-Round in Poly(œ-Methylstyrene) Mandrels by Increasing Interfacial Tension," *Fusion Technol.*, 38(1), 46 (2001).

[4.2.2-4] C.P. Lee, T. G. Wang, "The Centering Dynamics of a Thin Liquid Shell in Capillary Oscillations," *J. Fluid Mech.,* 188, 441, (1988).

[4.2.2-5] T. Norimatsu, "Modeling of the Centering Force in a Compound Emulsion to Make Plastic Shells for Laser Fusion Targets," Fusion Technol., 35, 147, (1999).

[4.2.2-6] B.W. McQuillan, A. Greenwood, “Microencapsulation Process Factors Which Influence the Sphericity of 1 mm O.D. Poly(α-Methylsyrene) Shells for ICF,” Fusion Technol., 35, 194 (1999).

[4.2.2-7] T. Jones, “Electromechanics of Particles”, Cambridge University press, New York, (1995) Z.-M. Bei, et al.,”Electric Field Mediated Droplet Centering,” Applied Physics Letters, 93, 184101, (2008).

[4.2.2-8] Z.-M. Bei, et al., “Electric Field Mediated Droplet Centering,” Applied Physics Letters, 93, 184101, (2008).

[4.2.2-9] Z.-M. Bei, et al., “Forming Concentric Double-Emulsion Droplets Using Electric Fields,” Journal of Electrostatics, 67, 173, (2009).

5 OMEGA TARGET DEVELOPMENT

5.1 Charm Targets

Experimenters from LLNL requested CH flat foil targets with a regularly-spaced array of bumps on the surface. These targets are used in Richtmyer-Meshkov ablative growth experiments. The bumps were to be nominally 12 μm tall, 25 μm full width half maximum (FWHM), and spaced 100 μm apart in a square array on top of a 60 μm thick CH disk. Target fabrication was performed by coating CH through a mask containing the hole array onto a CH disk. Individual targets are made by cutting them from the larger disk.

CH disks are made in the GDP coater on 1-inch silicon wafers. Typically, the parts are cut at a radius of ≥6 mm to maximize the number of parts per wafer. Masks are built by stretching Kapton film over a support ring and gluing the film in place. A 266 nm wavelength solid-state laser is used with a CNC-driven workstation to drill an array of holes in the Kapton mask. Typical conditions to drill through the Kapton were 2.6 W (output) with 250 pulses per spot. The laser beam is masked to produce the necessary drill hole size.

To produce the bump array, the mask is placed over the CH disk. The entire assembly is placed in the GDP coater. The gap between the mask and disk is critical to controlling the bump height as a function of coating time. If the gap is too large, the bump formation is limited and the width of the bump can spread. Typically, we were limited to a 5 μm tall growth when a poor gap between the mask and disk existed. By controlling the gap, two successful runs produced 18-20 μm tall bumps in 48 hrs, and 10-14 μm tall bumps in 30 hrs (at 6 mm radius).

The individual bump targets are produced by laser machining the CH base into the desired disk sizes. An example of the target is shown in Fig. 5-1 (a) and (b). Parts are released off the silicon wafer by submerging it in potassium hydroxide aqueous solution. Each target was characterized for bump height with the Wyko optical profiler, and measured for thickness with white-light interferometry.

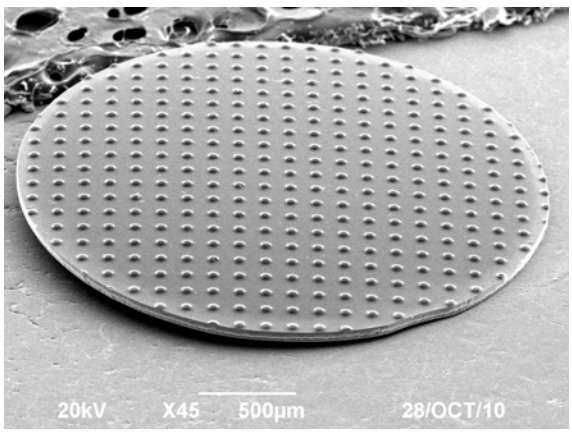

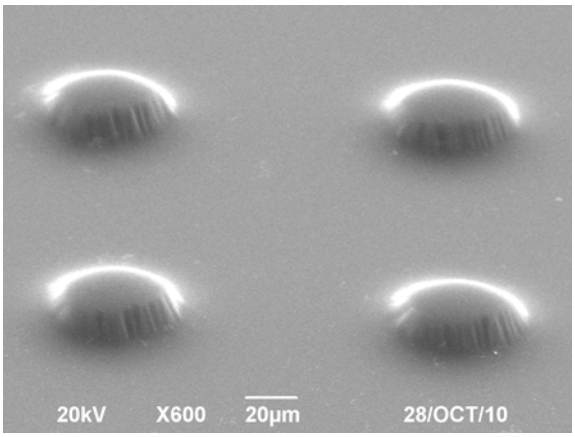

Fig. 5-1 (a) CH flat foil target with square array of bumps, and (b) bumps are nominally 12 μm tall, 25 μm FWHM, and spaced 100 μm apart on a 60 μm thick CH disk.

5.2 Refractive Index Measurements Of GDP & Ge-GDP at 532 nm Wavelength

Experimenters for the National Ignition Campaign use velocity of shock waves in glow discharge polymer (GDP) for equation-of-state measurements. These velocity measurements require precision to 1%–2%. Sensitivity of velocity measurements with VISAR is a function of refractive index $n(\lambda)$ of the host material. We are required to measure the refractive index of the GDP target at wavelength of the laser for VISAR experiments.

An interferometer with a light source filter (532 nm) in the illumination path was used to measure shift of a single fringe over a GDP bump placed in index-matching fluid. The fluid over the GDP sample was changed until the fringe shift was minimized. This occurs when the optical path lengths over the fluid and the bump/fluid are equal which is when the index of GDP and fluid match. The matching fluid (or fluid mixture) was measured with Abbé refractometer to produce n_D. The value of n_D was extrapolated to $n(532\ nm)$ via the Cauchy equation.

A smooth continuous GDP bump was an appropriate sample (as opposed to a step, for example) because a single fringe can be followed over the bump to the fluid. The bumps were made by depositing GDP through holes in a foil mask. The bumps were grown to about 80 μm tall and 600 μm wide. A frame around the GDP bumps was epoxied to the substrate surface. The frame was filled with a few drops of index matching fluid & covered with a glass cover slip. A schematic of the GDP bump in fluid is shown in Fig. 5-2. Reference arm mirrors were adjusted to produce ~2–3 fringes over the bump. The vertical travel stage was raised/lowered to follow a single (continuous) fringe over the bump. Photos were taken of the fringes over one bump with 532 nm filter in the illumination source. A line trace of the expected fringe path over the bump is made and the shift is recorded. This process was repeated with new index fluid, changing by ±0.002 index units. The best matching fluid was the one that minimized the fringe shift. In this case, the fringes most closely maintained their contour as if no bump was present. The index of the best matching fluid was measured using the Abbé refractometer and converted to the index at 532 nm by the Cauchy equation.

Images of GDP and Ge-GDP bumps are shown in Figs. 5-3 and 5-4, respectively. In each set of images, the index-matching fluid was changed around the bump and the fringe shift was recorded. Each set has a corresponding fluid that gives the minimum fringe shift (minimum deviation for expected contour). For GDP the best match occurred with the fluid index between 1.556 and 1.558; thus, we estimate $n_D = 1.557$. For Ge-GDP, the best match occurred at $n_D = 1.564$. After conversion with the Cauchy equation, we determine the refractive index at 532 nm for GDP and Ge-GDP is 1.563 and 1.570, respectively.

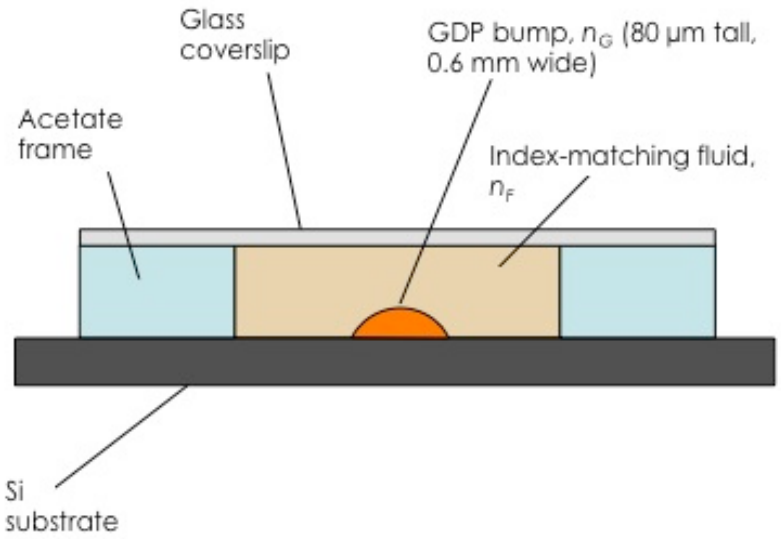

Fig. 5-2. Side-view schematic of GDP in index-matching fluid frame. The fluid was changed until the fringe shift by interferometry was minimized.

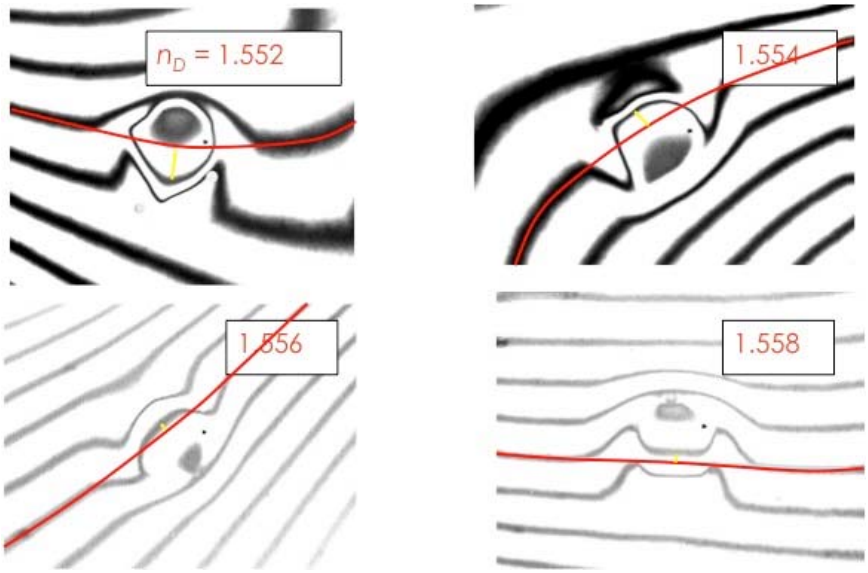

Fig. 5-3. Interference fringes for varying index-matching fluids over the GDP bump. The fringe shift was minimized with a fluid index n_D between ~1.556 and 1.558.

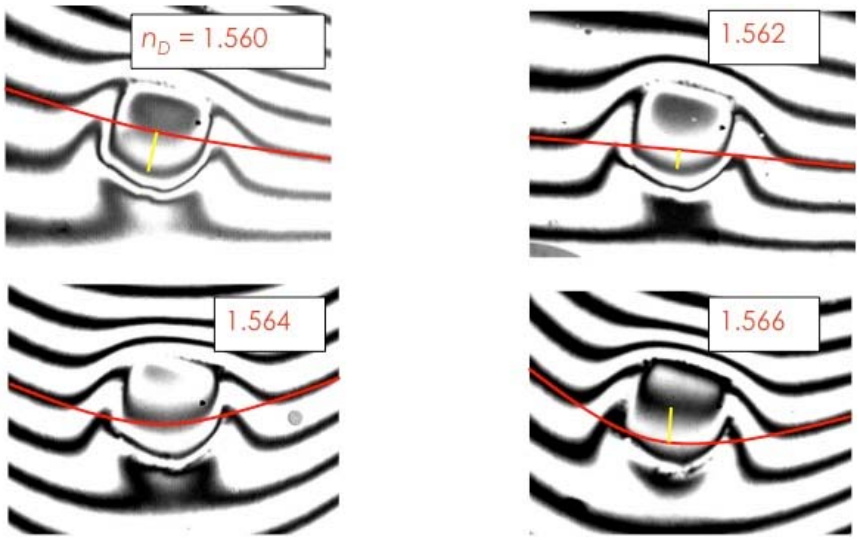

Fig. 5-4. Interference fringes for varying index-matching fluids over the Ge-GDP bump. The fringe shift was minimized with a fluid index n_D 1.564.

5.3 Improving Microstructure Detection On Xradia MicroXCT Microscope

High image resolution (~1.3 μm/pixel) and precision positioning capability make Xradia x-ray microscopy an attractive platform to study x-ray opacity variations. It can complement Precision Radiography (PR) as an instrument with much higher spatial resolution. PR measures x-ray transmission intensity variations down to 0.01% at 100 μm resolutions. Since the requirement to differentiate minute lateral variations in x-ray transmission intensity scales inversely with the spatial resolution, an x-ray imaging microscope such as X-radia MicroXCT can be useful if it measures the transmission intensity variations to <1%. In normal practice, a number of imaging artifacts limit the intensity measurement to only ~2% precision. Such artifacts include the thermal drift and the illumination uniformity of the x-ray source, and thickness variations in the scintillator plate and the beryllium x-ray tube window. The conventional flat-fielding technique is not effective against the dynamic interaction between the beryllium window texture and the moving shadow cast by a moving x-ray spot (Fig. 5-5), leading to an orange peel artifact (Fig. 5-6).

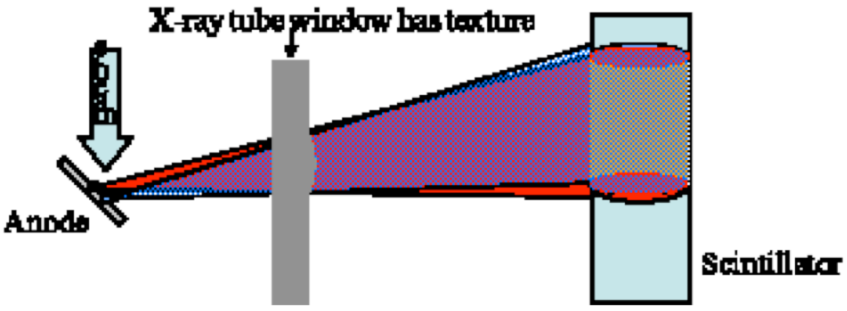

Fig. 5-5. Schematics of "orange peel" formation mechanism.

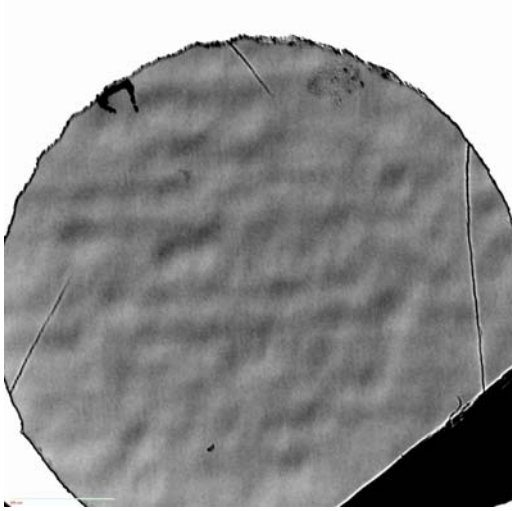
(a)
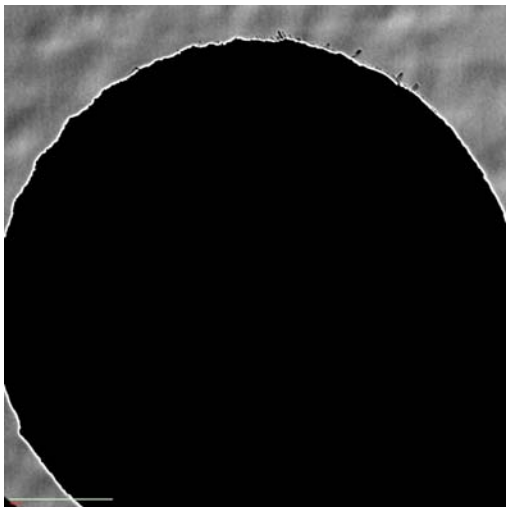
(b)

Fig 5-6. Distinctive "orange peel" pattern after flat-fielding affects both (a) the sample and (b) the background. The artifact limits the detection of subtle features in the sample.

We have modified the image processing routine so that the lateral variations in the transmitted intensity can be measured to ~0.3% precision on low-Z samples. This technique can be used to record microstructure variations in beryllium samples (Fig. 5-7). Currently the beryllium microstructures are characterized by Ultra Small Angle X-ray Scattering on a synchrotron source, which are not commonly accessible, expensive and have a long turn-around time. This Xradia based method has the potential to make it a routine measurement.

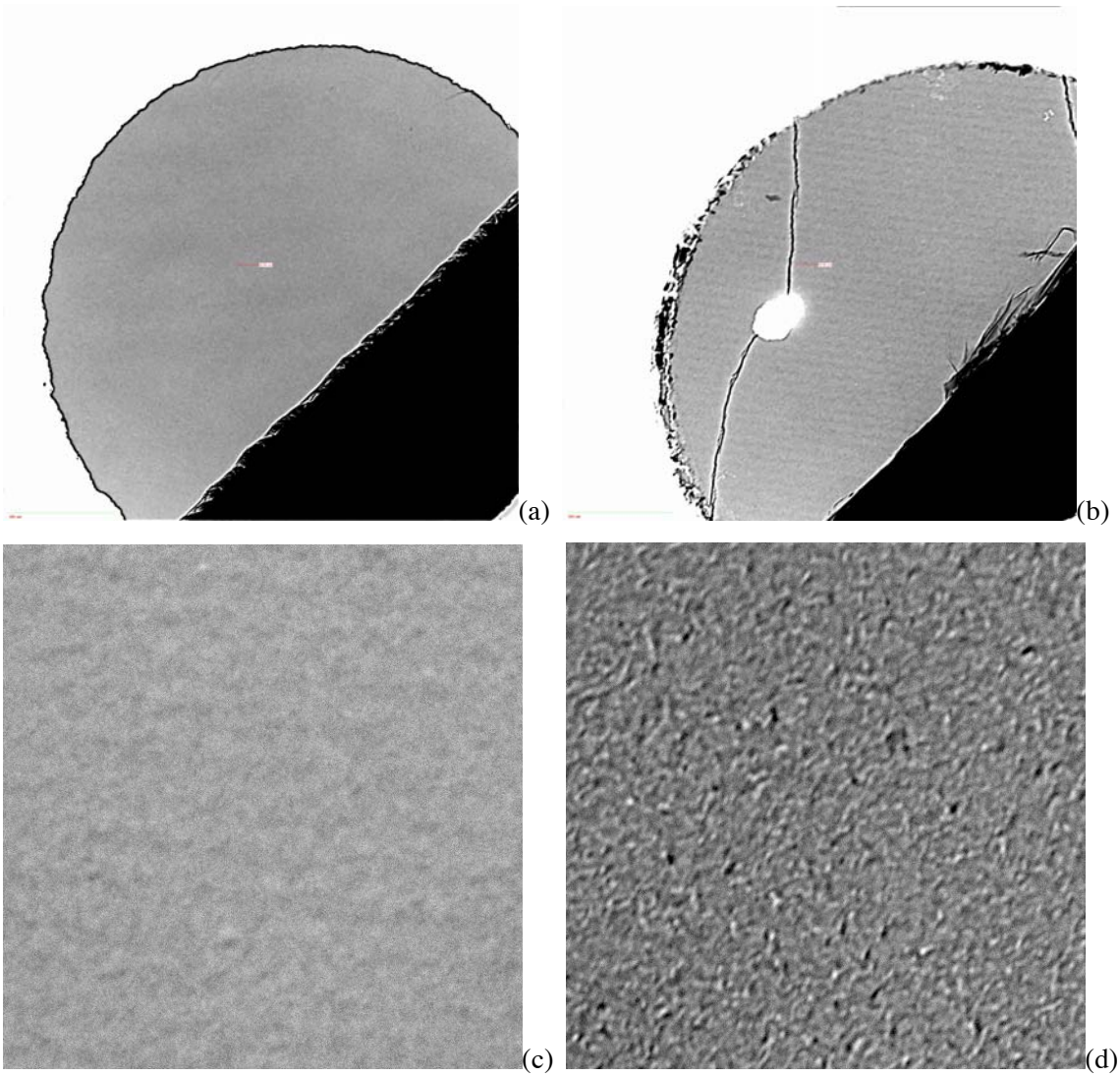

Fig. 5-7. New method enables the suppression of "orange peel" and the inspection of subtle sample details. (a) GB68-22: Sample with smooth surface; (b) GB14-22: Sample with machined sine wave with 25 μm periodicity, 0.25 μm peak-valley depth amplitude on 70 μm average thickness; (c) GB14-22: Sine wave details and residual grain texture; (d) GB65-19: Coarse grain texture of a bad sample.

5.4 Fabrication Of Backlighter And Enhanced Coupling Targets Via Lithography

There are a variety of ICF related laser experiments that require radiography as a diagnostic at the time of the experiment. In many of these situations it is convenient to use the emission from a secondary target to back light the primary experiment. Frequently, these backlighters are simple metal foils cut into squares hundreds of microns across. However, it is advantageous in some experiments, to have the backlighter approximate a small point source. To minimize the emission spot size, it is necessary to have a backlighter with a small cross section in the line of sight of the target. By using a micro-wire it is possible to have a small cross section yet still have a large enough object to easily target with the laser and to

create sufficient plasma volume. If the wire is supported by a low Z substrate, the background emission is relatively low compared to the backlighter signal. The challenge is then to produce these targets reproducibly and efficiently.

Lithographed wire targets have recently been fabricated at GA for use as backlighter targets for experimental campaigns at the OMEGA laser facility. Experiments such as CompRad, Brems, and 3ωCR required targets with 10 μm gold wires lithographed onto plastic. During FY10, a process was developed using lithography to make these targets via sputter coating and liquid solution removal of the resist (Fig. 5-8). One of the challenges overcome in developing this target was depositing the gold so that it would strongly adhere to the plastic. The quality of the lithographed targets was much better than targets made by other methods, such as gluing or thermal techniques. The lithographed targets were straighter, which is important in order to minimize the emission spot size at shot time. The lithographed targets also did not have problems with plastic or glue covering the wires, which can also reduce target emission, another challenge for gluing or thermal techniques. Lithography also allows a large number of similar targets to be made at once and cut out to the individual size needed, and a wide range of complex patterns or designs are possible using this technique.

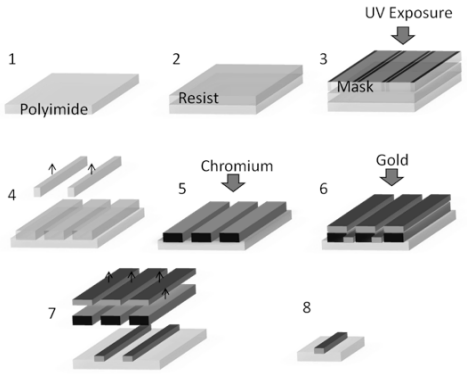

Fig. 5-8. Process steps of gold microwire fabrication. (1) Polyimide is mounted and cleaned. (2) Resist is coated. (3) UV light is exposed through a mask. (4) Resist is developed. (5) Cr seed layer is coated. (6) Gold layer is coated. (7) Resist and excess gold are removed. (8) Multiple targets containing a single wire are laser cut from larger substrate.

5.4.1 Fabrication of Backlighter Laser Targets via Lithography

Lithography is an ideal technique for fabricating backlighter targets. It is a powerful tool for creating small features that complements other laser target fabrication techniques such as mechanical micro-milling, diamond turning, laser machining and EDM. For these backlighters, a variety of alternative methods for fabrication of these targets are possible, but they lack the precision inherent in the lithographic technique. Although lithographic techniques are rather mature, they have only recently begun to be used for laser target fabrication. This may be because the general challenge of applying lithography is to design a process with compatible intermediate steps.

Backlighters were used for Compton radiography (CompRad), and cryogenic back-lighter (CryoBL) experiments at the OMEGA laser facility at the Laboratory for Laser Energetics

(LLE) in Rochester, NY (Figs. 5-9 and 5-10). This technique is suitably flexible so that other materials could be lithographed on plastic in a similar way.

In general, gold has poor adhesion to plastics, so a challenge in the lithography development was adhesion of the wires to the plastic substrate. At first, a plastic support film containing only carbon and hydrogen was requested as the laser target for these experiments. Polypropylene was attempted as a substrate because of its good chemical resistance to many of the materials used in the lithography process. Sputtering directly onto the plastic film, however, does not provide enough adhesion to survive the following steps of the process. In order to improve adhesion, a seed layer of 0.1 μm of chromium was applied before the gold layer. Unfortunately, the adhesion of polypropylene was still much lower than that of materials such as PET and polyimide, even when using a seed layer. It is most likely the reason for this difference in adhesion is in the chemical structure of the films: chromium creates a chemical bond to the polyimide while polypropylene does not. Goldberg, et al. proposed a mechanism for the surface interaction that requires Cr-O and Cr-N intermediates, which are not present at the surface of materials such as polypropylene.

Another adhesion challenge was caused by the resist not being developed to the bottom of the trench. When this happens, the deposited chromium does not form a bond to the surface of the substrate and the metal is removed during liftoff of the excess. This is not a problem once a set of optimum parameters for processes are chosen, but, when the process is being developed (or changed), this can be a problem. The difficulty lies in determining if the resist is developed all the way to the bottom of the trench. During development of the process this was done by sputter depositing a thin metal strip before the resist is coated onto the surface. This gives an interface that can be more easily seen via optical techniques such as interferometry. The substrate trenches in the resist can be further measured by SEM.

Another issue that had to be overcome was the liftoff process. At this step it is necessary for the excess gold and resist to be removed without damaging the substrate or removing the gold wires. This issue is closely related to the adhesion problems previously mentioned. Even with excellent adhesion between the metal wire and the substrate, this was still a problem. Although sputter coating is mostly directional in nature, it is conformal enough to create a thin layer along the sides of the trench that acts as a bridge between the gold wires and the gold excess on top of the resist. Having a trench depth that was much greater than the sputtered gold thickness solved this. At 27 μm thickness the trench was deep enough that the gold bridging between the excess and the wire was reduced to the point that it would tear before pulling the gold wire from the surface.

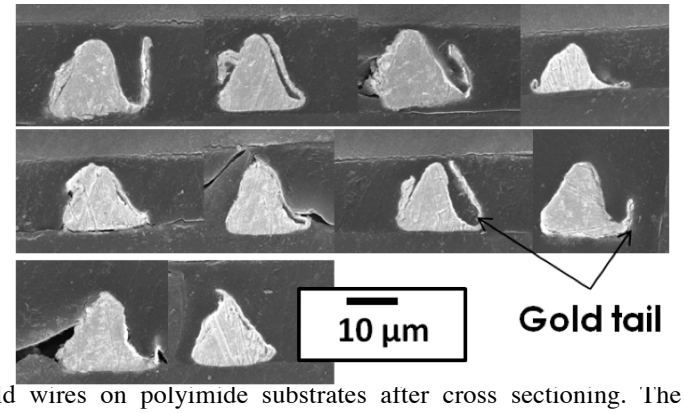

Fig. 5-9. SEM of gold wires on polyimide substrates after cross sectioning. The wires are consistently trapezoidal in cross section with the deposition parameters used.

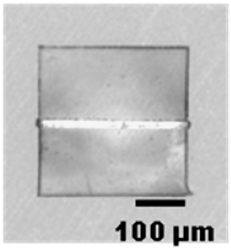

Fig. 5-10. Final gold wire target ready for mounting.

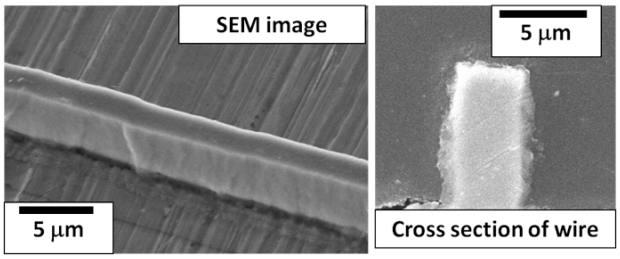

Fig. 5-11. SEM of electroplated copper wires on copper substrate. The image to the left is of a single wire out of an array, while the image to the right is after mounting and cross sectioning.

5.4.2 Lithography of Enhanced Coupling targets

We used a similar technique to produce the so-called enhanced coupling targets for LLE researchers which were fielded successfully at OMEGA. SEM images of such structure is shown in Fig. 5-12.

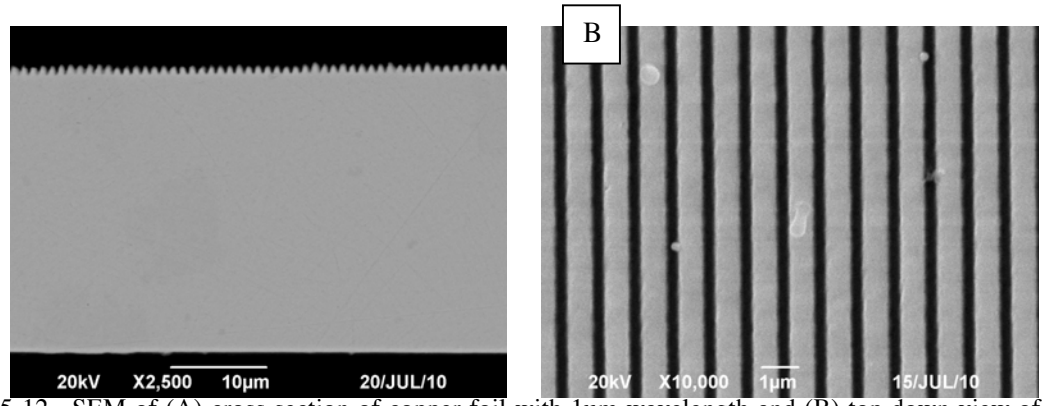

Figure 5-12. SEM of (A) cross section of copper foil with 1um wavelength and (B) top down view of copper foil.

5.5 Defect Capsule Fabrication Update

LANL is continuing investigations into equatorial perturbation effects. This investigation requires the use of banded targets. The desired bands consisted of trenches nominally either 5 or 8µm deep by ~30 µm wide.

This process starts with selecting a batch of PAMS mandrels with a very low mode 2 defect to achieve the best trench uniformity possible during the machining process. The PAMS mandrels were mounted individually on posts using a water-soluble glue. After mounting, the banded target was created in a stepwise fashion as illustrated in Fig. 5-13:

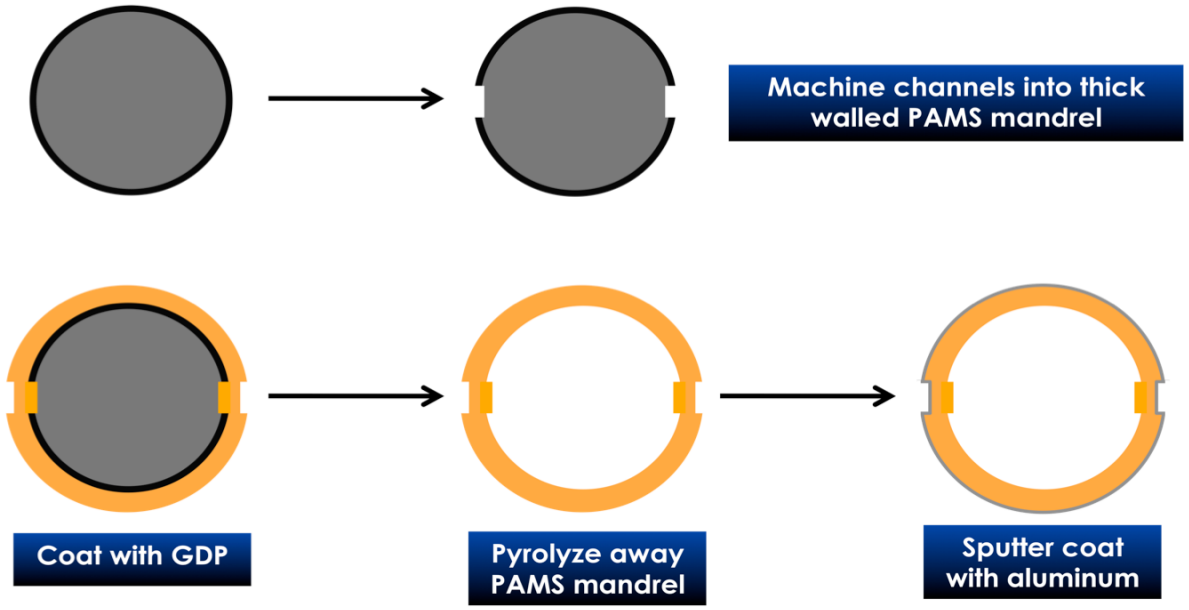

Fig. 5-13. Stepwise process for making a banded DImE target is depicted.

A 3D rendered example of a GDP capsule just prior to the Al coating step allows for much better visualization of the target and is shown in Fig. 5-14.

Fig. 5-14. 3D rendered trenched GDP mandrel.

After the GDP coating process each target had to be individually characterized 4π for diameter, wall thickness and uniformity using a combination of interferometry and x-ray radiography. Uniformity was determined by measuring the trench depth every 90 degrees by optical interferometry. Only capsules with a max-min trench depth of less than 1 μm were considered as potentially target quality. In addition to trench depth, the trench width and the thickness and geometry of the trench bottom needed to be measured. These latter parameters were determined by x-ray radiography. Fig. 5-15 shows the radiograph of a typical capsule.

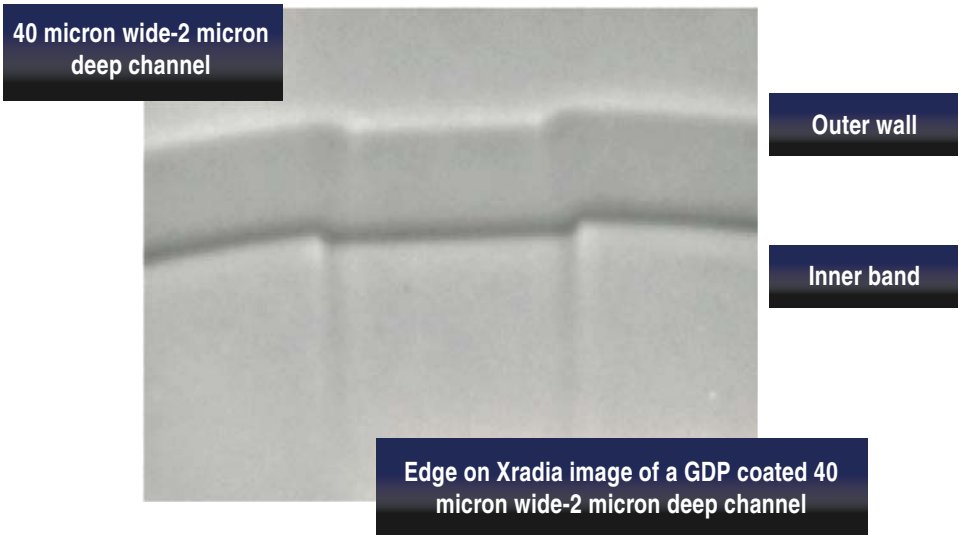

Fig. 5-15. X-ray radiograph of the banded capsule wall reveals the geometry, thickness, width and depth of the trench.

One of the final steps was to apply an Al coating to the capsules in order to form a gas barrier layer to allow for gas filling of the capsules. After the capsules were coated with Al, the individual D_2 half life for each capsule was measured by mass spectroscopy prior to delivery.

6 SNL TARGET DEVELOPMENT

6.1 GA Supported Research And Development

We have also undertaken research in support of the development of future target materials and types using GA's internal R&D funds. Four tasks were started in FY10. The first task was to produce germanium cylinders. Germanium is difficult to procure in the required dimensions and it is not readily machinable from an ingot. A fabrication process was devised in which pure powdered germanium was cast in a mold to the desired shape. To date, two cylinders have been prepared (Fig. 6-1).

Fig. 6-1. Germanium Cylinder after casting.

The second task was to study seven aluminum alloys for surface finish and strength. GA was able to locate a manufacturer of unique high strength, excellent surface finish alloys produced by a rapid solidification process. Three of these alloys will be included in the tests.

A third task was to fabricate cylinders out of materials that are difficult to machine. Examples of produced test parts include polished tantalum, aluminum coated sapphire, and beryllium coated sapphire. The tantalum part was polished down to exacting dimensions and mirror surface finish. The coated sapphire parts were over-coated with aluminum or beryllium and then back machined to achieve the desired dimensional and surface finish tolerances (Fig. 6-2).

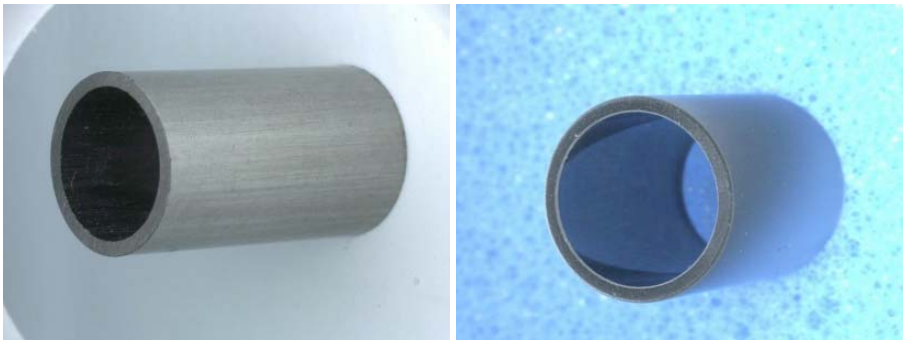

Fig. 6-2. Tantalum cylinder (left) and beryllium on sapphire (right).

The final task is to develop gradient density foams. The goal is to produce a foam with a 10 to 1 density reduction in 200 μm. The first approach was to add iron nanoparticles to a high density foam solution, then use magnetism to pull the nanoparticles to the bottom of the solution. The approach was not successful even though the nanoparticles did compact as needed. The flaw was that the nanoparticles aligned in layers, possibly aligning to the magnetic field. Further work is continuing using layers of solutions having the proper density.

6.2 Contract Supported Research And Development

The Z targets have been innovative in several regimes in FY10. This has lead to the need of new target designs and components. The beryllium cylinders required significant R&D to achieve the demanding dimensional and surface finish tolerances. While we had been machining flat beryllium parts for some time, the machining of cylinders presented new challenges. Thanks to focused attention to these challenges the first delivery occurred in February 2010 (Fig. 6-3). In addition to material research, GA also contributed to novel diagnostics for Z targets. We worked with the SNL VISAR diagnostic team to design a micromachined structure that will allow the VISAR diagnostic to probe the internal structure of the SNL targets.

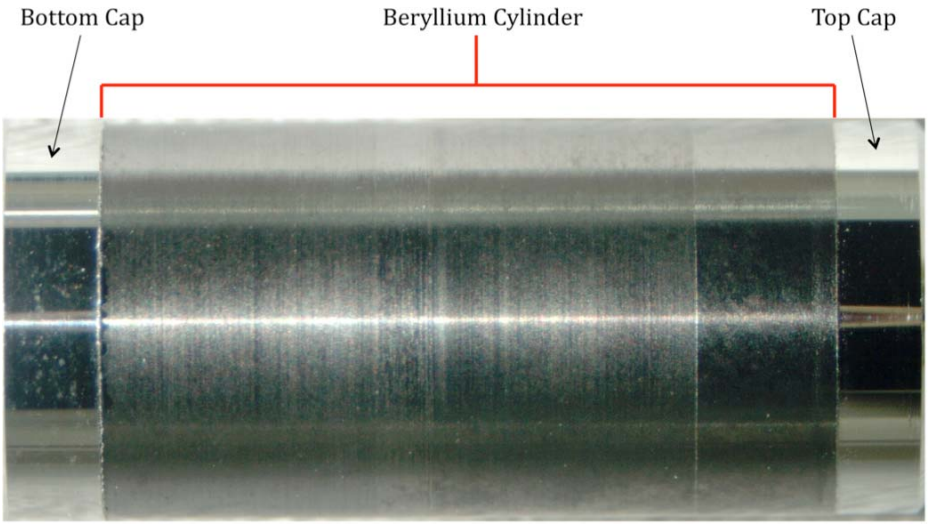

Fig. 6-3. This is an image of an assembled beryllium target. The center section is the beryllium cylinder. The two end caps are diamond turned aluminum.

The Dynamic Material Program also required the development of new techniques. The request was for 300 mg/cm^3 hydrocarbon foams. These foams were to be both pure CH_2 and to be doped 50% by weight with platinum nanoparticles. This was higher density than had been obtained before and was complicated by the challenge of a uniform doping at this high level. A technique was developed to use low molecular weight poly(4-methyl-1-pentene) polymer to make ~100 mg/cm^3 density solution and then using controlled solvent diffusion, allow the gel to become more dense before drying. The foams were made as circular disks

and then diamond turned to the required target dimensions. Figure 6-4 shows a 300 mg/cm^3 undoped foam after assembly into a panel.

Fig. 6-4. The white square in the center of the image is a 300 mg/cm^3 poly(4-methyl-1-pentene) foam.

7 OTHER TARGET DEVELOPMENT

7.1 Mass Fabrication Of Cones

In 2010, we have been investigating a number of methods for the mass fabrication of cones. These include injection molding of polymer mandrels, stamping of copper mandrels, a variation of the Guerin process of drawing, and cold forging. Where the process includes a mandrel, subsequent electroplating and mandrel dissolution steps are added.

For injection molding, we have built a mold for male cone mandrels for 30° cones, up to 2 mm long, see Fig. 7-1. After the polystyrene mandrel is removed from the mold, it is coated with a sub-micron layer of electrically conducting material (e.g. copper or gold using sputtering). The mandrel is then spray coated with photo-resist and exposed to UV using a contact mask to remove the photo-resist on the mandrel in the area of the cone. The mandrel is then electroplated. The result can be seen in Fig. 7-2. At this point, the mandrel is removed using solvents. If a definite exterior shape is needed, the cone can be machined on the mandrel before mandrel removal, or the cone can be used as a pre-form for cold forging to final shape.

Fig. 7-1. On the left is the injection mold machine, in the center is the four cavity mold for cone mandrels (mold face is 75 x75 mm), on the right are polystyrene mandrels as ejected from the mold, with runners still attached. Each mandrel is Ø3.2 x 34.3 mm long.

Fig. 7-2. Left, gold cones still on the photomasked, injection molded mandrels, mounted in electro-plating fixtures. Right, detail of tip. Gold cone height is 2 mm.

Gold cones with tapered walls have been formed by electroplating copper plates into which conical holes have been punched, see Fig 7-3. The wall thickness at the tip is very thin, <1 to 2 micron, for 2 mm deep 30° cones. The outer surface roughness of the cone formed in this way has been found to be similar to the surface roughness of the original punch.

Fig. 7-3. On left gold plated, punched copper plate, center shows gold cones fully released (cones 2 mm deep), right shows Xradia x-ray image of tip of a cone.

Aluminum cones have been fabricated in a variation of the Guerin process, wherein an aluminum sheet is placed on a polymer pad and a truncated conical punch pressed into the sheet. The polymer pad replaces the rubber pad of the usual Guerin process. Aluminum cones 1 mm deep with a 35° angle and 44 micron tip were fabricated with this process (Fig 7-4). The process produces parts with good repeatability. As an example, a set of 12 cones had an average tip diameter of 44 μm with a standard deviation of 1 μm, a tip thickness of 11.5 μm with a standard deviation of 0.6μm, an angle of 34.9° with a standard deviation of 0.1°, and a wall thickness at the mid-height of the cone of 23 μm with a standard deviation of 1 μm. As can be seen in Fig. 7-4, the outer tip is rounded. A second stamping operation can be used to produce a flat outer tip. Pressing on the tip with a flat plate, flattens the tip, see Fig. 7-5.

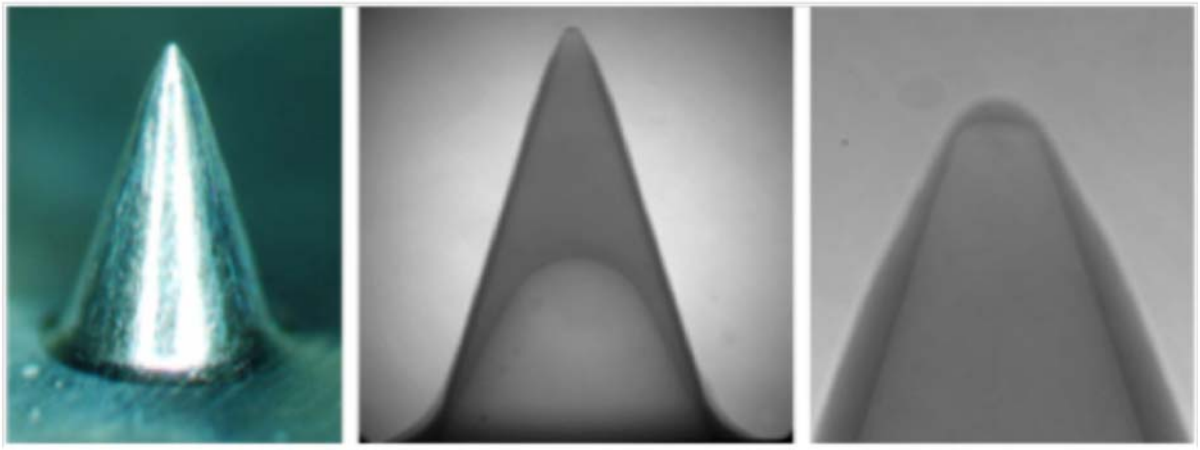

Fig. 7-4. On left 1 mm deep aluminum cone, center shows Xradia x-ray of cone right shows x-ray detail of tip. Tip diameter is 44 μm, tip thickness 11.5 μm.

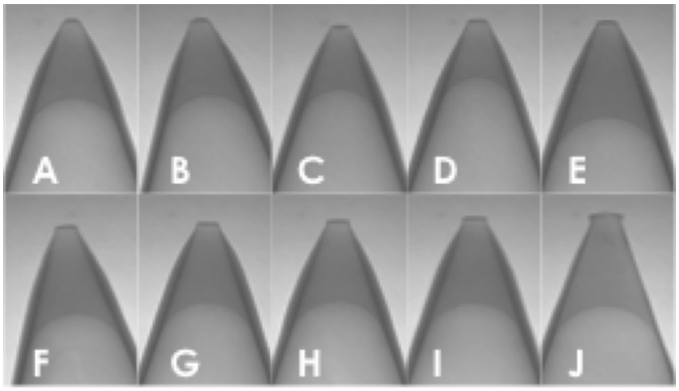

Fig. 7-5. Shows the tip of ten different 1 mm deep aluminum cones, after a second stamping operation to flatten the tip, each with a different applied force.

These techniques show promise for the mass production of cones. We plan to apply these methods to other target parts, such as hohlraums, in the future.

7.2 Automated Target Assembly System

GA continued development of an automated target assembly system. The system, shown in Fig 7-6, includes two commercial robot arms and a 3-axis piezoelectric stage to manipulate target components and glue them together at high throughput rates. A vision system with cameras at two orthogonal angles provides feedback to the piezo stage and robots for enhanced precision of parts placement. All operations are computer controlled.

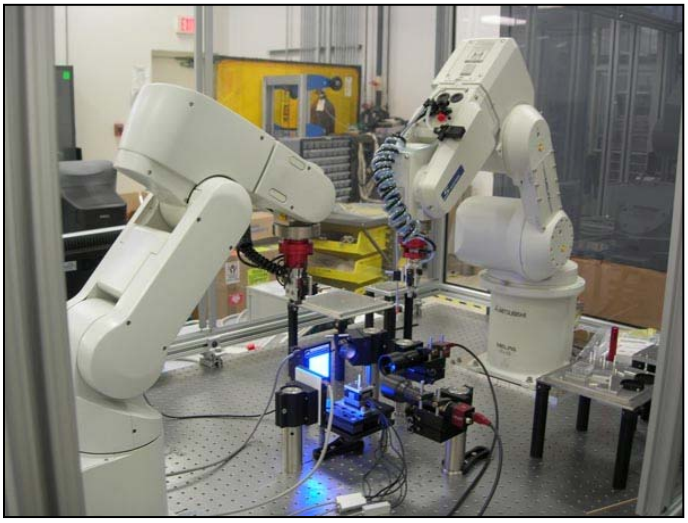

Fig. 7-6. GA-developed automated target assembly system.

Two types of targets were assembled using the system, cone-in-shell targets and "precision array" targets. The cone-in-shell targets consist of gold cones glued to PAMS shells that are mounted on carriers (Fig 7-7). The assembly system aligns the theoretical tip of the cone with the center of the shell to within ± 10 μm prior to gluing (see Fig 7-8). Operations are done in batches through the production process: a) glue shells to assembly

pegs, b) cut hole in tops of capsule with laser (done in separate station from the robot system), c) align and glue cones to capsules, d) glue carbon fiber mounting stalks to stainless steel carriers, and e) remove cone/capsule combination from handling post and glue to stalks on carriers. About 500 cone-in-shell targets can be assembled and mounted in a week.

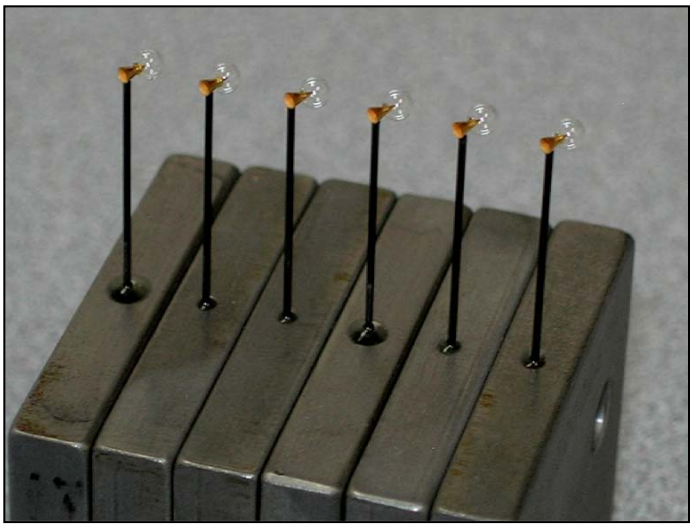

Fig 7-7. Cone-in-shell targets, assembled by GA's automated target assembly system.

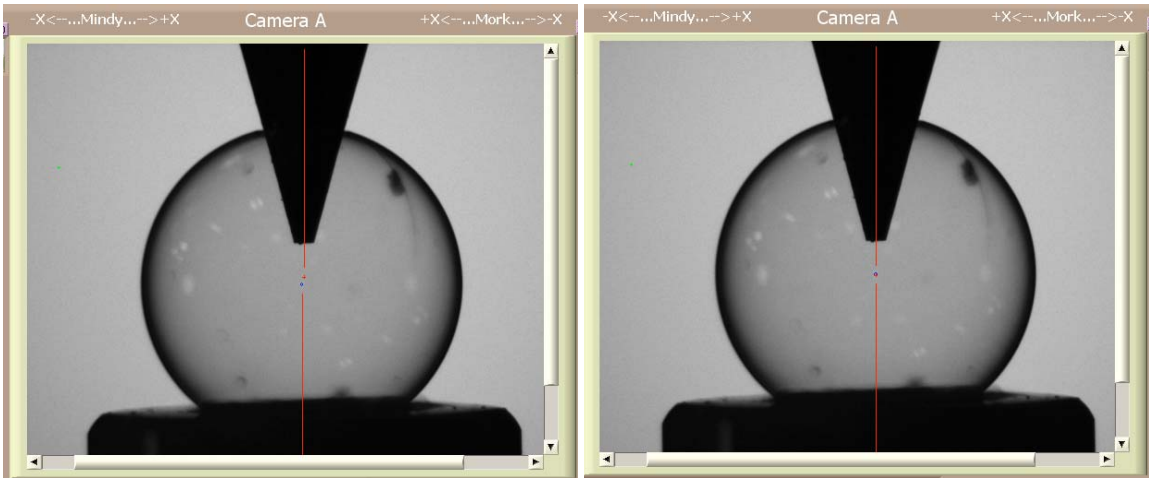

Fig 7-8. Screen shot showing how vision feedback is used to align cone and capsule. The blue circle represents a 10 μm region around the theoretical center of the capsule and the red cross represents the theoretical tip of the cone. The left photo shows the relative positions prior to alignment while the right photo shows after alignment

The precision array targets (Fig. 7-9) consist of 700 μm diameter discs cut from ~50 μm thick multi-layer foil and glued to graphite plates in a 10 by 10 array. Disk location uncertainty was kept <100 μm vertically and transversely to assure alignment during automated shot sequences. Some 1100 discs were assembled by the system in this manner.

The targets were characterized and later "shot" in experiments conducted by GA at the Rutherford Appleton Laboratory on the Gemini rep-rated laser.

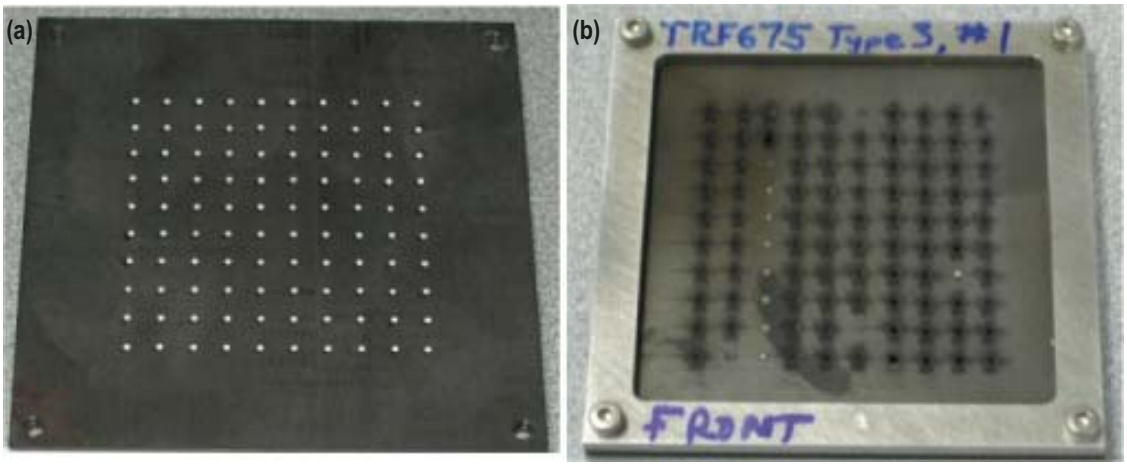

Fig 7-9. One set of some 1100 precision array targets assembled by the GA automated target assembly system, a) prior to testing and b) after being "shot" experiments at Rutherford Appleton Laboratory with the Gemini rep-rated laser.

The automated target assembly system is now being modified to assemble hohlraum components, including installation of thin films over the laser windows. New tooling and fixtures for this purpose have been designed and are being fabricated.

7.3 UV Polymerization of R/F

R/F aerogels are used in ICF experiments in the form of hollow microspheres (shells) for future direct and indirect drive targets at the National Ignition Facility (NIF) and for pilot Inertial Fusion Energy (IFE) power plant targets. These aerogels are synthesized using a 2-step (base/acid catalysis) polycondensation reaction developed by Pekala et al. An alternative method called dielectrophoresis (DEP) is being investigated to center and fabricate these R/F shells. DEP uses an electric field to move and center the shell while it is in its double emulsion form. The University of Rochester (U of R) has developed a 20 MHz device and technique that uses DEP to center a double emulsion of water-oil-water. The work done by Bei, et al. provided the parameters for the aerogel precursor solution to work in the device. One of these parameters is that the conductivity of the aerogel precursor solution needs to be in the 10^{-3} S/m range or lower, the other requirement is that the precursor solution must gel at room temperature (RT) in 20 minutes or less. Based on these requirements our traditional R/F formulation used to fabricate shells can not be used by the U of R DEP device due to it's high conductivity $5X10^{-2}$ S/m and it's current gelation time at RT (6-8 Hours). This issue led to the investigation of modifying the R/F formulation to fit these parameters.

Before modifying the traditional reaction, conductivity measurements were taken of each component in the formulation. The conductivity results shown in Fig. 7-10 show that it is the acid and base catalyst that increase the conductivity of the R/F precursor solution. This is an issue because these are the catalysts that drive this reaction. These results lead to the investigation of other ways to synthesize R/F, which led to the investigation of using UV-free

radical initiators to replace the current catalyst. One issue with using a UV free radical photo-initiated system is that it can only be used to gel or polymerize in the form of a thin film, but this works for our situation since our shells are a thin film in a spherical orientation.

Modification to the traditional formula were done two ways, the first (Modification 1) was done by replacing the acid catalyst with a UV free radical photo-initiator (Irgacure 819), the second modification (Modification 2) was to replacing both the acid and base catalyst with a UV free radical photo initiator (Irgacure 819). To test if the solution would gel, a droplet of the precursor solution was placed into a vial filled with mineral oil and sorbitan monooleate (Span 80). A small amount of tetrachloroethylene was added to keep the droplet suspended. The droplet was then exposed at RT with UV light using a Green Spot point source unit (American Ultraviolet); this unit uses a super-pressure 100-watt mercury lamp with peak intensity at 365 nm. An illustration of the vial test process is shown in Fig. 7-11. If the modification produced a gel, the precursor solution was used to fabricate shells using our triple orifice droplet generator (DG). A summary of these modification experiments that displays the gelation time, conductivity and its pH change during the gelation process and how it compares to the traditional process is shown in Fig.7-12.

Modification 1 starts off with the traditional base catalysis step; this would start the reaction and create the hydroxymethyl aggregates, which react with one another to form the primary particles to set up the hydrogel. After this step, 0.10wt% of the initiator (Irgacure 819) was added to the precursor sol and mixed to suspend or dissolve the photo-initiator. The results of the vial test show that the droplet of the modification 1 solution when exposed to UV light gels into a hydrogel in 5 minutes. The hydrogel was then solvent exchanged and dried using a CPD. SEM images in Fig. 7-13 show that the pore structure is similar to R/F synthesized with the traditional method. The SEM also has an energy dispersive x-ray analysis (EDX) that analyses the surface of the foam, which showed that the foam is still made up of carbon, hydrogen and oxygen. The density was also measured gravimetrically and is as calculated at 100 mg/cc. Optical images in Fig. 7-14 show that the surface has a rough skin, which could be an issue with the surface of the foam. Conductivity was also analyzed and the conductivity (3.3×10^{-2} S/m) was still too high for the DEP device due to the carbonate in the precursor solution. Despite the conductivity this showed that UV free radical photo initiators could be used to replace the acid catalyst and still form an R/F aerogel.

Because the modification formed a gel, it was then used to form shells in the droplet generator (DG). With the proper density matching modification R/F shells were successfully fabricated. Having the shells cure at RT will provide an advantage to the current DG process because we would no longer have to fight the density mismatch at a higher temperature. Also the faster cure time would be an advantage for production purposes. The shells and beads fabricated on the DG showed much less skin on the surface than the beads fabricated with the vial test (Fig. 7-15**).** This suggests that the skin may be due to the way the shells and beads were exposed to the light, the DG shells are rotated and more evenly exposed than the bead exposed in the vial test. SEM images of the DG shells pore structure are also similar to the aerogel fabricated using the vial test and the traditional R/F. Density, and EDX data was

similar to the R/F bead fabricated with the vial test. The pH of the R/F solution was also monitored; the results show that once the photo-initiator is added and activated with this modification that the pH goes from 5 to 3. This suggests that an acid is forming once the free radicals are initiated by reacting with the water, or the hydroxyl groups on the primary particles. From this one may suggest that the same reaction is occurring due to the changing of the pH. But because the solution gels from a water like liquid to a gel at RT a lot faster than the traditional method which takes 20 minutes at 70°C, it suggests that something else is driving the reaction besides the formation of an acid.

In Modification 2 both the base and acid catalyst are replaced with UV-free radical photo-initiator. The hope was to treat this still as a two step process in that a photo initiator would be used like the base catalyst to form the hydroxymethyl aggregates which react with one another to form the primary particles. This would be then followed with more initiators to bring these primary particles together to form the gel. In the first step the photo initiator (0.10 wt%) did not fully dissolve into the sol when exposed to the UV light as the first modification. Because of this we added acetonitrile to the precursor solution to help dissolve the photo initiator. The solution was then exposed with UV light for 15 min, the sol turned into a dark orange solution, without the acetonitrile the solution did not turn dark orange. The dark orange color is similar to the solution color of the traditional R/F solution, which is a good sign that the primary particles are forming. The pH of the solution at this stage went from 7 to 5. After this step, more initiator (0.10 wt%) was added to help bring these primary particles together to form the gel. The vial test results from modification 2 gelled in 10 minuets at RT. The solution in the curing step also changed in pH from 5 to 3, similar to the first modification 1. The measured conductivity of this R/F solution without the carbonate or acid was also measured to be an order of magnitude lower at 3.3×10^{-3} S/m, which meets the conductivity specification to be used in the DEP centering device. The gelation time of 10 minutes at RT also satisfies the second requirement for the DEP device, which makes this a candidate formulation.

Like the first modification the SEM images (Fig. 7-13) show that the pore structure is similar to the traditional R/F. Gravimetric density and EDX results are similar to modification 1. Like the beads fabricated using modification 1, the beads still have a skin on the surface; optical images are shown in Fig. 7-16A. This solution was also used in the DG process but the acetonitrile in the precursor solution made the emulsion unstable causing the uncured shell to collapse into a bead before the shells cured. Like the first modification the beads that survived the DG process had little to no skin (Fig. 7-16B). Despite these results, this shows the proof of principle that the R/F aerogel can be synthesized using only UV free radical initiators.

R/F Formulation Components	Conductivity (S/M)
DI Water	$6X10^{-6}$
Formaldehyde	$3.3X10^{-3}$
Carbonate Solution (Base)	$3.5X10^{-1}$
Benzoic Acid Solution	$2.83X10^{-2}$

Fig. 7-10. Conductivity results for each component of the traditional R/F formulation show that the acid and base catalysis are the components that increase the conductivity of the precursor solution.

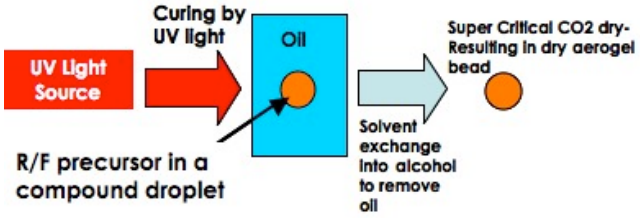

Fig. 7-11. Illustration of the vial test used to check if the modification using UV-Free radical initiators can synthesize and form the R/F hydrogel.

Modification	pH During Step 1	pH After Step 1	pH During Step 2	Conductivity (s/m)	Gelation time (vital test)	Gelation time (DG)	Meets DEP Centering device spec.
Traditional	10	6	3	5x10-2	20 min (70C)	2 hours (70°C)	No
1	10	6	3	3.3x10-2	5 min (RT)	15 min (RT)	No
2	6	3	3	3x10-3	10 min (RT)	20 min (RT)	Yes

Fig. 7-12. Summary chart of the modifications investigated in finding a formula that would work in the DEP centering device, and to test if UV Free radical initiators can synthesize R/F aerogels.

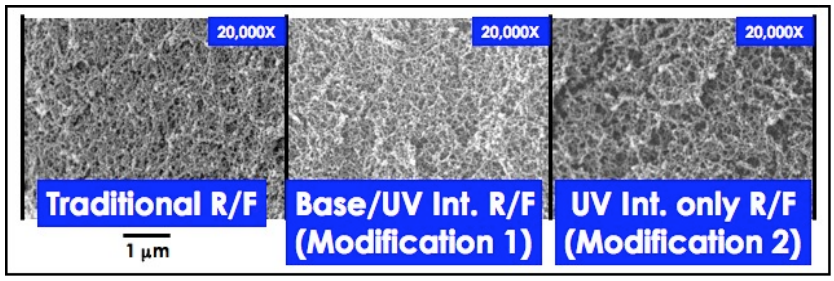

Fig. 7-13: SEM images of Traditional R/F, R/F made with replacing the acid catalyst with Photo-initiator (Modification 1) & R/F made with only UV initiator (Modification 2). Pore structure for all three look very similar with a pore size of less than 0.10 µm.

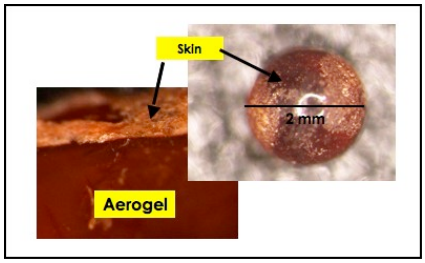

Fig. 7-14: Optical Image of a R/F aerogel bead fabricated by the vial test using modification 1 (Base/Photo Int.). The aerogel has a skin on the surface of the bead.

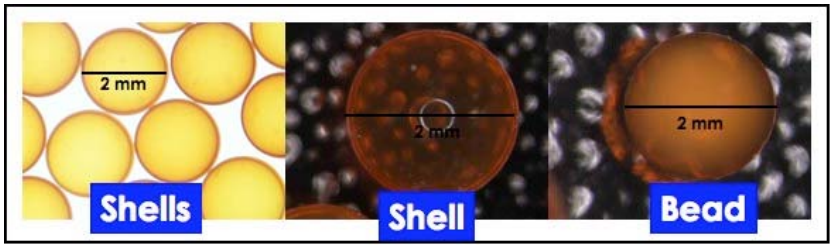

Fig. 7-15: Optical images of shells and beads fabricated using a DG with R/F modification 1 ((Base/Photo Int.). The shells and beads have little to no skin on the surface when compared to the beads fabricated with the vial test.

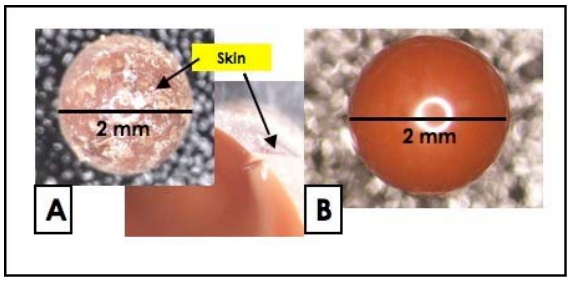

Fig. 7-16: Optical images of R/F aerogel beads made with the vial test using modification 2 (UV Int. only). Skin can be found on the surface of the bead. Optical image of a R/F aerogel bead made with the DG using modification 2 (UV Int. only). Little to no skin can be found on the surface of the bead when compared to the vial test.

Conclusion

These experiments helped produce a new way to synthesize R/F aerogel using UV-free radical initiators. These aerogels have a similar pore structure to the traditional R/F aerogel and can be cured at RT using a UV light source faster than the traditional method at RT and at 70°C. This was done by modifying the traditional formulation by either replacing the acid catalyst, or replacing both the acid and base catalyst. This work also produced formulations that are suitable to be used in the DEP centering device developed by U of R to center R/F shells, and these formulas also have the potential to be used in the traditional DG method to fabricate shells.

7.4 Deuterated Plastic Foils For Magnetic Recoil Spectrometer

In FY10 General Atomics supplied foils to NIF and OMEGA for use on Magnetic Recoil Spectrometers (MRS). The MRS diagnostic has been installed on both OMEGA and NIF for measuring the absolute neutron spectrum from experiments. The technique relies on a deuterated plastic (CD) foil to convert neutrons to deuterons (through forward scattering) that are then measured by a magnetic spectrometer. In this application, uncertainties in the deuteron density or uniformity of the foil will ultimately contribute to the relative error in the neutron measurement. Therefore it is essential to know the absolute deuteron density of the plastic foil and to fabricate a disk as uniform as possible. In FY10, GA was able to develop a reliable process to produce uniform foils and a method for characterizing them.

GA collaborated on this project with Kurt Fletcher of SUNY Geneseo, who had produced the original foils for the OMEGA MRS. However, two issues were apparent in the process when GA began. The foils had optical opacity non-uniformities that suggested a density variation in the foils, and no characterization for areal density uniformity was being done prior to use.

The non-uniformity of the foils was due to a high mode "blotchy" pattern and a low mode thickness non-uniformity. GA eliminated the high mode blotchy pattern by pressing the foils at a higher temperature in order to assure a more uniform melt while under pressure. The low mode thickness problem manifested itself as a wedge shape (with one side thicker than the other) or a flying saucer shape (with the middle thicker than the edges). The wedge shape was cause by uneven pressure applied, and the saucer shape was from insufficient applied pressure. Both thickness issues were mitigated by GA investing internal funds to acquire an industrial 4-post, computer controlled, hydraulic heat press. This press allowed much higher pressures to be applied and had a much higher degree of parallelism of the platens. It also allowed much better reproducibility from part to part in the pressing.

GA was able to quickly apply the contact radiography and analysis techniques developed for measuring dopant profiles of NIF ignition capsules in order to characterize the disks fabricated. As shown in Fig. 7-17, the blotchy pattern was visible in the radiographic image, qualitatively showing that the blotchy pattern was indeed due to an areal density non uniformity in the foil. Quantitative radiographic analysis verified that the improved GA technique produced foils that were much more uniform than the original Geneseo technique. As shown by the histogram and plot in Fig. 7-18, both the total variation and FWHM variation were dramatically improved. This data also provided important feedback to the PIs involved with the instrument.

As a result of this development work, 30 foils were supplied to NIF and 4 were supplied to OMEGA. Below is a comment from the customer, Johan Frenje, on the quality of GA's effort:

> "For an accurate neutron-yield measurement, using the MRS at the NIF or OMEGA, it is essential that the thickness, area and density of the DPE foil are well known. The deuterium-number density is another parameter that must be accurately known as well. These parameters were either poorly known or

displayed large unacceptable variations for the foils made by another manufacturer. To address this issue, we contacted GA who developed a new method for manufacturing these foils to well within specifications. The resulting GA-made foils are of such high quality that the systematic uncertainty associated with the neutron-yield measurement got reduced ~2 times, which has a big impact on the diagnosis of an ICF implosion."

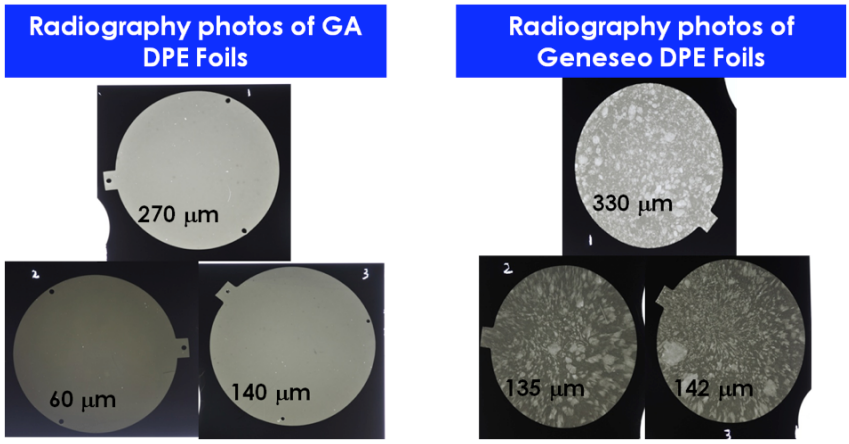

Fig. 7-17. Radiograph images of GA (A) and Geneseo (B) deuterated polyethylene. The diameters of all the disks shown are all 45mm. Qualitative differences in the areal density can easily be seen between the types of foils.

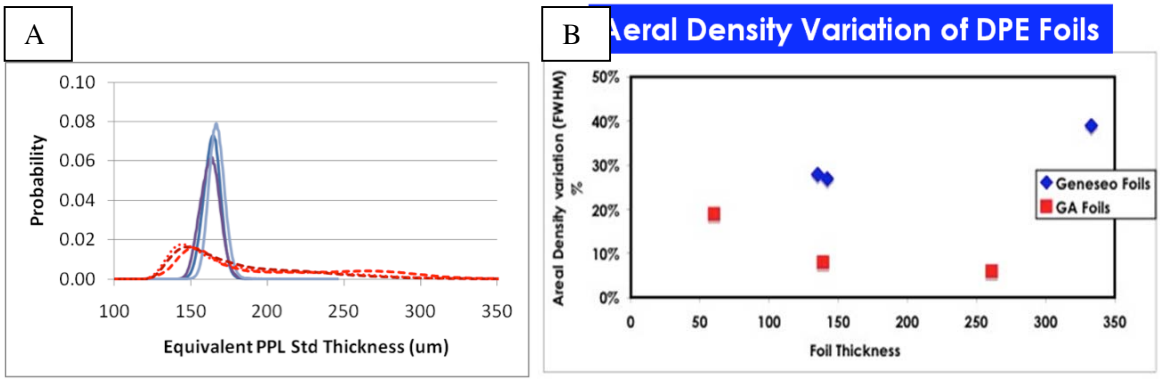

Fig. 7-18. (A) Histogram of areal density of 3 areas of the GA (blue solid lines) and Geneseo (red dotted lines) foils. (B) Plot of areal density variation comparing the full width half maximum (FWHM) of GA and Geneseo foils.

7.5 Electrowetting

Electrowetting (EW) technology offers precision droplet dispensing, transport, and merging without the use of pumps, valves, or even pipes. If a liquid partially bridges energized parallel plate electrodes, the liquid will move to fill the gap between those electrodes [Fig. 7-19(a)].

In FY2010, GA began work with electrowetting technology for capsule production. First, a photolithographic chip fabrication process was developed at GA. With photolithography,

GA can design electrode geometries for custom droplet manipulations [Fig. 7-19(b)]. Next, coating research was performed to make the EW chips more robust. With layout design and Labview control, GA built an automated droplet dispensing process [Fig. 7-19(c)]. Work is ongoing to build more complex processes.

GA made significant progress troubleshooting the biggest obstacles preventing this technology from capsule production and widespread use in industry: dielectric failure and satellite droplet formation. State-of-the-art atomic layer deposition (ALD) dielectric coatings were used to extend the chip lifetime from minutes to days. Furthermore, experiments and physical modeling of satellite droplet formation refined the notion of robust electrowetting processing. A publication is in preparation.

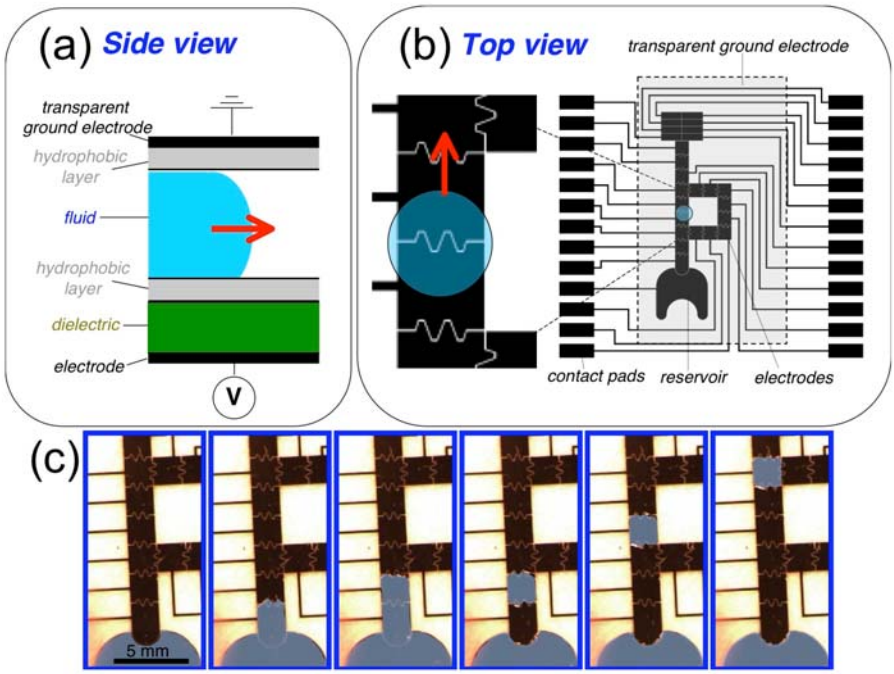

Fig. 7-19. (a) Side view of a droplet moving on an electrowetting chip, detailing the chip's layers. (b) Top view of a droplet moving on the electrowetting chip's grid of electrodes. (c) Top view of automated dispensing and transport of 0.5 μL of deionized water. The dielectric is 400 nm ALD alumina/30 nm Teflon, and the voltage source is 25 V_{rms} at 250 Hz. The water is appears blue with software enhancement.

7.6 Rippled Ta Targets For Material Strength Measurements Via Rayleigh-Taylor Instability

GA produced sputtered-rippled Ta targets for shots on OMEGA-EP to study Ta material strength via Rayleigh-Taylor instabilities. Figure 7-20 shows how the Ta target is utilized in the experimental setup.

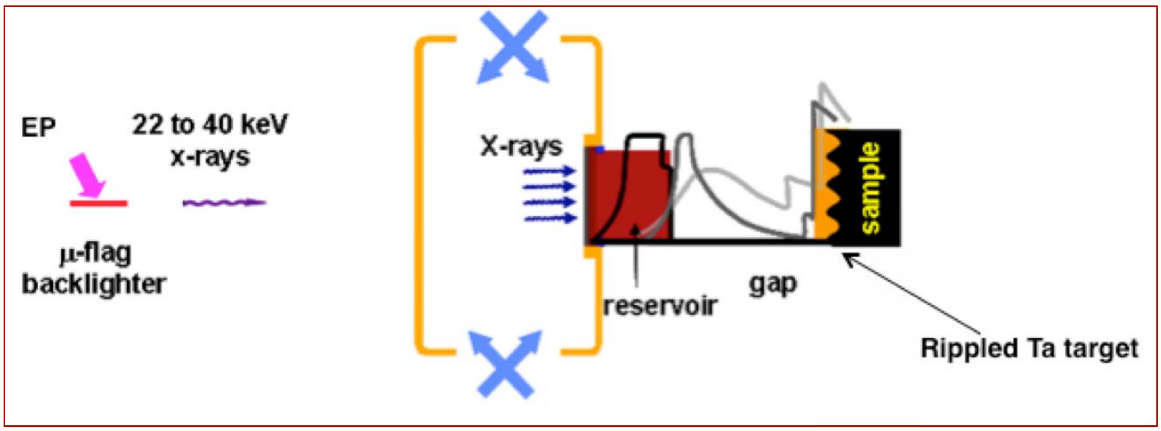

Fig. 7-20. Experimental setup using a rippled Ta target.

Bulk Ta has a larger grain size than sputtered Ta, smaller grain sizes are sought after to do a comparison of growth factor between larger grained bulk Ta and smaller grained sputtered Ta (Fig. 7-21).

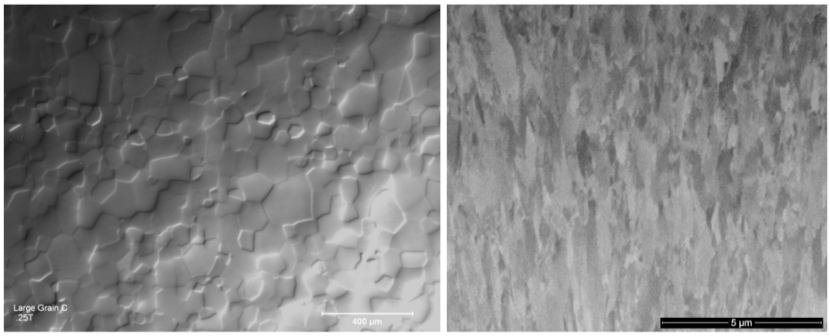

Fig. 7-21. Larger grained size sample on the left, smaller grained sputtered sample on the left.

The smaller grain size was achieved by heating the substrate during sputter deposition; this allows us to control the grain size. Specialized fixtures were developed at GA for this application. The sputter deposition took place on machined Cu molds that had the ripples machined into them using an off-axis diamond turning method to produce the ripples with as little arc as possible. Using diamond turning we achieved wavelengths of 50 and 100 μm that had peak-to-valleys of 5 μm. An Al release layer deposited on the surface of the machined Cu mold, following this precision masks were placed on top of the mold and Ta was sputtered onto the surface. The ripple features translated through the coating to yield ripples on the backside, these were removed by polishing since ripples were only called for on one side. Figure 7-22 shows the puck as deposited out of the coater and post polishing, note the absence of the ripples in the last photo.

Fig. 7-22. Shown here is the Cu puck with deposited Al and Ta at various stages of processing.

Finally the individual Ta pieces are leached off the Cu puck using NaOH to dissolve away the Al and release the free standing Ta. Figure 7-23 depicts a final part with the rippled side on the left and the polished side on the right.

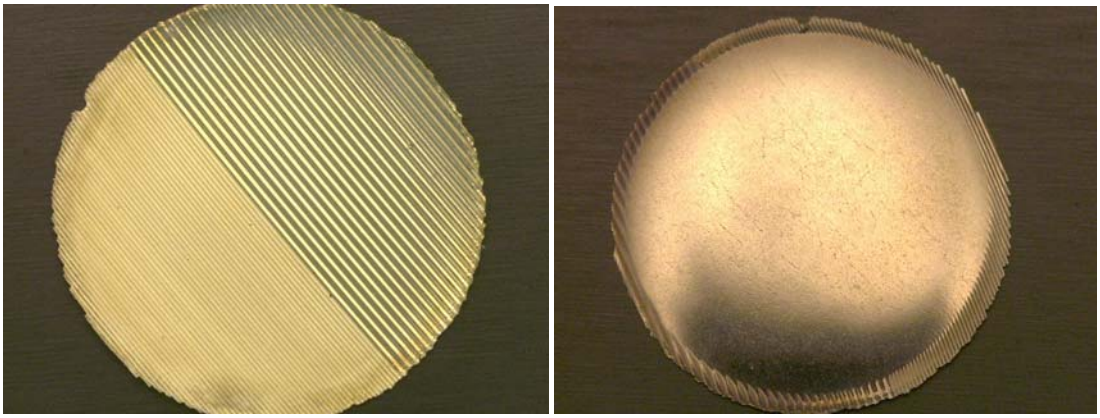

Fig. 7-23. Picture on the left shows the dual wavelength pattern. Picture on the right shows the polished side.

Next these parts undergo characterization for ripple wavelength, thickness, and density. Wavelengths are found using WYKO, see Fig. 7-24.

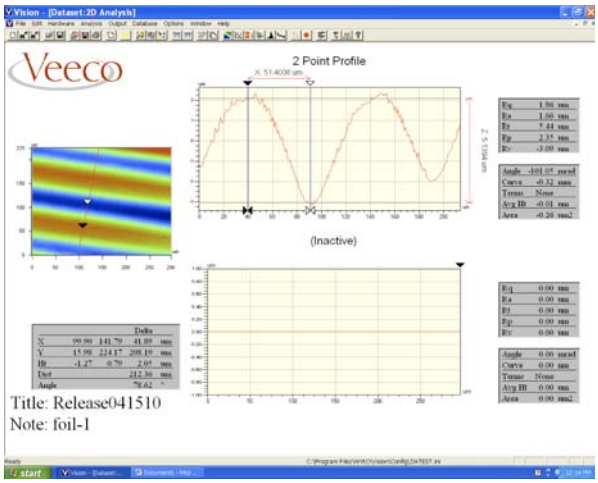

Fig. 7-24. Typical WYKO scan of rippled Ta part. This scan shows the peak to valley to be 5 μm and the wavelength to be 100 μm.

Density is measured using the Archimedes principle since the shape of the sample is irregular making the volume difficult to approximate. The Archimedes principle is well known and states that the buoyancy force equals the weight of displaced liquid. The sample is measured out in air then in a beaker of ethanol, the weight difference between the two measurements is equal to the volume of displaced liquid (Fig. 7-25). Assuming the volume of displaced ethanol is equal to the volume of the Ta part we find density by simply measuring the mass and dividing the mass by volume to get the density. The 1-sigma standard deviation is found by taking multiple density measurements using the same sample, and the accuracy is found by finding the density of a well-known standard.

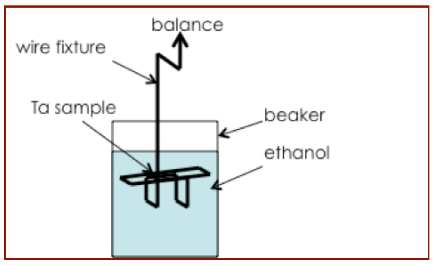

Fig. 7-25. Experimental setup of finding the volume of the sputtered Ta parts using the Archimedes volume technique.

Finding the metal thickness was achieved by using the dual confocal. It is essentially a laser interferometer that has a measurement error on the order of ±0.2 μm (Fig. 7-26).

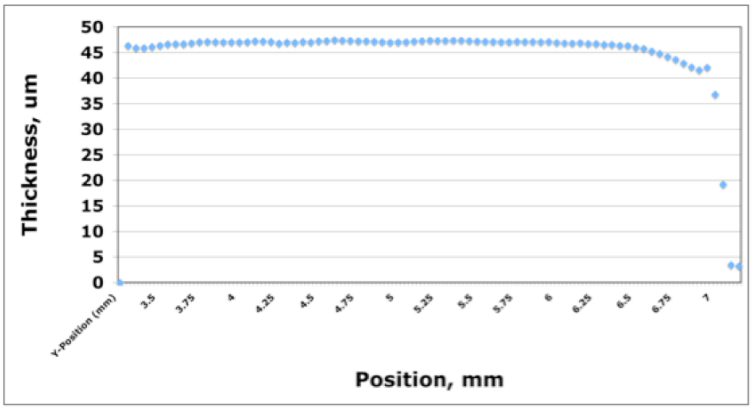

Fig. 7-26. Sample thickness as a function of its position along the Ta sample. Notice how the data drops off at the end indicating it has reached the end of the part.

8 PUBLICATIONS

8.1 List of Publications

Alfonso, E.L., Clark, A.A., Steinman, D.A., Stephens, R.B., "Techniques to Measure the Refractive Index of GDP and Ge-Doped GDP in Monochromatic Light for VISAR Experiments," Proc. the 19th Target Fabrication Mtg., Orlando, Florida, 2010, to be published in Fusion Sci. Technol.

Alfonso, E.L., Moreno, K.A., Wilkens, H.L., Jaquez, J.S., Nikroo, A., "Sub-Micron Gold Coating Measurements for Hohlraum Development," Fusion Sci. Technol. 55(4), 424 (2009).

Alger, E.T., Dzenitis, E.G., Mapoles, E.R., Klingmann, J.L., Bhandarkar, S.D., Reynolds, J.G., Florio, J.W., Lord, D.M., Castro, C., Segraves, K., "Experimental D-T Ice-Layering Target Assembly," Fusion Sci. Technol. 55(3), 269 (2009).

Alger, E.T., Kroll, J., Dzenitis, E.G., Montesanti, R.M., Hughes, J., Swisher, M., Taylor, J., Segraves, K., Lord, D.M., Reynolds, J., Castro, C., Edwards, G., "NIF Target Assembly Metrology Methodology and Results," Proc. 19th Target Fabrication Mtg., Orlando, Florida, 2010, to be published in Fusion Sci. Technol.

Boehm, K.J., Raffray, A.R., Alexander, N.B., Frey, D.T., Goodin, D.T., "Numerical and Experimental Analysis of a Fluidized Bed for IFE Target Layering," Fusion Sci. Technol. 56(1), 422 (2009).

Bousquet, J.T., Hund, J.F., Goodin, D.T., Alexander, N.B., "Advancements in Glow Discharge Polymer (GDP) Coatings for Mass Production," Fusion Sci. Technol. 55(4), 446 (2009).

Carlson, L.C., Tillack, M.S., Stromsoe, J., Alexander, N.B., Flint, G.W., Goodin, D.T., Petzoldt, R.W., "Completing the Viability Demonstration of Direct-Drive IFE Target Engagement and Assessing Scalability to a Full-Scale Power Plant," IEEE Trans. Plasma Sci. 38(3), 300 (2010).

Carlson, L.C., Tillack, M.S., Stromsoe, J., Alexander, N.B., Goodin, D.T., Petzoldt, R.W., "Improving the Accuracy of a Target Engagement Demonstration," Fusion Sci. Technol. 56(1), 409 (2009).

Carlson, L.J., Goodin, D.T., Tillack, M.S., "A Method for Characterizing and Improving the Damage Resistance of the Outer Metallic Coatings on Inertial Fusion Energy Targets," IEEE Trans. Plasma Sci. 38(3), 448 (2010).

Chen, K.C., Moreno, K.A., Lee, Y.T., Wu, J.J., Nguyen, A.Q.L., Huang, H., Sequoia, K.L., "CH Capsule Fabrication for Ignition Tuning Campaign," Proc. 19th Target Fabrication Mtg., Orlando, Florida, 2010, to be published in Fusion Sci. Technol.

Chen, K.C., Nguyen, A.L.Q., Huang, H., Eddinger, S.A., Nikroo, A., "Update on Germanium-Doped CH Capsule Production for NIF: Scale-Up Issues and Current Yields," Fusion Sci. Technol. 55(4), 429 (2009).

Dewald, E., Kozioziemski, B.J., Moody, J., Koch, J., Mapoles, E., Montesanti, R., Youngblood, K.P., Letts, S., Nikroo, A., Sater, J., Atherton, J., "Benchmarking the X-ray Phase Contrast Imaging for ICF DT Ice Characterization Using Roughened Surrogates," Fusion Sci. Technol. 55, 260 (2009).

Eddinger, S.A., Huang, H., Schoff, M.E., "3D Wall-Mapping Using Xradia with Distortion Correction," Fusion Sci. Technol. 55(4), 411 (2009).

Fong, J.R., Eddinger, S.A., Huang, H., Moreno, K.A., "Absorption Edge Spectroscopy for ICF Target Characterization," Fusion Sci. Technol. 55(4), 367 (2009).

Frederick, C.A., Forsman, A.C., Hund, J.F., Eddinger, S.A., "Fabrication of Tantalum Oxide Aerogel Targets for Radiation Transport Experiment Using Thin Film Fabrication and Laser Processing," Fusion Sci. Technol. 55(4), 499 (2009).

Gibson, C.R., Baltz, J., Malsburay, T., Atkinson, D., Brugmann, V., Coffield, F., Edwards, O., Heid, B., Locke, S., Shiromizu, S., Skulina, K., "Design of the NIF Cryogenic Target System," Fusion Sci. Technol. 55(3), 233 (2009).

Glenzer, S.H., MacGowan, B.J., Michael, P., Meezan, N.B., Sutter, L.J., Dixit, N., Kline, J.L., Kyrala, G.A., Bradley, D.K., Callahan, D.A., Dewald, E.L., Divol, L., Dzenitis, E., Edwards, M.J., Hamza, A.V., Haynam, C.A., Hinkel, D.E., Kalantar, D.H., Kilkenny, J.D., Landen, O.L., Lindl, J.D., LePepe, S., Moody, J.D., Nikroo, A., Parham, T., Schneider, M.B., Town, R.P.J., Wagner, P., Widmann, K., Whitman, P., Yuoung, B.K.F., VanWonterghem, B., Atherton, L.J., Moses, E.I., "Symmetric Inertial Confinement Fusion Implosions at Ultra-High Laser Energies," Science 327, 1228 (2010); Scienceexpress; www.scienceexpress.org; 10.1126/science 1185634.

Haid, B.J., Malsbury, T.N., Gibson, C.R., Warren, C.T., "Measurement of Total Condensation on a Shrouded Cryogenic Surface Using a Single Quart Crystal Microbalance," Fusion Sci. Technol. 55, 276 (2009).

Hansen, J.F., vanBreugel, W., Bringa, E.M., Graham, G.A., Remington, B.A., Taylor, E.A., Tielens, A.G.G.M., "A New Method to Generate Dust with Astrophysical Properties," to be published in a special issue of HEDLA, 2010.

Hoppe, M.L., Vermillion, B.A., "High Z Doping of Glass Shells," Fusion Sci. Technol. 55(4), 461 (2009).

Hoppe, M.L., Vermillion, B.A., Chen, K.C., "Developments in the Production of Doped and High Aspect Ratio Si-GDP to Glass Shells," Proc. 19th Target Fabrication Mtg., Orlando, Florida, 2010, to be published in Fusion Sci. Technol.

Huang, H., Eddinger, S.A., Schoff, M.E., "Quantitative Dimension Measurement of ICF Components Using Xradia," Fusion Sci. Technol. 55(4), 373 (2009).

Huang, H., Eddinger, S.A., Stephens, R.B., Nikroo, A., "Quantitative Data Analysis Method for Precision Radiography," Fusion Sci. Technol. 55(4), 380 (2009).

Huang, H., Fallon, R., Haan, S.W., Lee, Y.T., Moreno, K.A., Nguyen, A.Q.L., Nikroo, A., Sequoia, K.L., Stephens, R.B., Wu, J.J., "Metrology Statistics for NIF Tuning Campaign," Proc. 19th Target Fabrication Mtg., Orlando, Florida, 2010, to be published in Fusion Sci. Technol.

Huang, H., Nikroo, A., Stephens, R.B., Eddinger, S.A., Wall, D.R., Moreno, K.A., Xu, H.W., "Element Specific Dopant/Impurity Profiling for ICF Ablator Capsules," Fusion Sci. Technol. 55(4), 356 (2009).

Huang, H., Stephens, R.B., Eddinger, S.A., "Minimizing X-ray Imaging Artifacts of Low-Z Samples Using the X-radia MicroXCT Microscope," Proc. 19th Target Fabrication Mtg., Orlando, Florida, 2010, to be published in Fusion Sci. Technol.

Jaquez, J.S., Nikroo, A., Wilkens, H.L., "Fabrication and Characterization of Hohlraums with a Co-Mixed Gold-Boron Layer," Fusion Sci. Technol, 55(3), 313 (2009).

Johal, Z.Z., Crippen, J.W., Forsman, A.C., Lundgren, E.H., Moreno, K.A., Nikroo, A., "Robust Capsule and Fill Tube Assemblies for the National Ignition Campaign," Fusion Sci. Technol. 55(3), 331 (2009).

King, J.A., Akli, K.U., Freemen, R.R., Green, J., Hatchett, S.P., Hey, P., Jamangi, P., Key, M.H., Koch, J., Lancaster, K.L., Ma, T., MacKinnon, A.J., MacPhee, A., Norreys, P.A., Patel, P.K., Phillips, T., Stephens, R.B., Theobald, W., Town, R.P.J., Van Woerkom, L., Zhang, B., Beg, F.N., "Studies on the Transport of High Intensity Laser-Generated Hot Electrons in Cone Coupled Wire Targets," Phys. Plasmas 16, 020701 (2009).

Kurantz, C.C., Drake, R.P., Grosskopf, M.J., Budde, A., Krauland, C., Marion, D.C., Visco, A.J., Ditmar, J.R., Robey, H.F., Remington, B.A., Miles, A.R., Cooper, A.B.R., Sorce, C., Plewa, T., Hearn, N.C., Killebrew, K.L., Knauer, J.P., Arnett, D., Donajkowski, T.L., "Three-Dimensional Blast-Wave-Driven Rayleigh–Taylor Instability and the Effects of Long-Wavelength Modes," Phys. Plasmas 16, 056310 (2009); DOI:10.1063/1.3099320

Lee, G.E., Alexander, N.B., Diaz, E., Sheliak, J., "A Robotic System for High Throughput Rate Target Assembly," Proc. 19th Target Fabrication Mtg.," Proc. 19th Target Fabrication Mtg., Orlando, Florida, 2010, to be published in Fusion Sci. Technol.

Lee, Y.T., Johnson, M.A., Nikroo, A., Montesanti, R.C., Huang, H., Moreno, K.A., Chen, K.C., Chen, C., Nguyen, A.Q.L., "Increasing the Throughput of the Phase Shifting Diffraction Interferometer (PSDI)," Fusion Sci. Technol. 55(4), 405 (2009).

Lepape, S., Stephens, R.B., "Density Measurement of Shock Compressed Foam Using X–ray Radiography." to be submitted to Physics of Plasmas, 2008.

Li, C.K., Seguin, F.H., Frenje, J.A., Rosenberg, M., Petrasso, R.D., Amendt, P.A., Koch, J.A., Landen, O.L., Park, H.S., Robey, H.F., Town, R.P.J., Casner, A., Philippe, F., Betti, R., Knauer, J.P., Meyerhofer, D.D., Back, C.A., Kilkenny, J.D., Nikroo, A., "Charged-Particle Probing of X-ray-Driven Inertial-Fusion Implosions," Science 327, 1231 (2010); Scienceexpress; www.scienceexpress.org; 10.1126/science 1185747

Lundgren, E.H., Forsman, A.C., "Laser Forming of Shaped Fill-Holes in Beryllium Targets for Inertial Confinement Fusion Experiments," Fusion Sci. Technol. 55(3), 325 (2009).

Luo, R.W., Greenwood, A.L., Nikroo, A., Chen, C., "Properties of Silicon-Doped GDP Shells Used for Cryogenic Implosions at OMEGA," Fusion Sci. Technol. 55(4), 456 (2009).

Ma, T., MacPhee, A.G., Key, H., Akli, K.U., Barbee Jr., T.W., Mackinnon, A.J., Stephens, R.B., Van Woerkom, L.D., Zhang, B.-B., Beg, F.N. "Extreme ultraviolet imaging of electron-heated targets in petawatt laser experiments," IEEE Trans. Plasma Sci. 36, 1126-1127 (2008).

Mason, R.J., Faehl, R., Kirkpatrick, R., Ma, T., Wei, M.S., Beg, F.N., Key, M.H., and Stephens, R.B., "ePLAS Modeling of Hot Electron Transport in Nail-Wire Targets," J. Phys.: Conf. Ser. 244, 022047 (2010).

Monstesanti, R.M., Seugling, R.M., Klingmann, J.L., Dzenitis, E.G., Alger, E.T., Miller, G.L., Kent, R.A., Castro, C., Reynolds, J.L., Carrillo, M.A., "Robotic System for Precision Assembly of NIF Ignition Targets," Proc. American Society for Precision Engineering Annual Meeting, 2008.

Moreno, K.A., Chen, K.C., Crippen, J.W., Fallon, R., Huang, H., Lee, Y.T., Nguyen, A.Q.L., Nikroo, A., Sequoia, K.L., Wu, J.J., Xu, H.W., "Evolution of the Capsule Fill Tube Assembly Production Methods for the National Ignition Campaign," Proc. 19th Target Fabrication Meeting, Orlando, Florida, 2010, to be published in Fusion Sci. Technol.

Moreno, K.A., Eddinger, S.A., Fong, J.R., Lee, Y.T., Nguyen, A.Q.L., Nikroo, A., Huang, H., Rosano, R., Xu, H.W., "Overview of National Ignition Facility Capsule Metrology," Fusion Sci. Technol. 55(4), 349 (2009).

Nguyen, A.L., Eddinger, S.A., Huang, H., Lee, Y.T., Moreno, K.A., Schoff, M.E., "Characterization of Isolated Defects for NIF Targets Using PSDI with an Analysis of Shell Flipping Capability," Fusion Sci. Technol. 55(4), 399 (2009).

Paguio, R.R., Hund, J.F., Blue, B.E., Schroen, D.G., Saito, K.M., Frederick, C.A., Strauser, R.J., Quan, K., "Embedding Sapphire Spheres in Resorcinol Formaldehyde Aerogel for Astrophysical Jet Experiments," Fusion Sci. Technol. 55(4), 484 (2009).

Paguio, R.R., Jasion, D.J., Saito, K.M., Quan, K., Hund, J.F., Nikroo, A., "Development and Fabrication of NIF-Scale Resorcinol Formaldehyde Foam Shells for ICF Experiments," Proc. 19th Target Fabrication Mtg., Orlando, Florida, 2010, to be published in Fusion Sci. Technol.

Paguio, R.R., Nikroo, A., Saito, J.M., Hund, J.R., Castillo, E.R., Ravelo, N.M., Quan, K., "Improvements on Permeation GDP Coatings for Resorcinol Formaldehyde Foam Shells for Cryogenic Experiments on OMEGA," Fusion Sci. Technol. 55(4), 450 (2009).

Pasley, J., Wei, M., Shipton, E., Chen, S., Ma, T., Beg, F.N., Alexander, N., Stephens, R., MacPhee, A.G., Hey, D., LePape, S., Patel, P., MacKinnon, A., Key, M., Offermann, D., Link, A., Chowdhury, E., Van Woerkom, L., Freeman, R.R., "Nail-like targets for laser-plasma interaction experiments," IEEE Trans. Plasma Sci. 36, 1128-1129 (2008).

Petzoldt, R.W., Carlson, L.C., Hares, J., Stromsoe, J.D., "Target Steering and Electrostatic Acceleration for IFE," Proc. 23rd Symp. on Fusion Engineering (SOFE), San Diego, California, to be published in IEEE Trans. Plasma Sci., 2009.

Petzoldt, R.W., Valmianski, E.I., Carlson, L.C., Stromose, J., Hares, J.D., "Target Injection With Electrostatic Acceleration," Fusion Sci. Technol. 56(1), 417 (2009).

Saito, K.M., Hund, J.F., Paguio, R.R., Nikroo, A., Crippen, J.W., Johal, Z.Z., Shearer, C.H., Giraldez, E.M., "Fill Tube Development for Foam Shells for OMEGA, NIF, and Fast Ignition Application," Fusion Sci. Technol. 55(3), 337 (2009).

Saito, K.M., Hund, J.F., Wittman, M., Nikroo, A., Crippen, J.W., Jaquez, J.S., Giraldez, E.M., "Improvements to Fill Tube Design for Direct Drive NIF and Fast Ignition Applications," Proc. 19th Target Fabrication Mtg., Orlando, Florida, 2010, to be published in Fusion Sci. Technol.

Sequoia, K.L., Huang, H., Stephens, R.B., Moreno, K.A., Chen, K.C., Nikroo, A., "Increased X-ray Opacity of GDP Capsules from High Intensity X-ray Exposure," Proc. 19th Target Fabrication Mtg., Orlando, Florida, 2010, to be published in Fusion Sci. Technol.

Sethian, J.D., Boehm, K., Alexander, N.B., Goodin, D.T., Hund, J.F., Paguio, R.R., Petzoldt, R.W., Schroen, D.G., Sheliak, J.D., "The Science and Technologies for Fusion Energy with Lasers and Direct-Drive Targets," IEEE Trans. Plasma Sci. 38(4), 690 (2010).

Stephens, R.B., Akli, K.U., Bartel, T., Beg, F.N., Chawla, S., Chen, C.D., Divol, L., Fedosejevs, R., Freeman R.R., Friesen, H., Giraldez, E., Hey, D.S., Higginson, D.P., Jarrot, C., Kemp, G.E., Key, M.H., Krygier, A., Larson, D., Le Pape, S., Link, A., Ma, T.Y., MacKinnon, A.J., MacLean, H.S., MacPhee, A.G., Murphy, C., Ovchinnikov, V., Patel, P.K., Ping, Y., Sawada, H., Schumacher, D., Tsui, Y., Turnbull, D., Wei, M.S., Van Woerkom, L.D., Westover, B., Wilks, S.C., Yabuuchi, T., "Divergence of Laser-Generated Hot Electrons Produced in a Cone Geometry," J. Phys.: Conf. Ser. 244, 022064 (2010).

Stephens, R.B., Akli, K.U., Bartel, T., Beg, F.N., Chawla, S., Chen, C.D., Chen, H., Chen, S., Chrisman, B., Freeman, R.R., Hey, D., Key, M., Kemp, A., King, J., Lancaster, K., LePape, S., Link, A., Ma, T., MacKinnon, A.J., MacPhee, A.G., Norreys, P., Offerman, D., Ovchinnikov, V., Pasley, J., Patel, P., Schumacher, D., Sentoku, Y., Tsui, Y., Wilks, S., Van Woerkom, L.D., Wei, M.S., Yabuuchi, T., "Energy Injection for Fast Ignition," Plasma and Fusion Research: Review Articles 4, 016-1 (2009).

Theobald, W., Stoeckl, C., Jaanimagi, P., Nilson, P., Storm, M., Meyerhofer, D.D., Sangster, T.C., Hey, D., MacKinnon, A.J., Park, H.-S., Patel, P., Shepherd, R., Snavely, R., Key, M., King, J.A., Zhang, B., Stephens, R.B., Akli, K., Highbarger, K., Weber, R., Van Woerkom, L., Freeman, R.R., Green, J., Gregori, G., Lancaster, K., and Norreys, P.A., "A Dual-Channel, Curved-Crystal Spectrograph for Petawatt-Laser X-ray Backlighter," Rev. Sci. Instrum. 80, 083501 (2009).

Vermillion, B.A., Hoppe, M.L., Alfonso, E.L., Giraldez, E.M., Hoppe Jr., M.L., Fooks, J.A.," The Production and Characterization of Banded GDP Capsules for Defect Implosion Experiments on OMEGA," Proc. 19th Target Fabrication Mtg., Orlando, Florida, 2010, to be published in Fusion Sci. Technol.

Vermillion, B.A., Hoppe, M.L., Andrews, R.E., "The Assembly and Characterization of Dynamic Hohlraum Double-Shell Targets," Fusion Sci. Technol. 55(3), 296 (2009).

Wei, M.S., Chawla, S., Mishra, R., MacPhee, A.G., Paradkar, B.S., Akli, K.U., Batani, D., Chen, C.D., Chen, H., Fedosejevs, R., Foord, M., Friesen, H., Hey, D., Higginson, D., Jarrott, L., Key, M.H., Larsen, J.T., Le-Pape, S., Mackinnon, A.J., Mariscal, D., McLean, H.S., Morace, A., Murphy, C.W., Nakami, N., Pasley, J., Patel, P.K., Ping, Y., Sawada, H., Sentoku, Y., Stephens, R.B., Tiedje, H., Tsu, Y., Westover, B., Yabuuchi, T., Beg, F.N., "First Direct Divergence Measurement of a Fast Ignition Relevant Electron Beam," submitted to Phys. Rev. Letters, 2010.

Wong, B.Y., Brown, L.C., Schaube, F., Tamme, R., Sattler, C., "Oxide Based Thermochemical Heat Storage," Proc. SolarPaces 2010, Perpignan, France, to be published in Journal of Hydrogen Energy.

Youngblood, K.P., Alford, C.S., Bhandarkar, S., Hayes, J., Moreno, K.A., Nikroo, A., Xu, H.W., "Increasing the Uniformity of the Radial Argon Concentration in Beryllium Shells," Proc. 19th Target Fabrication Meeting, Orlando, Florida, 2010, to be published in Fusion Sci. Technol.

8.2 List of Presentations

Alexander, N., "A Rep-Rated Target Insertion System for High Power Lasers," 19th Target Fabrication Meeting; Orlando, Florida, February 21–26, 2010.

Alger, E., "NIF Target Assembly metrology Methodology and Results," 19th Target Fabrication Meeting; Orlando, Florida, February 21–26, 2010.

Alfonso, N., "Techniques to measure the refractive index of GDP and Ge-doped GDP in monochromatic light for VISAR experiments," 19th Target Fabrication Meeting; Orlando, Florida, February 21–26, 2010.

Back, C., "Developments in Target Fabrication Applicable to HEDLA Experiments," 8th International Conference on High Energy Density Laboratory Astrophysics, California Institute of Technology, March 15–18, 2010.

Blue, B., "Shock-Clump Interaction Studies in the Laboratory," 51st APS Meeting of Division of Plasma Physics, Atlanta, Georgia, November 2–6, 2009.

Blue, B., "Target Basics," OMEGA Laser Facility Users Group Workshop, University of Rochester, April 28, 2010.

Brown, L., "Thermochemical Heat Storage for Concentrated Solar Power - Cycle Identification," Project Review Meeting at GA, March 15–17, 2010.

Brown, L., "SO2-H2O Disproportionation Thermodynamics," Solar Project Meeting held at DRL, UK, September 14, 2010.

Buckingham, R., "TES Flowsheeting and Costing Method Update," Solar Project Meeting held at DRL, UK, September 14, 2010.

Chen, B., "Progress in Hohlraum Process Improvement — Delamination Issue," General Atomics, June 3, 2010.

Chen, K.C., "Improvements in CH Capsule Production," 19th Target Fabrication Meeting; Orlando, Florida, February 21–26, 2010.

Crippen, J., "Capsule and Fill Tube Assembly and Metrology for NIC," 19th Target Fabrication Meeting; Orlando, Florida, February 21–26, 2010.

Farrell, M., "Effect of Cooling on Helium Half Life in Hoppe Glass," Video Conference with LLNL, June 10, 2010.

Farrell, M., "FY2009-2010 NLUF Components & Assemblies" Internal Presentation for Lois Buitano at DOE/NNSA HQ, October 22, 2010.

Fooks, J., "Investigation of a New Cryogenic Target Design," 19th Target Fabrication Meeting; Orlando, Florida, February 21–26, 2010.

Forsman, A., "The Study of Warm Dense Matter: Both a Servant to and a Beneficiary of High Aspect Laser Drilling," 2010 Ion Beam Driven High Energy Density Physics Workshop, Pleasanton, California, June 23–24, 2010.

Frederick, C., "Fabrication of CH Microbump Arrays on Planar CH Foils," 19th Target Fabrication Meeting; Orlando, Florida, February 21–26, 2010.

Giraldez, E., "Overview of New Components and Targets Fabricated at GA in FY09 for Shots in OMEGA, NIF, and Titan," 19th Target Fabrication Meeting; Orlando, Florida, February 21–26, 2010.

Greenwood, A., "Drop Tower Glass Shell Composition as a Predictor of He Half-life," 19th Target Fabrication Meeting; Orlando, Florida, February 21–26, 2010.

Hansen, F., "A Method to Generate Dust with Astrophysical Properties," 8th International Conference on High Energy Density Laboratory Astrophysics, California Institute of Technology, March 15-18, 2010.

Hein, N., "AuU Hohlraum Surface Categorization/Assessment," LLNL, February 3, 2010.

Hein, N., "Tiger Team Specification: Affect on Hohlraum Production," General Atomics, September 22, 2010.

Hein, N., "LANL Hohlraum Machining; Tolerances and Surface Roughness for NIF Hohlraums," General Atomics, September 22, 2010.

Hoppe, M. Jr., "Fabrication and Characterization of the 4th Rise Keyhole Cone for NIF," 19th Target Fabrication Meeting; Orlando, Florida, February 21–26, 2010.

Hoppe, M. Sr., "Developments in the Production of Doped and High Aspect Ratio-Si-GDP Glass Capsules," 19th Target Fabrication Meeting; Orlando, Florida, February 21–26, 2010.

Hoppe, M. Sr., "Large Hoppe Glass for FY11 Exploding Pusher Experiments," Video Conference with LLNL, June 16, 2010.

Huang, H., "Metrology Statistics for ICF Targets" 19th Target Fabrication Meeting; Orlando, Florida, February 21–26, 2010.

Huang, H., "Minimizing Artifacts in X-radia measurement of Low-Z Samples," 19th Target Fabrication Meeting; Orlando, Florida, February 21–26, 2010.

Hund, J., “Fabrication of Backlighters and Other Laser Targets Via Lithography,” 19th Target Fabrication Meeting; Orlando, Florida, February 21–26, 2010.

Jaquez, J., “Recent Developments in Fabrication and Characterization of AuB Lined Au Hohlraums,” 19th Target Fabrication Meeting; Orlando, Florida, February 21–26, 2010.

Jaquez, J., “Initial IR&D Summary of SS-304 Coating as a Liner for Epoxy Cylinders,” General Atomics, June 3, 2010.

Jasion, D., “Molten Salt – Ion Exchange Effects on Glass Capsule Half-Life,” 19th Target Fabrication Meeting; Orlando, Florida, February 21–26, 2010.

Kilkenny, J., “Review of NIC Sponsored Workshops on Target Diagnostics,” HED Planning Workshop, LANL, April 14, 2010.

Killebrew, K., “New Characterization Techniques for Wire Arrays at Z Facility.” 19th Target Fabrication Meeting; Orlando, Florida, February 21–26, 2010.

Lee, G., “A Robotic System For Assembly and Mounting of Targets, ” 19th Target Fabrication Meeting; Orlando, Florida, February 21–26, 2010.

Lundgren, E., “Laser Forming of Shaped Fill Holes in Be Capsule Update,” 19th Target Fabrication Meeting; Orlando, Florida, February 21–26, 2010.

Lundgren, E., “Rapid Production of Precision Pinholes by Laser-Machining,” 19th Target Fabrication Meeting; Orlando, Florida, February 21–26, 2010.

Luo, R., “Fabrication of ICE BCCMetal target for OMEGA experiment,” 19th Target Fabrication Meeting; Orlando, Florida, February 21–26, 2010.

Miller, W., “ISO orientation,” Presentation to ICF personnel, October 6, 2009.

Miller, W., “Management Review of the IFT Quality System,” ISO Management Review held at GA, October 26, 2009.

Miller, W., “Are the Measurements Good Enough? Performing a Measurement System Analysis,” 19th Target Fabrication Meeting; Orlando, Florida, February 21–26, 2010.

Moreno, K., “Evolution of the Capsule Fill Tube Assembly Production Methods for the National Ignition Campaign,” 19th Target Fabrication Meeting; Orlando, Florida, February 21–26, 2010.

Moreno, K., “CFTA Process Assessment - How Clean is the Process Today? Update 3,” General Atomics, June 3, 2010.

Nguyen, A., “Minimizing Contaminants Due to Mandrels in Beryllium Sputter Coated Capsules,” 19th Target Fabrication Meeting; Orlando, Florida, February 21–26, 2010.

Paguio, R., “Embedding Ruby Spheres & Al2o3 Nanoparticles into a Resorcinol Formaldehyde Target for Astrophysical Jet Experiments,” 19th Target Fabrication Meeting; Orlando, Florida, February 21–26, 2010.

Paguio, R., “Improving the Wall Uniformity of NIF-Scale Resorcinol Formaldehyde Foam Shells for ICF Experiments,” 19th Target Fabrication Meeting; Orlando, Florida, February 21–26, 2010.

Paguio, R., “Synthesis of Resorcinol Formaldehyde Aerogel Using UV Photoinitiators or Photoacids,” 19th Target Fabrication Meeting; Orlando, Florida, February 21–26, 2010.

Paguio, R., “Characterization of SUNY Geneseo's DPE Foils.” General Atomics, June 8, 2010.

Paguio, R., “Comparison of GA and Geneseo DPE Foils for MRS.” Telecon with Geneseo, June 9, 2010.

Petzoldt, R., “Injector Selection for LIFE,” LLNL, June 29, 2010.

Quan, K., “2009-2010 Uranium Hohlraum Storage Study,” General Atomics, June 3, 2010.

Randall, G., “Microfluidic Droplet Processing for Inertial Fusion Targets,” 19th Target Fabrication Meeting, Orlando, Florida, February 21–26, 2010.

Randall, G., “Digital Microfluidics’ Process Engineering,” Advertisement for Outside Applications, August 4, 2010.

Russ, B., “Results of the Sulfur-Iodine Process Integrated Lab Scale Experiment,” American Nuclear Society Meeting, June 15, 2010.

Saito, K., “Improvements to Fill Tube Design for Direct Drive NIF and Fast Ignition Applications,” 19th Target Fabrication Meeting, Orlando, Florida, February 21–26, 2010.

Schroen, D., “Extending the Possibilities of TPX Foams,” 19th Target Fabrication Meeting, Orlando, Florida, February 21–26, 2010.

Schroen, D., “Sandia National Laboratories Z Targets - After the Refurbishment,” 19th Target Fabrication Meeting, Orlando, Florida, February 21–26, 2010.

Sequoia, K., “Increased X-ray Opacity of GDP Capsules from High Intensity X-ray,” 19th Target Fabrication Meeting; Orlando, Florida, February 21–26, 2010.

Sohn, R., “Utilizing Computer Aided Manufacturing in the Fabrication of Components for the National Ignition Campaign,” 19th Target Fabrication Meeting, Orlando, Florida, February 21–26, 2010.

Stephens, R., “Cone Geometry Modified Divergence of Laser-Generated Hot Electrons,” 51st APS Meeting of Division of Plasma Physics, Atlanta, Georgia, November 2–6, 2009.

Stephens, R., “Perspectives for collaborations from the US point of view,” HiPer WP10-WP12 Meeting, United Kingdom, January 25, 2010.

Stephens, R., “Scaling Up Super-Penetration on EP,” Informal Shock and Fast Ignition Physics Meeting, University of Rochester, April 27, 2010.

Stephens, R., “Electron Transport in Warm Dense Matter,” Fusion Science Center Meeting at LLNL, August 5, 2010.

Stephens, R., “IFE Technology at GA,” Symposium on Fusion Technology, Oporto, Portugal, September 28, 2010.

Stephens, R., “Hot Electron Generation for Fast Ignition,” 23rd IAEA Fusion Energy Conference, Daejeon, Korea, October 11–16, 2010.

Stephens, R., “Precision Measurements of Electron Generation and Transport,” 11th Int. Workshop on Fast Ignition of Fusion Targets; Shanghai, China, October 17–21, 2010.

Vermillion, B., “The Production and Characterization of Banded GDP Capsules for Defect Implosion Experiments on OMEGA,” 19th Target Fabrication Meeting, Orlando, Florida, February 21–26, 2010.

Wilkens, H., “Update on Thick C Coating,” Presented to FarTech at GA, April 2010.

Wilkens, H., “Update on Thick C Coating,” Presented to FarTech at GA, June 2010.

Wilkens, H., “Be steps, Measurements of step height and surface roughness with white light interferometry.” Presented to Carolyn Kuranz, NLUF, September 14, 2010.

Wilkens, H., “SiC target composition summary and SiC/C bilayers,” Presented to FarTech at GA, September 14, 2010.

Wong, B., “Thermochemical Heat Storage for Concentrated Solar Power,” DOE CSP Project Review on February 9, 2010.

Wu, D., “Determining Measurement Uncertainty in NIF Capsule Production Environment,” 19th Target Fabrication Meeting, Orlando, Florida, February 21–26, 2010.

Xu, H., “SiC and C coating on zirconia beads, heat treatment results,” Presented to FarTech at GA, September 14, 2010.

Younan, S., “Hohlraum Interior Surface Roughness – Improving the Current Surface Roughness Measuring Process” Presented to LLNL, April 16, 2009.

Younan, S., “Hohlraum Interior Surface Roughness – Improving the Current Surface Roughness Measuring Process” Presented to IFT group at GA, April 7, 2010.